

**Low-temperature thermochronology as a control on vertical movements for semi-quantitative source-to-sink analysis**

**A case study for the Permian to Neogene of Morocco and surroundings**

Charton, Rémi; Bertotti, Giovanni; Duval Arnould, Aude; Redfern, Jonathan; Storms, Joep E.A.

**DOI**

[10.1111/bre.12517](https://doi.org/10.1111/bre.12517)

**Publication date**

2020

**Document Version**

Final published version

**Published in**

Basin Research

**Citation (APA)**

Charton, R., Bertotti, G., Duval Arnould, A., Redfern, J., & Storms, J. E. A. (2020). Low-temperature thermochronology as a control on vertical movements for semi-quantitative source-to-sink analysis: A case study for the Permian to Neogene of Morocco and surroundings. *Basin Research*, 33 (2021)(2), 1337-1383. <https://doi.org/10.1111/bre.12517>

**Important note**

To cite this publication, please use the final published version (if applicable). Please check the document version above.


**Copyright**

Other than for strictly personal use, it is not permitted to download, forward or distribute the text or part of it, without the consent of the author(s) and/or copyright holder(s), unless the work is under an open content license such as Creative Commons.

**Takedown policy**

Please contact us and provide details if you believe this document breaches copyrights. We will remove access to the work immediately and investigate your claim.

# Low-temperature thermochronology as a control on vertical movements for semi-quantitative source-to-sink analysis: A case study for the Permian to Neogene of Morocco and surroundings

Rémi Charton<sup>1</sup>  | Giovanni Bertotti<sup>1</sup> | Aude Duval Arnould<sup>2</sup> | Joep E. A. Storms<sup>1</sup> | Jonathan Redfern<sup>2</sup>

<sup>1</sup>Department of Geoscience and Engineering, Delft University of Technology, Delft, The Netherlands

<sup>2</sup>School of Earth and Environmental Sciences, The University of Manchester, Manchester, United Kingdom

## Correspondence

Rémi Charton, Department of Geoscience and Engineering, Delft University of Technology, P.O. Box 5048, 2600 GA Delft, The Netherlands.

Email: r.j.g.charton@tudelft.nl

## Funding information

North Africa Research Group; The Netherlands Research Centre for Integrated Solid Earth Science

[Correction added on 9 November 2020, after first online publication: The first citations of Figures 4-22 and Tables 1-3 have been updated and Figure 15 has been corrected in this version.]

[Correction added on 9 November 2020, after first online publication: The order of the last two authors and the affiliation of Joep E. A. Storms have been corrected in this version.]

## Abstract

Continental passive margins and their hinterlands in the Atlantic realm have been the locus of many Low Temperature Thermochronology (LTT) and time-Temperature (t-T) modelling studies that evidence pre-, syn- and post-rift episodic km-scale exhumation and burial episodes. In this study, we integrate data from over 30 published LTT and t-T modelling studies from Morocco and its surroundings using a three-step workflow to obtain: (a) exhumation/burial rates, (b) erosion rates and (c) palaeoreconstructions of source-to-sink domains, between the Permian and the Present. Our synthesis of available t-T modelling results predicts high exhumation rates in the Anti-Atlas (0.1 km/Myr) during the Early to Middle Jurassic, and in the High Atlas (0.1 km/Myr) and Rif (up to 0.5 km/Myr) during the Neogene. These rates are comparable to values typical of rift flank, domal or structural uplifts settings. During the other investigated periods, exhumation rates in the Meseta, High-Atlas, Anti-Atlas and Reguibat shield are around  $0.04 \pm 0.02$  km/Myr. Interpolation of the exhumation rates at the regional scale allow calculation of the volume of rocks eroded. Estimates of erosion rates are between  $0.2 \times 10^3$  and  $7.5 \times 10^3$  km<sup>3</sup> (in the Meseta and the Reguibat Shield respectively). Ten erosional (quantitative, from interpolation results) and depositional (qualitative, from data synthesis) “source-and-sink” maps have been constructed, with emphasis on the Jurassic and Cretaceous periods. The maps integrate the extent of exhumed domains, using information from geological maps, lithofacies and biostratigraphic data from new geological fieldwork and well data from onshore and offshore basins. The results illustrate changes in the source-to-sink systems and allow for a better understanding of the Central Atlantic margin hinterlands evolution.

## KEYWORDS

exhumation rates, exhumation/burial, Morocco, palaeoreconstruction, time-temperature modelling

This is an open access article under the terms of the Creative Commons Attribution License, which permits use, distribution and reproduction in any medium, provided the original work is properly cited.

© 2020 The Authors. *Basin Research* published by International Association of Sedimentologists and European Association of Geoscientists and Engineers and John Wiley & Sons Ltd

# 1 | INTRODUCTION

Continental passive margins and their hinterlands (Figure 1) are the locus of a significant amount of Low-Temperature Thermochronology (LTT) studies that evidence pre-, syn- and post-rift episodic km-scale upward (i.e. exhumation) and downward (i.e. burial) movements (e.g. Gallagher, Hawkesworth, & Mantovani, 1994; Green et al., 2018). Such movements are an important component of source-to-sink systems (e.g. Bhattacharya et al., 2016; Helland-Hansen et al., 2016).

A number of exhumation episodes are recorded on the margins of the Atlantic Ocean. Pre-rift movements are well documented (e.g. Japsen, Green, Bonow, Chalmers et al., 2016; Jelinek et al., 2014; Juez-Larre & Andriessen, 2006; Ruiz et al., 2011). Syn-rift exhumation is observed along the Atlantic rift flanks (e.g. Charton et al., 2018; Japsen, Green, Bonow, Chalmers et al., 2016; Jelinek et al., 2014; Oukassou et al., 2013; Wildman et al., 2015) and several hundreds of kilometres into the plate interior (e.g. Leprêtre et al., 2014). Syn-rift burial episodes in the unstretched continental crust have also been documented, although in fewer places (e.g. Ghorbal et al., 2008; Gouiza et al., 2019; Juez-Larre & Andriessen, 2006). Lastly, post-rift km-scale exhumation/burial have been documented along the North (e.g. Japsen et al., 2006; Japsen, Green, Bonow, Chalmers et al., 2016; Japsen, Green, Bonow, Hinchey et al., 2016), Central (e.g. Amidon et al., 2016; Bertotti & Gouiza, 2012; Frizon de Lamotte et al., 2009), Equatorial (e.g. Hayford, Lisker, & Apaalse, 2008; Ye, 2016; Wildman et al., 2019) and South (e.g. Jelinek et al., 2014; Wildman et al., 2015) Atlantic margins.

Vast regions along Atlantic rifted continental margins expose pre-rift rocks, which can be examined using LTT and time-Temperature (t-T) modelling techniques to provide unique understanding of the thermal history. Low-temperature thermochronology ages record the cooling of rock samples, which can be caused by either thermal relaxation and/or exhumation (also called denudation when erosional in nature; e.g. Malusà & Fitzgerald, 2019b; Pagel et al., 2014). This is especially valuable for geologically ill-constrained areas characterized by no or little sedimentary cover (e.g. Gallagher et al., 1998; Ghorbal et al., 2008; Japsen et al., 2009; Japsen, Bonow et al., 2012; Japsen, Chalmers et al., 2012; Jelinek et al., 2014; Teixell et al., 2009). Results of these techniques can be used as proxies to reconstruct exhumation/burial events (e.g. Teixell et al., 2009) and provide a key constraint on sediment source (e.g. Helland-Hansen et al., 2016).

Bertotti and Gouiza (2012) proposed that unpredicted km-scale exhumation episodes are concurrent with excessive downward movements in the subsiding domain along the Moroccan Atlantic margin. This relationship was further tested and documented in different segments of the

## Highlights

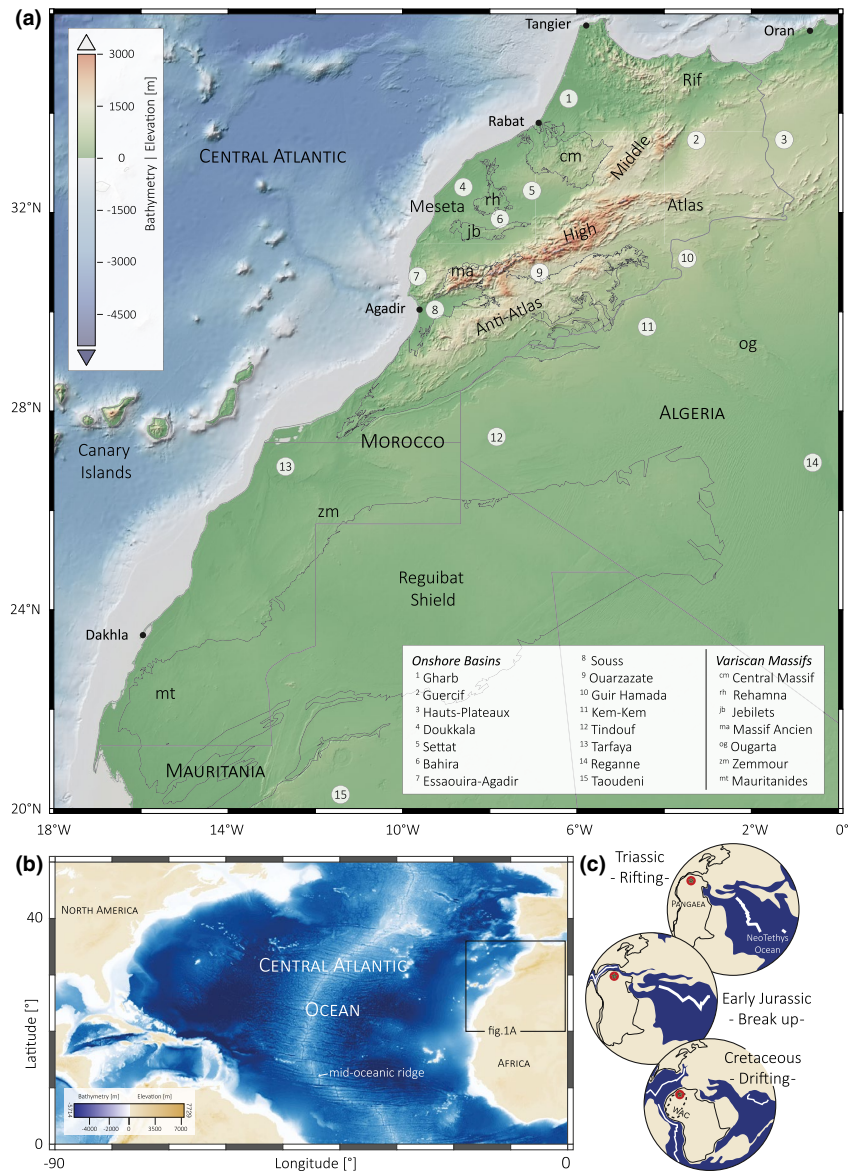
- The illustrated workflow uses time-temperature models as inputs to reconstruct past source-and-sink domains.
- Definition of criteria for the selection of time-temperature models is crucial and should be based on up-to-date geological constraints.
- On average, Meso-Cenozoic exhumation rates in Moroccan massifs are around  $0.04 \pm 0.02$  km/Myr.
- Ten erosional and depositional “source-and-sink” maps are constructed (Permian to Neogene).
- We observe two shifts in sedimentary sources between the Anti-Atlas and the Meseta during the Mesozoic.

same margin (Charton et al., 2018). Exhumation and burial episodes occur at the same time in regions characterized by nonstretched lithosphere, demonstrating that processes other than rifting are at work, or that the effects of the rifting and drifting extend beyond the rifted margin and their direct flanks (e.g. Gouiza et al., 2017, 2018). Several authors have tested aspects of these km-scale movements with numerical models (e.g. Cloetingh & Burov, 2011; Gouiza, 2011; Leroy et al., 2008; Yamato et al., 2013). However, to better constrain the models, quantification of exhumation/burial events over geological time and at the scale of the margin and beyond is required (e.g. Wildman et al., 2019; Ye et al., 2017).

In this study we integrate data from over 30 LTT and t-T modelling studies published in Morocco and its surroundings (see supplementary file 1), including detrital LTT. The majority of the derived LTT ages span the period between the Variscan and Atlas orogenies (ca. 300–40 Ma; Charton, 2018) and the Atlasic inversion event (e.g. Frizon de Lamotte et al., 2009; ca. 40–0 Ma). These cooling ages were interpreted to record vertical movements relative to Earth's surface (e.g. Ghorbal et al., 2008; Sebti et al., 2009; Leprêtre et al., 2014; Gouiza et al., 2017; Charton et al., 2018), although currently the mechanism that generates the vertical movements within the passive margin hinterland remains enigmatic (e.g. Ghorbal et al., 2008).

The objectives of this study are to (a) illustrate a simple workflow that quantifies erosion rates from studies of basement LTT/t-T data, using Morocco as a test area, and (b) provide insights into the post-Variscan palaeogeographic evolution of Morocco and its surroundings via the construction of Source-and-Sink maps integrating t-T data.

**FIGURE 1** (a) Geography of Morocco and its surroundings (data: GEBCO\_2014\_1D) with main geological domains, sedimentary basins and Variscan Massifs superimposed. (b) Morphology of the Central Atlantic seafloor and conjugate margins (data: GEBCO\_2014\_1D). (c) Simplified plate tectonic evolution is after Stampfli and Borel (2002). WAC: Western African Craton



This study presents a technique for investigation of source-to-sink systems, to define and quantify sediments pathways and fluxes along continental margins and their hinterlands. The Source-and-Sink maps do not precisely define the palaeo-drainage systems, as the resolution of available datasets is too coarse, but illustrate the dominant source-and-sink areas, and provide insight into the dynamic nature of these systems during the Phanerozoic post-orogenic, syn-rift and post-rift phases.

## 2 | GEOLOGICAL SETTING AND HISTORY OF MOROCCO

The Central Atlantic continental margins extend from Morocco to Guinea in the east and from Canada to the USA to the west (Figure 1b; Davison, 2005; Withjack & Schlische, 2005). Morocco is located where the Central

Atlantic oceanic crust, the West African Craton and the Atlas orogenic system meet. The present-day topography (Figure 1a) varies from high mountainous regions (Rif and Atlas belts), elevated plains (Hauts Plateaux and Ouarzazate Basin), high massifs (Central Massif, Rehamna, Jebilets, Massif Ancien, Anti-Atlas, Reguibat Shield and Ougarta), nonelevated coastal plains (Meseta, Souss Basin, Tarfaya Basin and Dakhla Basin) and the Saharan domain marked by ergs and sabkhas (salt flats).

The geological history of Morocco (Figure 2a) is marked by a number of major events from the Precambrian to the present day. Prior to Central Atlantic rifting (Figure 1c), Morocco was subjected to the Palaeoproterozoic and Neoproterozoic Eburnean and Panafrican orogenies (Piqué et al., 2006). These orogens are exposed in the Reguibat Shield, the Mauritanides and in the core of the Anti-Atlas. Early Palaeozoic clastic-dominated marine sedimentation deposited in the Palaeo-Tethys Ocean is preserved and exposed

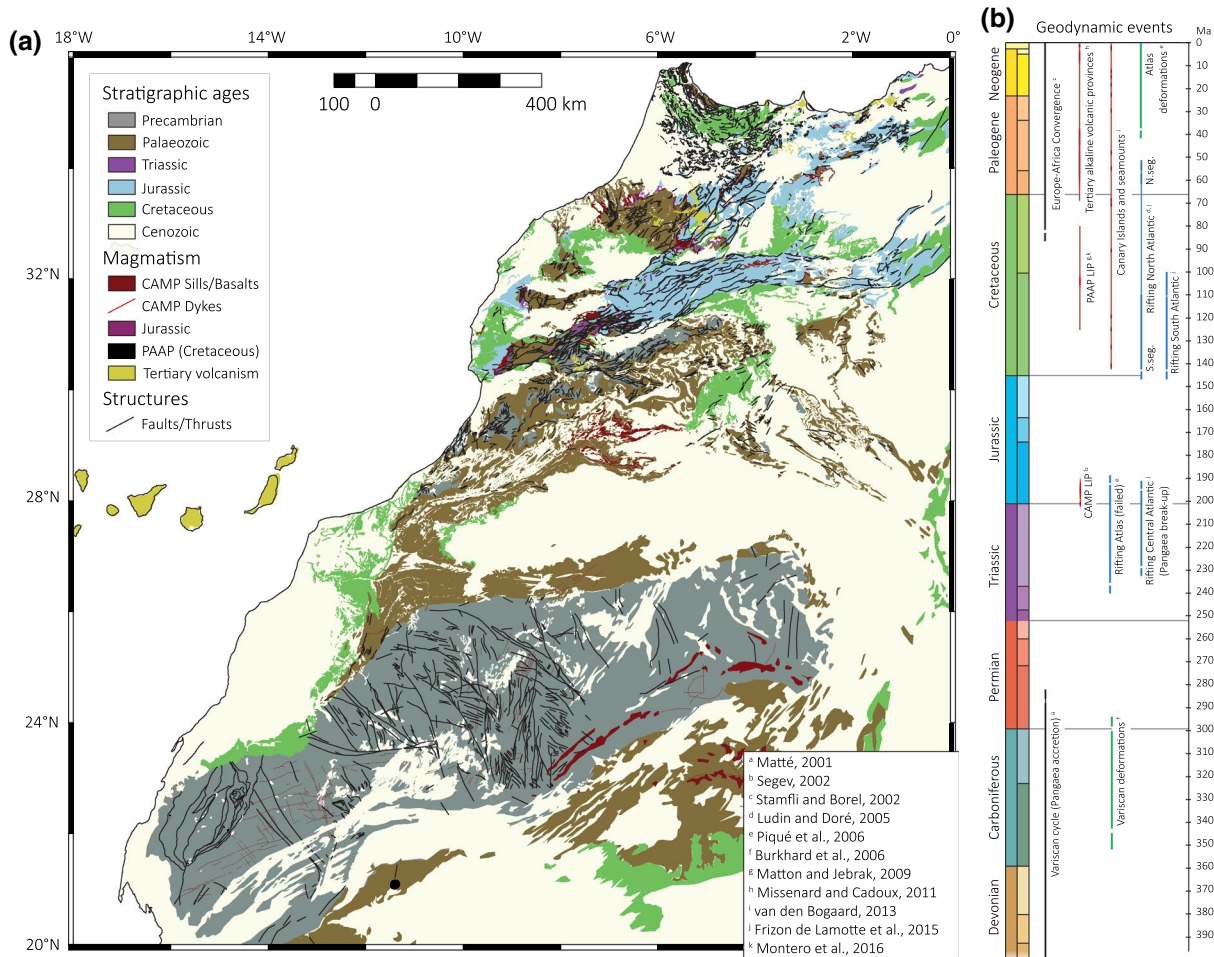


**FIGURE 2** (a) Geological map of Morocco and its surroundings (after Hollard et al., 1985). CAMP: Central Atlantic Magmatic Province (Triassic); PAAP: Peri-Atlantic Alkaline Province (Cretaceous). (b) Tectonic chart of the Atlantic realm and Morocco, see references therein (numerical ages after ICS 2016/12). LIP, Large Igneous Province

in the Meseta massifs, Anti-Atlas and Tindouf basin (Michard et al., 2008).

The Late Palaeozoic Variscan orogeny (Figure 2b; basin inversion, crustal folding, intense thrusting and strike-slip faulting, granitic intrusion...) affected the Precambrian basement of the Meseta, High Atlas and Anti-Atlas and its Palaeozoic cover (e.g. Ellero et al., 2020; Michard et al., 2010). It was followed between the Late Permian and Early Triassic by a post-orogenic collapse, which is part of the Variscan (or 'Hercynian') unconformity (e.g. Frizon de Lamotte et al., 2013).

Morocco experienced two partly coeval episodes of rifting during Triassic and Jurassic times: The Central Atlantic (ca. 230–190 Ma; Frizon de Lamotte et al., 2015; Labails et al., 2010) and Atlasic (aborted; ca. 240–185 Ma; Piqué et al., 2006; Figure 2b) rifts. The Central Atlantic rift partly reactivated Variscan faults, with rift structures often controlled by, and parallel to, the trend of the Palaeozoic belt. The Atlasic rift belongs to the Tethysian realm and is oriented at ca. 45° to the Central Atlantic rift (Figure 2). The rifts, grabens and half-grabens were filled with continental syn-rift

deposits in the Doukkala, Argana/Essaouira-Agadir, Tarfaya coastal basins and High/Middle Atlas basins (Figures 1a and 2a). At ca. 201 Ma, emplacement of mafic dykes and sills (e.g. Davies et al., 2017), followed by flood basalts (dated until ca. 190 Ma; Verati et al., 2007) characterizes the Central Atlantic Magmatic Province (CAMP; Figure 2).

The onset of Pangaea break-up, marking continental drift and initiation of the proto-Central Atlantic occurred at the beginning of the Jurassic, between 190 and 170 Ma (e.g. Davison, 2005; Labails et al., 2010; Sibuet et al., 2012). The development of the Moroccan passive margin during the Jurassic and Early Cretaceous witnessed the accumulation of neritic and deeper marine sediments offshore, and continental to paralic deposits in the coastal basins, the High/Middle Atlas and in the Meseta basins. The Peri-Atlantic Alkaline Pulse (PAAP) is recorded by plutons and flood basalts in the conjugate margins of the Central and South Atlantic oceans, between 125 and 80 Ma (Matton & Jébrak, 2009; Montero et al., 2016).

The opening of the South Atlantic at ca. 135 Ma (Collier et al., 2017) led to African-European plate convergence

and sustained far-field intraplate stresses. The related Atlas Orogeny peaked in the Eocene, and is characterized by exhumation and deformation of the Middle and High Atlas (Figure 1a; Guiraud, 1998; Michard et al., 2008). Finally, Cenozoic volcanism (Missenard & Cadoux, 2011) and surface uplift, observed along two axes, from the Canary Islands to the Siroua massif (Anti-Atlas) and from the Siroua Massif to the Rif belt (Figures 1 and 2), have been interpreted as associated with a mantle anomaly (Missenard, 2006; Teixell et al., 2005; Zeyen et al., 2005). Although such interpretation has been questioned by more recent work (e.g. Ellero et al., 2020), Lanari et al. (2020) suggest that the crustal deformation controlled the exhumation pattern and uplift on a short scale, with coexisting mantle dynamics that control both large-wavelength topography and short-wavelength crustal deformation.

### 3 | FROM TIME-TEMPERATURE MODELS TO SOURCE-TO-SINK MAPS: WORKFLOW, INTERMEDIATE RESULTS AND UNCERTAINTIES

#### 3.1 | Key steps of the workflow

The workflow, illustrated in Figure 3, is composed of the following three steps:

Step 1. From t-T to ‘exhumation/burial rates’ (part 3.2):

- 1.1. Digitalization of published produced t-T curves (open source tool: web plot digitizer);
- 1.2. Selection of t-T models based on review of geological constraints and other conditions;

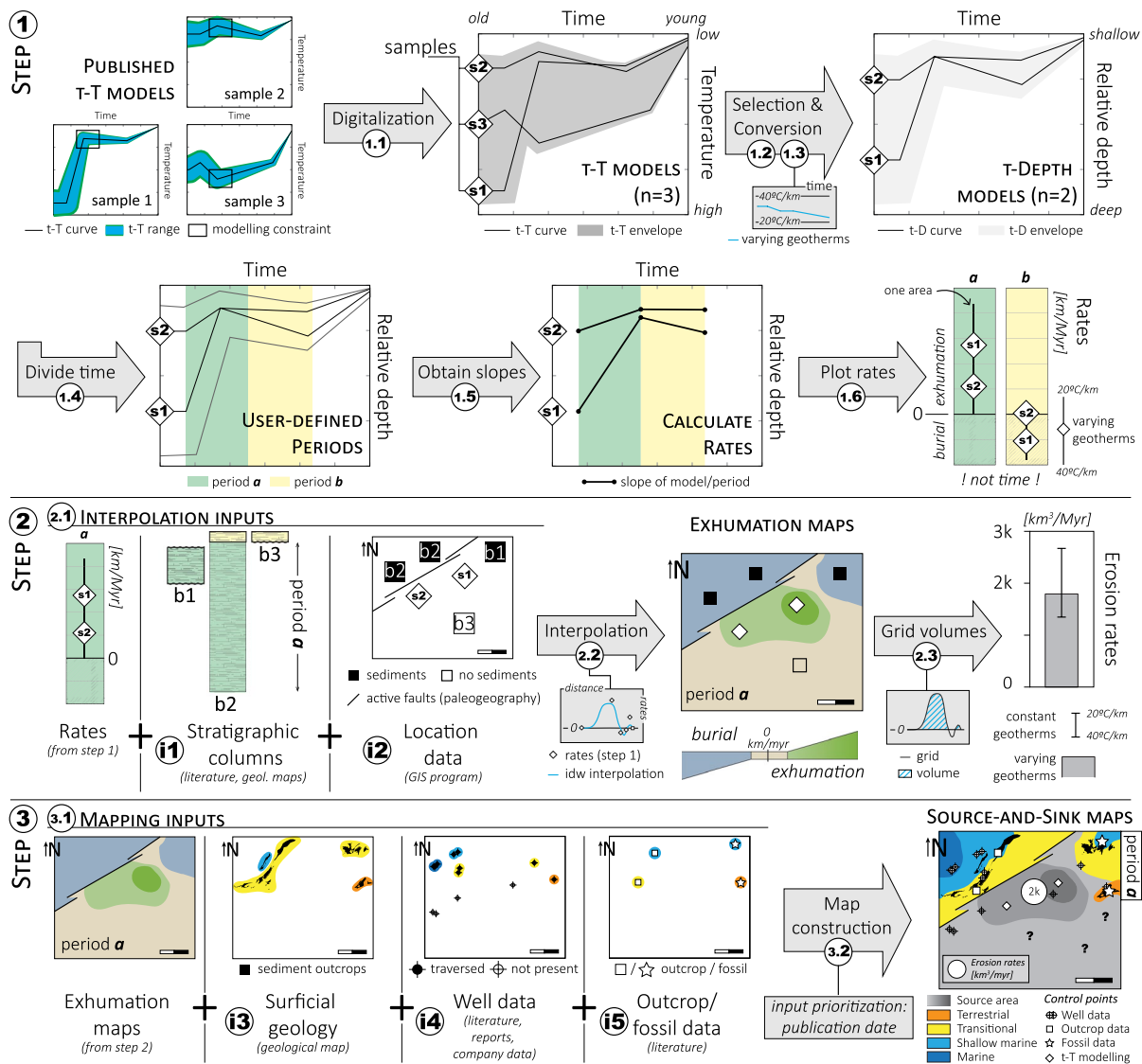


**FIGURE 3** Workflow used in this work. See details in the text in part 3.1. Step 1) From time-temperature (t-T) models to exhumation/burial rates (part 3.2); S1: sample 1. Step 2) From exhumation/burial rates to exhumation maps (part 3.3); b1: basin 1. Step 3) From exhumation maps to source-and-sink maps (part 3.4)

- 1.3. Temperature-to-depth conversion using varying and constant geothermal gradient from present-day analogues, assuming that cooling means erosional exhumation and heating means burial;
- 1.4. Divide investigated time into periods according to main trends in t-T models and stratigraphic boundaries;
- 1.5. Obtain slopes for t-Depth models based on start and end of previously defined periods, which assumes that a strong exhumation followed by burial in one period is similar to an overall milder exhumation (as it cancels out peaks within each period);
- 1.6. Plot rates and ranges based on the depth conversion using varying and constant geothermal gradients respectively.

Step 2. From exhumation/burial rates to 'exhumation maps' (part 3.3):

- 2.1. Interpolation inputs for exhumation maps:
  - (i) Compilation of stratigraphic columns to use as constraint in the interpolation, assuming that sediment preserved in a basin means burial for the related;
  - (ii) Localization of input data with a GIS program. Digitalization of active faults for defined periods from palaeogeographies, for instance, which may then be used as interpolation limits. This assumes that all faults have similar effect on the exhumation rates;
- 2.2. Interpolation of data using the "Inverse Distance Weighted" (IDW) algorithm in the Surfer program (Figure 10). Using this method means that we assume a linearly weighted variation of exhumation/burial rates between points;
- 2.3. Volumetric calculations are performed using the Surfer program, for values higher than 0 km/Myr, which yields the amount of material which has been removed per million years (erosion rate in km<sup>3</sup>/Myr). Clipping polygons are used to estimate the contribution of each considered area. The range is given by running the interpolation and the volume calculations using rates obtained with constant geothermal gradients.

Step 3. From exhumation maps to 'Source-and-Sink (SandS) maps' (part 3.4):

- 3.1. SandS mapping inputs:
  - (i) Surficial geology from the geological map (2a; Hollard et al., 1985) with associated depositional environment when described;
  - (ii) Well data (and location) with associated or interpreted depositional environments from literature or company reports;
  - (iii) Outcrop and fossil data with associated or interpreted depositional environments from the literature;

- 3.2. Map construction using defined depositional environment categories. In areas with no control points, we use existing palaeogeographies to guide limits of source/sink domains.

The detail of the method of each step of this workflow and methods for calculation of exhumation/burial rates and generation of exhumation maps is summarized in the following sections, which include a brief description of the intermediate results, and for each of the steps, the assumptions and limitation.

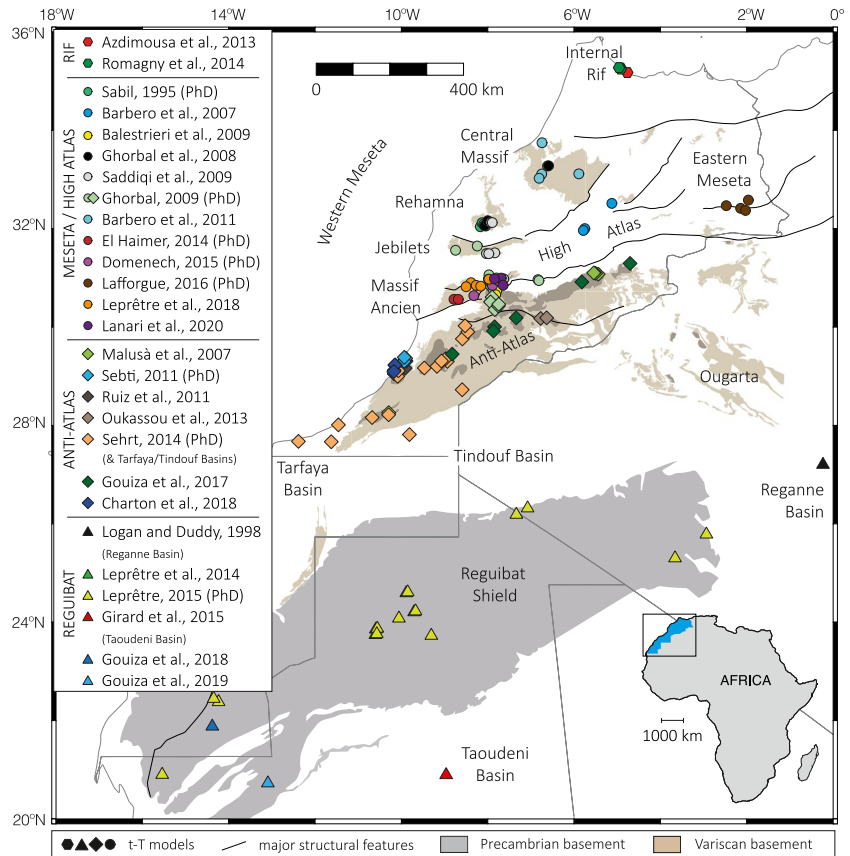
## 3.2 | Step 1: From time-Temperature (t-T) models to exhumation/burial rates

### 3.2.1 | t-T modelling database

In Morocco and its surroundings, over 30 LTT published studies have been conducted in the last 30 years (e.g. Ghorbal et al., 2008; Lanari et al., 2020; Malusà et al., 2007; Mansour, 1991; Ruiz et al., 2011; see supplementary file S1). This provides an extensive database of over 1,000 LTT ages including; (U-Th)/He ages from apatite crystals (AHe), Apatite Fission Track (AFT) ages; (U-Th)/He ages from zircon crystals (ZHe) and Zircon Fission Track (ZFT) ages. Exposed Precambrian crystalline basement rocks, Palaeozoic metapsamites within an otherwise marine metapelite dominated column, Meso-Cenozoic clastic sediments and dykes/sills of all ages were the most sampled lithologies.

LTT studies often use the calculated ages, fission track density and length as inputs for t-T inverse modelling (e.g. Pagel et al., 2014; Malusà & Fitzgerald, 2019a). This inverse modelling technique allows testing of several t-T paths by guiding model realizations with user-defined constraints. This method provides a comprehensive assessment of the thermal history of the analysed sample. Twenty published studies had performed and published t-T modelling, resulting in 141 t-T models (Figures 4 and 5; Table 1). The programs that were used in these studies for the inverse modelling of LTT data are as follows: HeFTy (Ketcham, 2005), AFT Solve (Ketcham et al., 2000) and QTQt (Gallagher, 2012; also, see Vermeesch and Tian (2014) for a comparison of HeFTy and QTQt codes), which provide comparable thermal histories. The program outputs are labelled as 'acceptable', 'good', 'best-fit' or 'weighted average' (referring to a goodness of fit) paths for HeFTy/AFTSolve and 'probability' range, 'maximum likelihood' or 'expected' paths for QTQt. Weighted average/expected curves were digitized when available, or if weighted average was not available, the best-fit/maximum likelihood curves, using WebPlotDigitizer (Ankit Rohatgi; <https://automeris.io/WebPlotDigitizer/>). All digitized curves for each study are available in the supplementary file 2.

**FIGURE 4** Location of t-T models (see reference details in Table 1). Note that the location of t-T models from Logan and Duddy (1998) in the Reganne basin was approximated and Leprêtre (2015) conducted one t-T modelling in the Western Anti-Atlas and all others in the Reguibat Shield



### 3.2.2 | Geological constraints

In the study area, two types of geological constraints are used in considered t-T modelling studies: (a) sediments of known stratigraphy that overlay the sampled basement, with or without an erosion gap, provide a constraint to surface temperatures (ca. 10–40°C) at the time of deposition. In the case of detrital LTT, the stratigraphic age of the sampled sediments is used as a time constraint for surface temperatures; (b) when the age and temperatures of emplacement of igneous body or metamorphism of the sample are known, a corresponding radiometric age constraint is applied to the subsurface temperatures.

In the Rif belt,  $^{40}\text{Ar}/^{39}\text{Ar}$  and K-Ar radiometric dating of Pliocene and Miocene sediments were used as constraints (Azdimoussa et al., 2013; Romagny et al., 2014). In the Meseta, the age of Variscan granite emplacement and the Permian, Triassic and Cenomanian sedimentary record in the basins surrounding the Variscan massifs were utilized in the t-T modelling (Barbero et al., 2011; Ghorbal et al., 2008; Saddiqi et al., 2009). In the Variscan High Atlas (Massif Ancien), Triassic and poorly dated Lower Cretaceous sediments overlying Precambrian basement rocks provided the surface-temperature age constraint (Ghorbal, 2009; Balestrieri et al., 2009; Barbero et al., 2007; Domènech et al., 2016). In the central High Atlas, emplacement timing of Jurassic intrusives was used. (Barbero et al., 2007). In the Tarfaya basin, Sehrt et al., (2017b) used the Aptian and Albian stratigraphic age

of sampled sediments in the t-T modelling. In the Reguibat Shield, a geological constraint at surface temperatures was defined for the Early/Middle Cretaceous, from sediments (poorly dated) exposed in the Tarfaya and Tindouf basins (Leprêtre et al., 2014, 2015; Leprêtre et al., 2017). In the eastern Reguibat Shield, the poorly dated Upper Cretaceous sediments of the Reganne Basin were used to guide t-T models (Leprêtre et al., 2017). A review of these studies suggests that the use of geological constraints was applied in a fairly consistent manner in all published studies, conforming to the most likely geological history (e.g. Michard et al., 2008).

Radiometric dating of Variscan metamorphism (Charton et al., 2018; Malusà et al., 2007; Ruiz et al., 2011) and emplacement of the CAMP dykes (see Gouiza et al., 2017) were used to constrain the time when the sampled rocks were at great temperature/depths (i.e. higher than LTT retention temperatures). Evidence that the presently exhumed Anti-Atlas basement rocks were close to surface temperatures in the past came from observation of the relationship with overlying sedimentary packages. This included the contact with Triassic sediments (Ghorbal, 2009), Middle Jurassic sediments (Charton et al., 2018) in the north, poorly dated terrestrial Infra-Cenomanian sediments in the western, central and eastern Anti-Atlas (e.g. Oukassou et al., 2013; Ruiz et al., 2011) and Cenomanian fluvial sediments overlying the Variscan basement on the eastern Anti-Atlas (Gouiza et al., 2017).



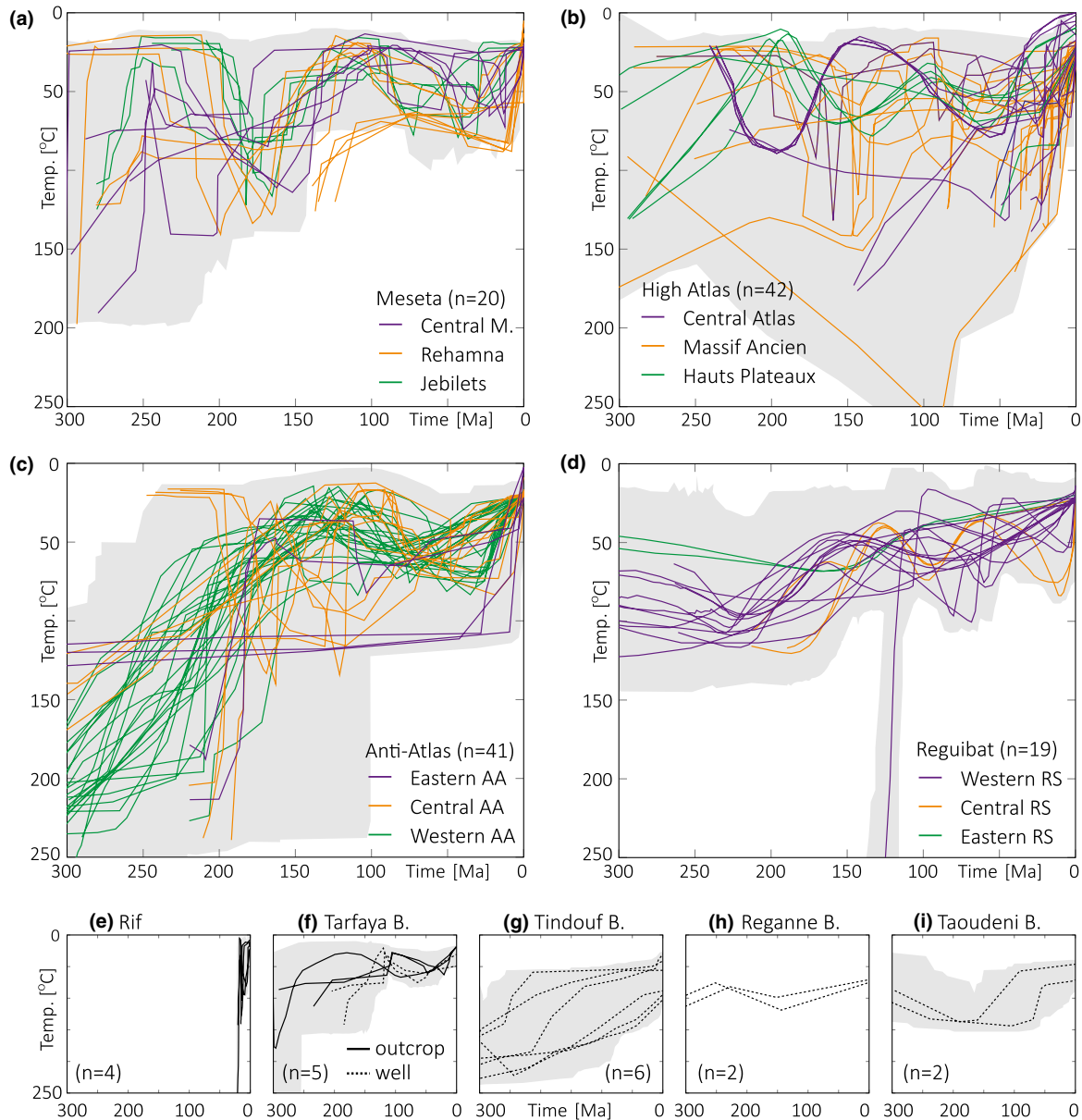


**FIGURE 5** Digitized t-T modelling weighted averages for considered regions (a-i), best-fit curves and acceptable envelopes (grey area) for HeFTy results or expected curves, maximum likelihood curves and limits of  $2\sigma$  confidence level (grey area) for QTQt results (see references in Table 1). AA, Anti-Atlas; B., Basin; Central M., Central Massif; RS, Reguibat Shield

However, comparison between t-T models of the Anti-Atlas indicates some major discrepancies (e.g. Oukassou et al., 2013 vs. Gouiza et al., 2017; Figure 5c). Most of these discrepancies can be attributed to the use of different t-T modelling constraints. An example is the use of an Early Cretaceous modelling geological constraint (Early Cretaceous sediment overlying Basement) in the Anti-Atlas (Ghorbal, 2009; Oukassou et al., 2013; Ruiz et al., 2011; Sehrt et al., 2017a). Recent biostratigraphic work has re-dated much of the terrestrial to shallow marine sediment in the Tarfaya area (mapped as Lower Cretaceous) as being conclusively Bathonian (Middle Jurassic) or older Jurassic/

Triassic, with implications for the modelling (Arantegui et al., 2019; Charton et al., 2018). Finally, in the western Anti-Atlas, recent work by Arantegui (2018) presents new biostratigraphic data that conclusively dates the local redbeds (mapped as Lower Cretaceous) as Bathonian (Middle Jurassic) or older. Extensive palaeontological work has also shown that the clastics overlying basement in parts of the Anti-Atlas are Cenomanian in age (Late Cretaceous; e.g. Benyoucef et al., 2015). In the central Anti-Atlas, no recent biostratigraphic study on the undifferentiated Mesozoic clastic sediments has been conducted, but the Cenomanian limestones positioned higher in the stratigraphic column can be

**TABLE 1** Selection of t-T models for temperature-to-depth conversion and for exhumation and subsidence rate calculations

t-T modelling reference ↓ years	Location	t-T modelling software	t-T models n = 141 Figure 5	Failed to meet conditions (see text for details; n = 73)				t-depth models n = 68 Figure 7	Comments (on failing to meet selection conditions)
				i	ii	iii	iv		
Sabil, (1995)	Meseta	Gallagher et al. (1993)	4	—	4	—	—	—	Program: Gallagher et al., (1998)
Logan and Duddy, (1998)	Reganne	—	2	—	2	—	—	—	Program: no program
Barbero et al., (2007)	High Atlas	AFT-Solve	3	—	3	—	—	—	t-T: no best-fit or weighted average
Malusà et al., (2007)	Anti-Atlas	HeFTy	3	—	—	—	3	—	Anti-Atlas: no relevant Mesozoic exhumation
Ghorbal et al., (2008)	Meseta	HeFTy	4	—	—	—	—	4	—
Balestrieri et al., (2009)	Anti-Atlas	HeFTy	2	—	—	—	2	—	Anti-Atlas: E. Cretaceous exhumation
Ghorbal, (2009)	Meseta/High Atlas/AA	HeFTy	23	1	—	2	—	4	time: model start is younger than 20Ma; newer: re-modelled in Leprière et al., (2018); Anti-Atlas: E. Cretaceous exhumation
Saddiqi et al., (2009)	Meseta	AFT-Solve	4	—	—	—	—	4	—
Barbero et al., (2011)	Meseta	HeFTy	5	—	—	—	—	5	—
Ruiz et al., (2011)	Anti-Atlas	HeFTy	5	—	—	—	5	—	Anti-Atlas: E. Cretaceous exhumation
Sebt, (2011)	Anti-Atlas	HeFTy	4	—	—	—	—	4	Anti-Atlas: E. Cretaceous exhumation
Azdimousa et al., (2013)	Rif	HeFTy	2	1	—	—	—	1	time: model start is younger than 20Ma
Leprière et al., (2014)	Reguibat Shield	HeFTy	4	—	—	4	—	—	newer: corrected models in Leprière (2015)
Oukassou et al., (2013)	Anti-Atlas	HeFTy	2	—	—	—	—	2	Anti-Atlas: E. Cretaceous exhumation
El Haimer (2014)	High Atlas	HeFTy	1	—	1	—	—	—	t-T: no best-fit or weighted average
Romagny et al., (2014)	Rif	QTQt	2	1	—	—	—	1	time: model start is younger than 20Ma
Sehrt, (2014)*	Tarfaya/Anti-Atlas/Tindouf	HeFTy	24	—	—	—	4	14	t-T: results from borehole samples; Anti-Atlas: E. Cretaceous exhumation
Girard, Eichenseer, Kabbej, Taoudeni & Idris, (2015)	High Atlas	HeFTy	2	—	—	—	1	—	t-T: results from borehole samples
Domenech, (2015)	High Atlas	QTQt	3	—	—	—	3	—	t-T: modelled for vertical profiles
Leprière, (2015)*	Reguibat Shield/AA	QTQt	14	—	—	—	—	1	Anti-Atlas: E. Cretaceous exhumation
Lafforgue, (2016)	High Atlas	QTQt	4	—	—	—	—	—	—
Gouiza et al., (2017)	Anti-Atlas	HeFTy	6	—	—	—	—	—	—
Charton et al., (2018)	Anti-Atlas	HeFTy	2	—	—	—	—	—	—
Gouiza et al., (2018)	Reguibat Shield	QTQt	1	—	—	—	1	—	t-T: modelled from several LTT ages
Leprière et al., (2018)	High Atlas	QTQt	10	—	—	—	6	—	t-T: modelled for vertical profiles or several samples
Gouiza et al., (2019)	Reguibat Shield	QTQt	1	—	—	—	—	—	—
Lanari et al., (2020)	High Atlas	QTQt	4	1	—	—	3	—	t-T: modelled for vertical profiles; time: model start is younger than 20Ma

Note: Conditions: The t-T modelling results had to (i) start before 20 Ma, (ii) be based on HeFTy, AFT solve or QTQt results and display a favoured curve, as opposed to envelopes only, (iii) be from the most recent realizations, if different models using the same LTT data exist, (iv) be based on single rock sample as opposed to vertical profiles and other combined modelling, or from shallowest sample from borehole data, and (v) be compatible with valid geological constraints as discussed in the text. \* In the case of Sehrt (2014) and Leprière (2015) theses, more recent publications of Leprière et al., 2017 and Sehrt et al., 2017 and 2018 reused the same t-T models and are thus not listed here.

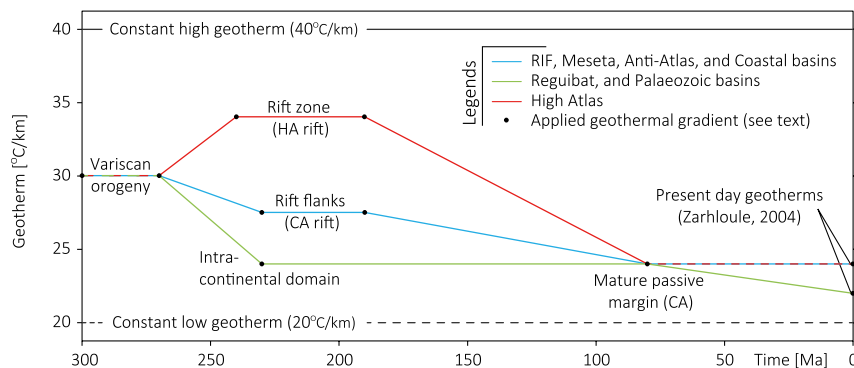


**FIGURE 6** Varying geothermal gradients used for the temperature-to-depth conversion of the t-T curves. Forty and 20°C/km were selected as the constant geothermal gradients used for obtaining ranges in subsequent calculations (Figure 3; step 2); Applied geothermal gradient: Geothermal gradients documented in literature, from present-day or recent settings similar to ones in Moroccan geological past. See description of the geotherms considered as analogues in the text. CA, Central Atlantic; HA, High Atlas

used as a time constraint (e.g. Fetah et al., 1990). The underlying clastics could, hence, be Cenomanian in age, similarly to the sediments in eastern Anti-Atlas.

Overall, this invalidates the use of an Early Cretaceous constraint in time-temperature modelling that was previously used to force basement rock surface temperatures in the Anti-Atlas. Moreover, it is also unclear whether Cretaceous sedimentary cover was continuous over all the Anti-Atlas or not (Malusà et al., 2007). In this work, we have used the above-mentioned new modelling constraints for the Anti-Atlas, and disregard published models using surface temperatures for the Early Cretaceous as a geological constraint (e.g. Oukassou et al., 2013; Ruiz et al., 2011; Sehr, 2014).

### 3.2.3 | Temperature-to-depth conversion

In order to quantify the volume of material that was subsequently eroded above presently exposed rocks and shallowest samples from borehole data, a temperature-to-depth conversion is applied on selected t-T results (Figures 6 and 7). This conversion is often used in t-T model to estimate exhumation rates and was already applied in some of the previous studies considered in this work (e.g. Gouiza et al., 2017). One of the assumptions to apply such a conversion to t-T modelling results is that cooling must be due to exhumation, not thermal relaxation (see Malusà & Fitzgerald, 2019b, for a comprehensive review). Exhumation, as defined in England and Molnar (1990), is a decrease in the distance between a considered rock and the Earth's surface. It does not mean 'uplift', as exhumation may occur by the erosion and denudation of a rock overburden, without involving motion of the rock with respect to the geoid or the undeformed reference lithosphere.

The conclusion reached in nearly all t-T studies, in Morocco and surroundings, is that samples with cooling ages younger than their stratigraphic ages recorded burial and exhumation. When supported by the identification of local or regional detrital sediments of ages similar to the modelled cooling (i.e. the eroded product), it supports the

use of identified cooling events as periods of exhumation. Exceptions were applied to samples that may have exhibited thermal relaxation, such as in the High Atlas (post-rift sampled Jurassic dykes; Barbero et al., 2007), in the Canary Islands (Cenozoic post-volcanism; Wipf et al., 2009) and in the Siroua massif (Cenozoic post-magmatism/volcanism thermal relaxation; Ghorbal, 2009).

The interpretation of heating due to burial requires the presence of truncated sediments of coeval age in the rims of the sampled basement massif, or remnants of formerly emplaced thrust sheets that could have loaded the basement (e.g. Cerrina Feroni et al., 2010), or alternatively the absence of evidence for heating by volcanism/magmatism.

Five conditions were applied to the selection of representative and valid t-T curves, resulting in a total of 68 t-T curves (approximately half of initial dataset were disregarded; detailed in Table 1).

Published modelling results had to:

- (i) start before 20 Ma (approximately the duration of youngest considered period),
- (ii) be based on HeFTy, AFT solve or QTQt results and display a best fit/weighted curve, as opposed to envelopes only,
- (iii) be the most recent realizations, if different models using the same LTT data exist,
- (iv) be based on single rock samples as opposed to vertical profiles and other combined modelling, or from shallowest sample from borehole data, (justified by the fact that we use points for the spatial interpolation) and
- (v) be compatible with geological constraints discussed above.

To achieve the temperature-to-depth conversion (Figure 7), different palaeogeothermal gradients were used based on the location of the selected t-T curves (Figure 6) and keeping surface temperature constant at 20°C. The applied geothermal gradients are based on several studies, including studies of similar geodynamic settings that serve as analogues for Morocco. Luth and Willingshofer (2008; see

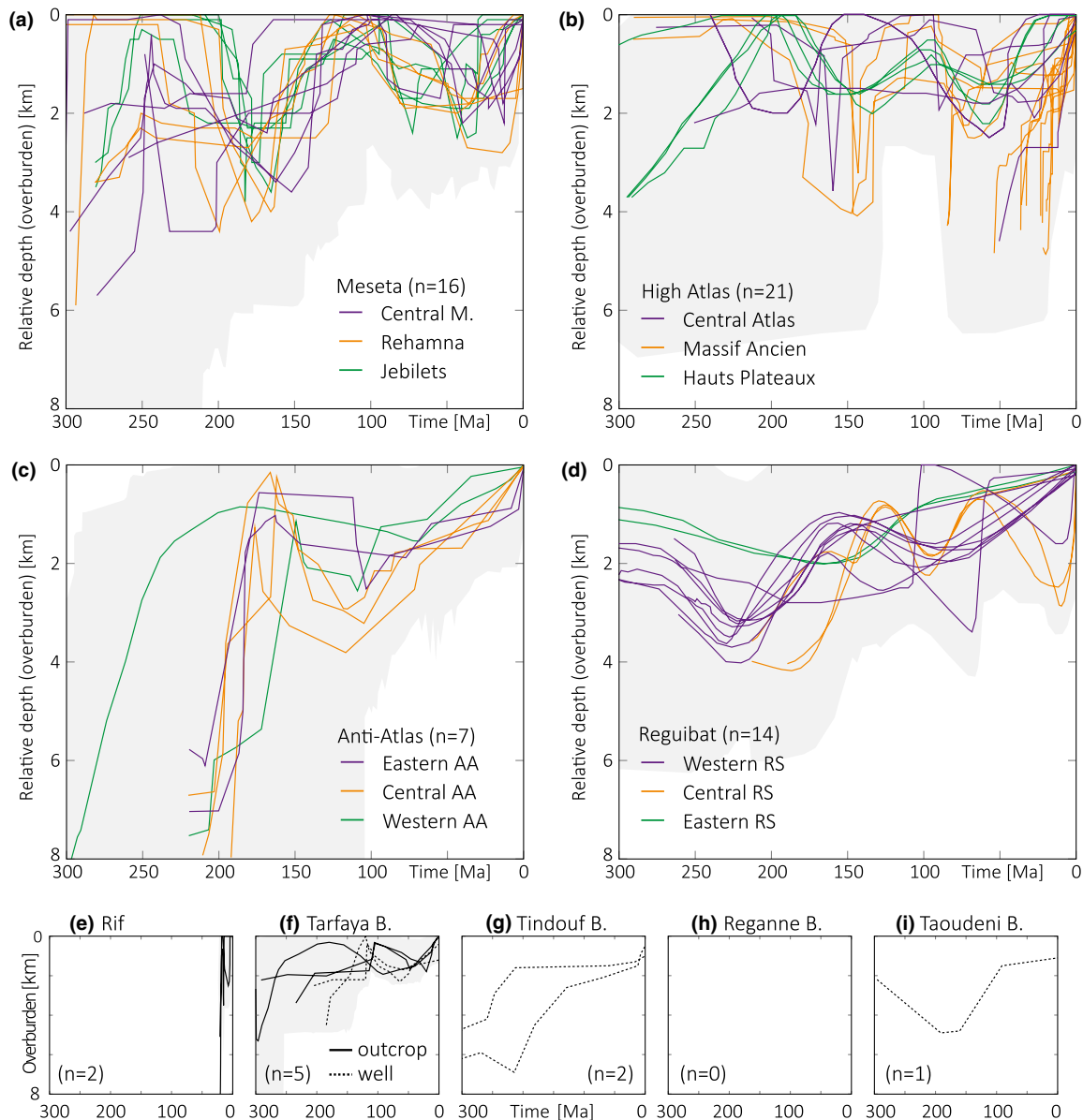


**FIGURE 7** Time-depth curves converted from t-T curves for considered regions (a-i) and shown in Figure 5, assuming geothermal gradients evolving as illustrated in Figure 6 and assuming a surface temperature of 20°C. The thicker lines display vertical movement rate calculations; nonselected thinner curves, in the backgrounds, were also converted into depth but were not used in the later study; conditions for result selection are detailed in Table 1. The upper and lower limits of the t-Depth envelope (thick dashed lines) are calculated with geothermal gradients of 40 and 20°C/km respectively

references therein) obtained geothermal gradients of 23–35°C/km for the Alps. Based on these values, we considered an average geotherm of 29°C/km for the Variscan orogeny. The geothermal gradient in the rift zone of the present-day East African Rift system is ca. 40°C/km (van der Beek et al., 1998) and between 25 and 32°C/km in the Rio Gande Rift (Bridwell, 1976). We applied a geotherm of 34°C/km as representative for the High Atlas Rift zone. The flanks of the East African Rift systems today display geothermal gradients between 25 and 30°C/km (van der Beek et al., 1998) and using this as an analogue, in Morocco 27°C/km was applied for the Central Atlantic/High Atlas rift flanks. For

the post-rift Moroccan passive margin ca. 100 Ma after the continental break-up (mature passive margin) and for the intra-continental domain of the Reguibat Shield, we applied a geotherm of 24°C/km (Zarhloule, 2004). Zarhloule (2004) reports present-day values from Moroccan Passive margin of 20 to 35°C/km and these values were applied to their respective areas. Note that as the selected geotherms are based on distinct geodynamic context, they take into account the thermal relaxation that follows the rift-related heating phase.

Applying a varying palaeogeothermal gradient that is also specific for each area is required to 1) match the changing thermal conditions of the upper crust based on known

geodynamic events (e.g. High Atlas rifting; e.g. Gouiza et al., 2017), and 2) define a preferred model to obtain values of exhumation/burial rates and erosion rates with their associated ranges (Figure 3), as opposed to only ranges using constant geotherms (see following paragraph).

To calculate the range of depth-converted results, two constant palaeogeothermal gradients of 20 and 40°C/km were used, together with both a low case (10°C) and high case (30°C) surface temperature. Both gradients are within the range of present-day values of geothermal gradients in Morocco (Zarhoulou, 2004), and are considered as “end-member” values. The low and high constant geotherms, applied to the digitized temperature envelopes, expectedly yield the maximum and minimum depths throughout the considered period of time respectively (Figure 7). Both sets of low and high constant geotherms and surface temperatures are later used to calculate the range of exhumation/burial rates (Figure 3).

### 3.2.4 | Defined time periods and burial/exhumation rates

Exhumation and burial rates (km/Myr; Figure 8) were calculated from the depth-converted t-T curves (Figure 7). Seven periods of time were defined (periods *a* to *g*), resulting in up to seven exhumation/burial rate calculations for each curve: Permian (*a*; 299–252 Ma), Triassic (*b*; 252–201 Ma), Early to Middle Jurassic (*c*; 201–163 Ma), Late Jurassic to Early Cretaceous (*d*; 163–125 Ma), middle-late Cretaceous (*e*; 125–66 Ma), Palaeogene (*f*; 66–23 Ma) and Neogene (*g*; 23–0 Ma). The selection of time periods is based on the stratigraphy, and as much as possible on the timing of exhumation and burial events as recorded by t-Depth models. The calculated rates range from –0.09 to 0 (burial) and from 0 to 0.49 (exhumation) km/Myr. The rates calculated from t-Depth models are based on the start and end of the above-defined periods. This implies that, for instance, a strong exhumation followed by

burial has a similar overall rate of exhumation in any given time period to an overall milder exhumation and vice versa.

Figure 8 illustrates that there were four periods of active and widespread denudation in the study area: Permian, Early-Middle Jurassic, Late Jurassic-Early Cretaceous and Neogene (periods *a*, *c*, *d* and *g* respectively), in line with results of previous work. During the Permian (period *a*), sampled basement in the Meseta (e.g. Ghorbal et al., 2008) and the Anti-Atlas (e.g. Oukassou et al., 2013) were exhumed up to 0.12 km/Myr, while the Reguibat Shield (e.g. Leprêtre et al., 2015) showed a slower rate of exhumation of ca. –0.01 km/Myr. During the Triassic (period *b*), exhumation in the Meseta and the Anti-Atlas slows down (0.01 to 0.05 km/Myr). The High Atlas and most of the Meseta and Reguibat samples were being buried (down to –0.08 km/Myr). In the Early to Middle Jurassic (period *c*), the basement of the Anti-Atlas (Gouiza et al., 2017) was mildly to strongly exhumed (rate increases up to 0.16 km/Myr). For this region, we observe an acceleration of the exhumation rates from the Triassic to the Jurassic, characterized by the highest rates recorded in this study, with the exception of Neogene exhumation rates. Concomitantly, the regions surrounding the Anti-Atlas were mostly subsiding in the north (down to –0.09 km/Myr) and mildly exhuming in the south (up to 0.06 km/Myr). The Late Jurassic-Early Cretaceous period (*d*) is marked by stability or limited burial of the Anti-Atlas (down to –0.05 km/Myr), whereas the sampled basement of the Meseta (e.g. Saddiqi et al., 2009), the Reguibat shield (e.g. Leprêtre, 2015) and the High Atlas to some extent (e.g. Ghorbal, 2009) were exhuming (0 to 0.09 km/Myr). During the middle-late Cretaceous (period *e*), the Meseta, the High Atlas and the Reguibat Shield regions become stable (weak exhumation and burial) with vertical motion rates relative to Earth's surface between ca. 0.03 and –0.03 km/Myr. Exhumation is renewed along the eastern and western rims of the Anti-Atlas during the Palaeogene (period *f*; 0.01 to 0.03 km/Myr), while other areas remain characterized by low rates, similar to those of

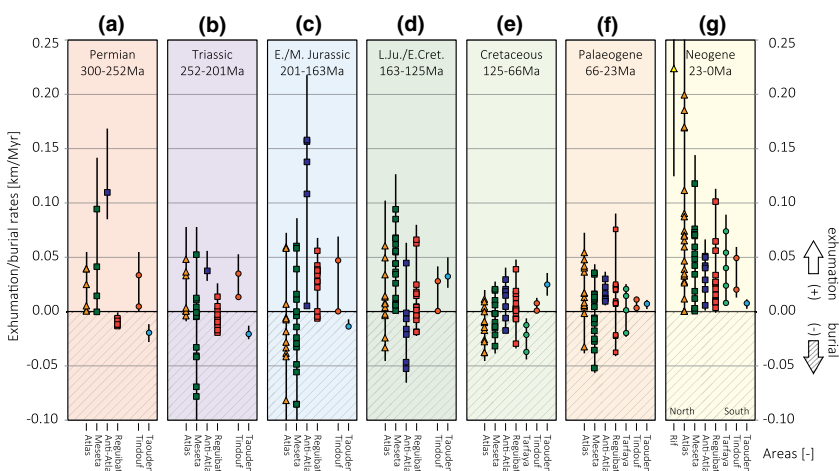


**FIGURE 8** Exhumation and burial rates calculated from the 68 selected depth converted curves of Figure 7 using the variable geotherms shown in Figure 6. The seven defined periods *a* to *g* span between 300 and 0 Ma. The combined ranges are extracted from the results of rate calculations using constant geotherms (Figure 3). North and South are only marked for period *g* because Morocco has been significantly rotated since the Permian (e.g. Scotese, 2012). Note that the x-axis is not time

the middle-late Cretaceous. Finally, the Neogene period (**g**) is characterized by widespread exhumation with a clear orogenic signal; which increased from a typical value below 0.10 and 0.20 km/Myr in the High Atlas, and 0.49 km/Myr in the Rif belt, after conversion of Ghorbal (2009) and Romagny et al., (2014) t-T models, respectively.

### 3.2.5 | Uncertainties and limitations of step 1

In addition to the ranges, other uncertainties need to be recognized to fully understand the limitations of the first step of the workflow. Typically, LTT ages in Morocco have ~10% error for both (U-Th)/He and FT systems (Charton, 2018). The t-T modelling shows a substantial temporal and thermal uncertainty associated with all models (e.g. good and acceptable envelopes for HeFTy) and this uncertainty increases with time (Figure 5).

Furthermore, nearly all t-T modelling studies reviewed in this work (Table 1) consider post-Variscan cooling events as resulting from erosional exhumation. As reviewed in Malusà and Fitzgerald (2019b), cooling does not exclusively mean erosional exhumation, but may be linked to thermal relaxation after a regional heating event or tectonic exhumation (e.g. footwall of a normal fault), depending on the geological context. The interpretation that cooling exclusively records erosional exhumation (assumed by previous workers and in this study) has a direct control on the related t-T path(s) used to obtain exhumation rates. If this assumption is incorrect, results would need to be modified, which would in turn results in different exhumation maps.

In this study, the t-T modelling does not consider the erodibility of the overburden. While it has been documented as having a potentially strong impact on the interpretation of erosion histories (Flowers & Ehlers, 2018) because of the lack of published palaeogeology maps, this study could not consider rock erodibility. This is an area for future refinement of the models.

Palaeogeothermal gradients and the assumption that the surface temperature remains constant will also have an impact on the error range. In this modelling, assumptions made regarding the thermal structure of the crust for each region, the gradients and surface temperature are invariable. However, surface temperature will vary temporally, locally and regionally, while the geotherms may be influenced locally by independent parameters (e.g. crustal heat production, volcanism, large salt province; e.g. Mareschal & Jaupart, 2004). Another assumption has been that palaeogeotherms are not dynamically modified as a function of erosion and deposition, although it is known that both processes can impact the upper crust thermal structure. Erosion may lead to an increase in the palaeogeotherm while sedimentation may lead to its decrease (Ehlers, 2005; Gouiza et al., 2017).

The use of different analogues for geothermal gradients may also have an impact on the workflow. For instance, in the

Mediterranean Sea, a palaeogeothermal gradient of  $>80^{\circ}\text{C}/\text{km}$  was constrained based on t-T modelling for the rift zone of the Tethysian rifting (Malusà et al., 2016). Thus, the applied value of  $34^{\circ}\text{C}/\text{km}$  during rifting in this work might be seen as low. However, assessing the sensitivity of this study, we estimate that using such high gradient in the syn-rift would not affect greatly the obtained exhumation/burial rates, as considered t-T realizations for the rifting period in the High Atlas show a flat path fairly close to surface temperature (Figure 5b). However, using gradients higher than the  $40^{\circ}\text{C}/\text{km}$  (used in range calculation, in the rift flanks during the Triassic, for example) would result in significantly lower exhumation rates.

## 3.3 | Step 2: From exhumation/burial rates to exhumation maps

### 3.3.1 | Inputs for interpolation of exhumation/burial rates

In order to estimate the volume of material that has been removed through time in the exhumed areas, seven 'exhumation maps' (Figure 3) have been constructed, using the calculated exhumation rates recorded by t-T modelling and regional stratigraphy (Figures 9, 10, and 11). This step qualitatively considers burial rates and the onshore and offshore basins published stratigraphic columns (Figure 9) to define areas undergoing burial.

The dataset, composed of exhumation/burial rates, is characterized by dense-data (basement massifs in Meseta/Anti-Atlas) and sparse-data areas (e.g. Reguibat Shield). Areas of burial were included to add geological meaning to the exhumation maps (Figure 9). For each preserved sedimentary basin, one or several points were created depending on the extent of the area, and positioned either in the centre of small basins (e.g. Souss Basin) or at the edges of larger basins (e.g. Tindouf Basin). If sediments were deposited during one of the selected periods and are still preserved in a basin, we attribute a negative rate to all the synthetic points of this basin. When sediments are not recorded in a basin because they were not deposited or not preserved, we attribute to synthetic points a rate of 0 km/Myr.

Synthetic points away from the present-day coastline, to account for subsidence in the rifted margin, have been added along the Continental-Ocean Boundary (COB; Miles et al., 2012). Prior to the Jurassic, there was no oceanic crust, and therefore no COB was present. Nevertheless, for the Permian and Triassic interpolations (periods **a** and **b**), we consider the same COB location in order to add synthetic rates in the Variscan chain and Central Atlantic rift zone respectively.

For the Permian only, points along the COB line are attributed exhumation rates of 0.1 km/Myr. This is to account for the tectonic collapse and associated denudation of the

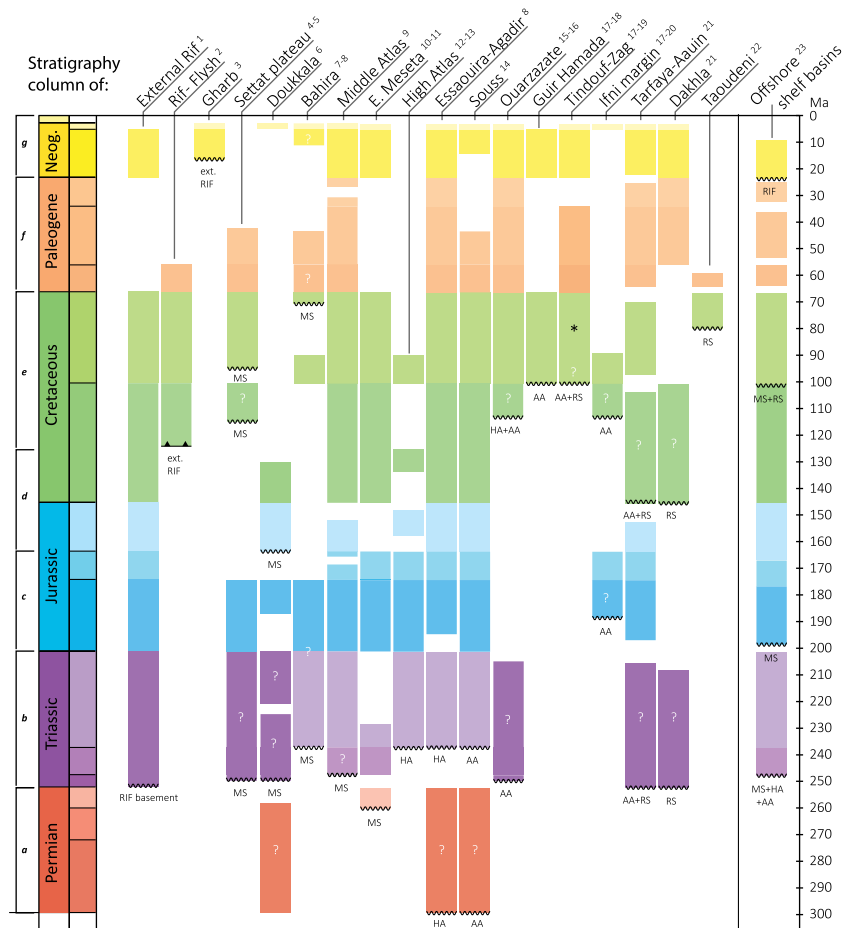


**FIGURE 9** Compilation of simplified stratigraphic columns. The name of the corresponding Variscan/Precambrian basement is shown below the unconformity surfaces (MS: Meseta, HA: High Atlas, AA: Anti-Atlas and RS: Reguibat shield basements). The seven selected periods (a to g) are shown on the left. \*Late Cretaceous in the Tindouf basin is present in the eastern and western parts, but not in its central part (Hollard et al., 1985). <sup>1</sup>Frizon de Lamotte et al. (2004); <sup>2</sup>Groune et al. (2013); <sup>3</sup>Michard et al. (2008); <sup>4</sup>TAN-101 well report; <sup>5</sup>Boleli (1952); <sup>6</sup>Echarfaoui et al. (2002); <sup>7</sup>Karroum et al. (2014); <sup>8</sup>Hafid et al. (2006); <sup>9</sup>Michard et al. (2008) after A. Charrière, unpubl.; <sup>10</sup>Manspeizer et al. (1978); <sup>11</sup>Gomez et al. (2000); <sup>12</sup>Haddoumi et al. (2010); <sup>13</sup>Michard et al. (2011); <sup>14</sup>Samaka and Bouhaddioui (2003); <sup>15</sup>El Harfi et al. (2001); <sup>16</sup>Fiechtner et al. (1992); <sup>17</sup>Hollard et al., (1985); <sup>18</sup>Benyoucef et al. (2015); <sup>19</sup>Zouhri et al. (2008); <sup>20</sup>Arantegui et al. (2019); <sup>21</sup>Ranke et al. (1982); <sup>22</sup>Hill et al. (2008); <sup>23</sup>Tari and Jabour (2013)

Variscan chain, which is documented in Morocco as occurring somewhere between the Carboniferous and the Triassic (e.g. Michard et al., 2008). Similar exhumation rates during post-orogenic collapse have been used in other published models and documented between 0.15 and 0.7 km/Myr (e.g. Casini et al., 2015; Clift et al., 2004; Mazzoli et al., 2010). In this study, we applied a lower exhumation rate of 0.1 km/Myr, comparable to the highest rate we calculated for the Permian (period *a*).

From the Triassic onwards (periods *b* to *g*), we attributed a burial rate to the COB of  $-0.01$  km/Myr (smaller than the colour bar limit for stable domain, defined between  $-0.005$  and  $0.005$  km/Myr). This is equivalent to adding a number of synthetic points with burial rates in the slope and/or basal domains. These values are not necessarily realistic, but are acceptable as volumes in the buried domain are not the focus of this study.

### 3.3.2 | Interpolation method

For the interpolation of the exhumation/burial rates, an Inverse Distance Weighting (IDW) algorithm was used. This algorithm does not extrapolate the rates above and below input values and functions with an interpolation grid that allows for the addition of active faults. The interpolation grid extends between 0 to  $-18^{\circ}$ W and 20 to  $36^{\circ}$ N (with a  $10 \times 10$  km spacing) and ends at the COB in the west. For the Triassic, Palaeogene and Neogene periods (*b*, *f* and *g* respectively), the Atlas fault system is defined according to Frizon de Lamotte et al. (2004). Here, we assume that exhumation rates change following a normal distribution between data points (Figure 3; step 2.2) and the interpolation method (IDW) calculates each cell value using a linearly weighted combination of surrounding input points (unless interrupted by faults).

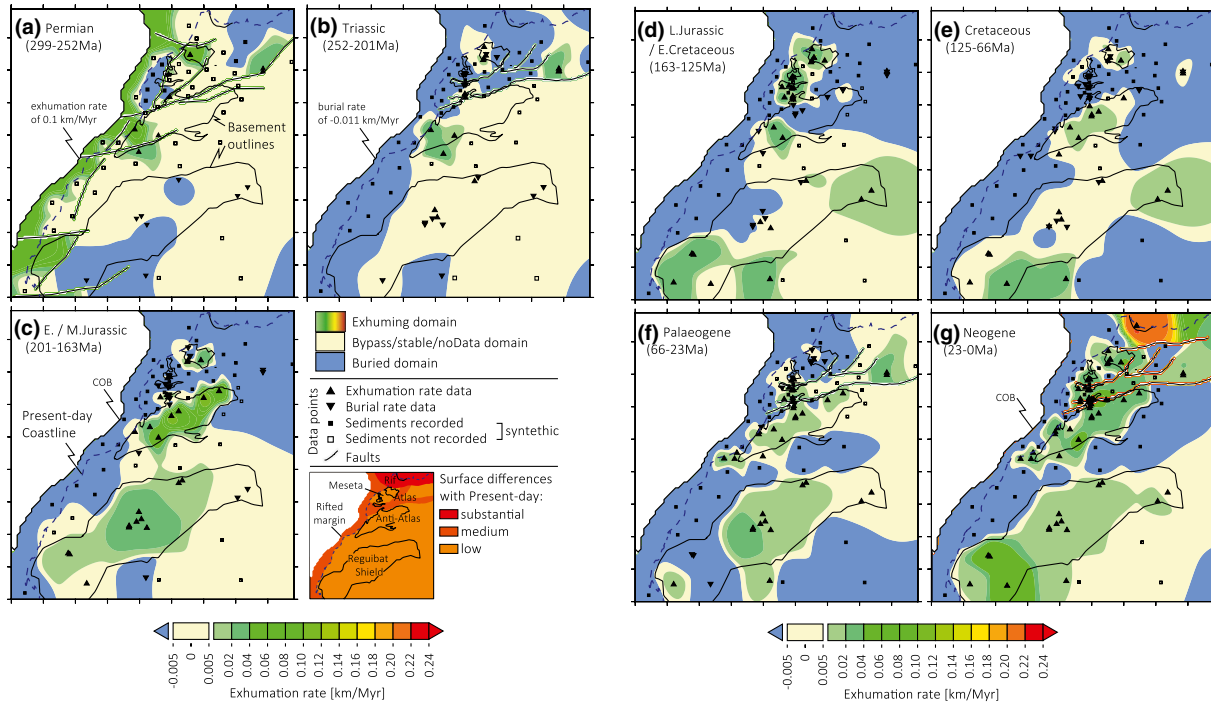


**FIGURE 10** Exhumation maps for the seven selected periods (a-c on this page and d-g on the next one) after stratigraphic column compilation (Figure 9) and exhumation/burial rates (Figure 8). Three domains are defined on the exhumation maps: a subsiding domain with rates  $\leq -0.011$  km/Myr, a stable domain characterized by rates between  $-0.01$  and  $0.01$ , and an exhuming domain with rates  $\geq 0.011$  km/Myr. Note that the western boundary is the Continent-Ocean Boundary (COB). The insert grades differences in areas, between the Permian and the Present-Day, and is based on the geological history of Morocco (Michard et al., 2008)

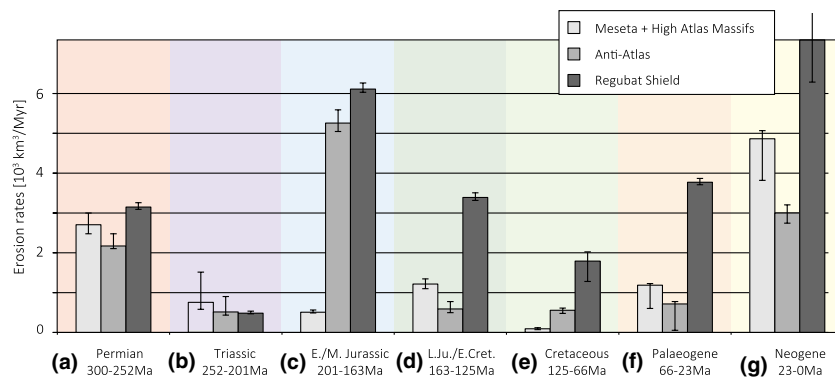


**FIGURE 11** Estimated erosion rates for the three main sediment sources (Meseta/High Atlas, Anti-Atlas and Reguibat Shield) for the seven defined periods (a-g). The erosion rates are obtained with the varying geotherms. The ranges are given by calculations done with two constant geotherms of 20 and 40°C/km in the supplementary file 2

The descriptions of the exhumation maps are presented alongside the source-to-sink maps (section 4).

### 3.3.3 | Erosion rates

Volume calculations of eroded material, hereafter, called “erosion rates”, are performed using the Surfer software between the interpolated surface and the plane of null denudation rate (0 km/Myr). Volumes are separately calculated

for the following areas (based on polygons of the present-day extent of the basement exposure): Meseta, High Atlas, Anti-Atlas and Reguibat Shield (Figure 11; Table 2). The erosion rates are an estimation of the volume of removed material, per million years, during the seven considered erosion periods (see similar approaches in other areas: Guillocheau et al., 2012; Grimaud et al., 2018; expressed in km<sup>3</sup>/Myr). They are the calculated upper limit for the total detrital sediment flux, which is especially important for carbonate successions possibly undergoing dissolution and in the case



**TABLE 2** Erosion rates and surface areas from Permian (a) to Neogene (g)

	Periods (duration) [–]						
	a (45 Myr)	b (51 Myr)	c (38 Myr)	d (38 Myr)	e (59 Myr)	f (43 Myr)	g (23 Myr)
Erosion rates [ $10^3 \text{ km}^3/\text{Myr}$ ]							
Entire interpolation grid	25.0	2.6	13.1	9.2	6.1	7.1	33.6
Meseta & High Atlas	2.8	0.8	0.5	1.3	0.2	1.2	4.8
Anti-Atlas	2.2	0.6	5.2	0.6	0.6	0.7	3.0
Reguibat Shield	3.2	0.6	6.1	3.3	1.8	3.8	7.5
Surface area [ $10^6 \text{ km}^2$ ]							
Exhumation/No Data	1.1	0.4	0.9	1.2	0.6	1.0	1.4
Subsidence/Burial	1.3	2.0	1.5	1.2	1.7	1.4	1.0

of bypassing the shelf and slope to more distal sinks. The minimum and maximum values (Figure 11) are obtained by running the same interpolation and subsequent volume calculation using exhumation rates calculated with the high and low constant geothermal gradients.

The calculated erosion rates for the seven exhumation maps range from c.  $3 \times 10^3$  to  $34 \times 10^3 \text{ km}^3/\text{Myr}$  for the Triassic and Neogene respectively (Figure 11; Table 2). For regions of specific interest, these rates are between ca. 600 and  $7,500 \text{ km}^3/\text{Myr}$  for the Reguibat Shield, ca. 600 and  $5,200 \text{ km}^3/\text{Myr}$  for the Anti-Atlas and ca. 200 and  $4,800 \text{ km}^3/\text{Myr}$  for the Meseta and High Atlas massifs (Figure 11).

### 3.3.4 | Uncertainties and limitations of step 2

The nonrestored base maps used for the exhumation maps contain an element of uncertainty, as some areas may have changed in shape and/or surface (the High Atlas rift before the Cenozoic shortening for instance). The use of null exhumation/burial rates for synthetic points where no stratigraphy is recorded also introduces a potential error, as the lack of sediments may be linked to either deposition/erosion (i.e. burial rates should have been used during the assumed time of deposition) or nondeposition (i.e. null exhumation rates). A final uncertainty is the use of published stratigraphy columns as reference, which may be incomplete and/or incorrect.

Potential errors associated with the interpolation algorithm and volume calculations are difficult to quantify. Such errors include the choice of interpolation algorithm and selected parameters, mathematical approximations, using all types of fault in a similar fashion, and the placement of the synthetic points for the stratigraphic columns.

In conclusion, it has not proved possible to estimate an error for the calculated erosion rates in this workflow, only

ranges using arbitrary high and low geothermal gradients may be presented at this stage.

## 3.4 | Step 3: From exhumation maps to Source-and-Sink maps

### 3.4.1 | Source-to-sink maps: principle and inputs

The availability of robust sedimentary, stratigraphic, geochronological and provenance studies, and LTT and numerical (e.g. Landscape Evolution Modelling) analyses allows integration to improve source-to-sink models (e.g. Bhattacharya et al., 2016; Helland-Hansen et al., 2016). Source-to-sink studies have limitations, depending on the spatial and temporal resolutions of each data, or simply on the existence and quality of the sedimentary record. Because the nature of data used in this contribution does not constrain or depend on the transport of sediments ('to'), the presented maps are not labelled as 'Source-to-Sink' but instead as Source-and-Sink (SandS) maps.

A recent effort at generating palaeogeography maps by combining AFT data with more classical datasets has been carried out in southern NW Africa (Ye et al., 2017), at the sub-continental scale. The work resulted in several palaeoreconstructions around the equatorial Atlantic African margin since the early Mesozoic. This work allowed the inclusion of exhuming areas, as based on LTT and t-T results, onto what can also be described as qualitative SandS maps. Overall, Ye et al. (2017) and our contribution are similar in terms of deliverables, and therefore our maps are, by design, greatly inspired from the former.

As the initial control of the SandS maps, the geological map of Morocco at 1:1,000,000 (Hollard et al., 1985) was digitized, or for neighbouring regions, the UNESCO geological map of NW Africa compiled in 1990 (Figure 2a). This

**TABLE 3** References used in the third step of this work to construct the SandS maps

SandS map	Outcrop data	Fossil data
Permian (Figure 13)	Wrtiti et al., (1990)   Central Massif Chalouan et al., (2008)   Rif basin	Doubinger, (1956)   Central Massif Broutin et al., (1989)   Argana valley
Triassic (Figure 14)	Brown, (1980)   Argana valley Chalouan et al., (2008)   Rif basin Oujidi and Elmi, (2000)   Hauts Plateaux	Chalouan et al., (2008)   Rif basin Kammerer et al., (2011)   Argana valley Lagnaoui et al., (2016)   Argana valley
Early Jurassic (Figure 15)	Steiner et al., (1998)   Canary Islands Sanders et al., (2015)   Rif basin Merino-Tomé et al., (2017)   Eastern High Atlas	Jenny and Jossen, (1982)   Central High Atlas Lee, (1983)   Central High Atlas Beauvais, (1986)   Eastern High Atlas Bourillot et al., (2008)   Central High Atlas
Middle Jurassic (Figure 16)	Oujhain et al., (2011)   Essaouira-Agadir basin Charrière and Haddoumi, (2016)   Central High Atlas Merino-Tomé et al., (2017)   Central High Atlas Benvenuti et al., (2017)   Ouarzazate basin	Monbaron and Taquet, (1981)   Central High Atlas Mahammed et al., (2005)   Eastern High Atlas Haddoumi et al., (2015)   Central High Atlas Oukassou et al., (2016)   Middle Atlas
Late Jurassic (Figure 17)	Fabre et al., (1996)   Taoudeni Steiner et al., (1998)   Canary Islands Mekahli et al. (2004)   Eastern High Atlas Oujhain et al., (2011)   Essaouira-Agadir basin Charrière and Haddoumi, (2016)   Central High Atlas Benvenuti et al., (2017)   Ouarzazate basin	Ourribane et al., (2000)   Essaouira-Agadir basin Nouri et al., (2011)   Central High Atlas Hssaida et al., (2014)   Rif basin
(early) Early Cretaceous (Figure 18)	Fabre et al., (1996)   Taoudeni basin Steiner et al., (1998)   Canary Islands Ali et al., (2014)   Tarfaya basin Charrière and Haddoumi, (2016)   Central High Atlas Benzaggagh, (2016)   Rif basin	Monbaron, (1978)   Middle Atlas Middlemiss, (1980)   Essaouira-Agadir basin Benest, (1985)   Rif basin Ettachfini et al., (1998)   Doukkala basin
Middle Cretaceous (Figure 19)	Choubert et al., (1966)   Tindouf basin Fabre et al., (1996)   Taoudeni basin Steiner et al., (1998)   Canary Islands Aquit et al., (2013)   Tarfaya basin Benyoucef et al., (2015)   Guir Hamada	Dhondt et al., (1999)   Tarfaya basin Aït Boughrouss et al., (2007)   Guir Hamada Cavin et al., (2010)   Kem Kem beds Ibrahim et al., (2014)   Kem Kem beds Benzaggagh et al., (2017)   Rif basin
(mid-late) Late Cretaceous (Figure 20)	Choubert et al., (1966)   Tindouf basin Fabre et al., (1996)   Taoudeni basin Chalouan et al., (2008)   Rif basin  Aquit et al., (2013)   Tarfaya basin Arab et al., (2015)   Rif basin	Andreu and Tronchetti, (1994)   Middle Atlas Dhondt et al., (1999)   Tarfaya basin Ambroggi and Lapparent, (1954)   Essaouira-Agadir basin Mulder et al., (2000)   Essaouira-Agadir basin Rage and Wouters, (1979)   Settât basin Hill et al., (2008)   Taoudeni basin
Palaeogene (Figure 21)	Trappe, (1991)   Ouarzazate basin Chalouan et al., (2008)   Rif basin	Tabuce et al., (2005)   Ouarzazate basin Jouve et al., (2005)   Settât basin Gaffney et al., (2006)   Rif basin Adaci et al., (2007)   Kem Kem beds Hill et al., (2008)   Taoudeni basin Zouhri et al., (2014)   Dakhla basin Gingerich and Zouhri, (2015)   Tarfaya basin Marivaux et al., (2017)   Dakhla basin

(Continues)

TABLE 3 (Continued)

SandS map	Outcrop data	Fossil data
Neogene (Figure 22)	-	Darteville & Schwetz (1937)   Canary Islands Ennouchi, (1954)   Rif Chevalier & Choubert, (1962)   Safi basin Koeniguer, (1967)   Dakhla Rage, (1976)   Middle Atlas Best & Boekschoten, 1981   Porto Santo Saint-Martin (1990)   Rif Blain et al. (2013)   Hauts Plateaux
<b>SandS Map</b> Permian (Figure 13)	<b>Palaeo-reconstruction*</b> Broutin et al., (1998)   Meseta Ellouz et al., (2003)   Atlas Systems Chopin et al., (2014)   Atlas Systems Najih et al., (2019)   N Morocco	<b>Provenance study</b> Perez et al., (2019)   High Atlas
Triassic (Figure 14)	Ranke et al., (1982)   Tarfaya basin Roy et al., (1997)   Atlantic Shelf Ait Brahim et al. (2002)   Atlas Systems Leleu et al., (2016)   Morocco Benvenuti et al., (2017)   Massif Ancien	Baudon et al., (2009)   Massif Ancien Domènech et al., (2018)   Massif Ancien Perez et al., (2019)   High Atlas
Early Jurassic (Figure 15)	Laville and Piqué, (1992)   Atlantic Ellouz et al., (2003)   Atlas Systems Serge et al., (2009)   Rif basin Sibuet et al., (2012)   Atlantic	Domenech et al., (2018)   Western High Atlas Krencker et al., 2020   Central High Atlas
Middle Jurassic (Figure 16)	Ellouz et al., (2003)   Atlas Systems Guiraud et al., (2005)   Morocco Nemčok et al., (2005)   Morocco Frizon de Lamotte et al., (2011)   Tethys	Stets, (1992)   Massif Ancien Pratt et al., (2015)   Middle Atlas
Late Jurassic (Figure 17)	Ranke et al., (1982)   Tarfaya basin Ellouz et al., (2003)   Atlas Systems Nemčok et al., (2005)   Morocco Sibuet et al., (2012)   Atlantic Leprêtre et al., (2018)   Rif-Tethys	Stets, (1992)   Rehamna
(early) Early Cretaceous (Figure 18)	Sibuet et al., (2012)   Atlantic Aloui et al., (2012)   Algeria Ye et al., (2017)   Reguibat Shield Luber (2017)   Essaouira-Agadir basin Gimeno-Vives et al., (2019)   Rif basin	Ali et al., (2014)   Tarfaya basin Leprêtre, (2015)   Reguibat Shield Pratt et al., (2015)   Rif basin Luber, (2017)   Essaouira-Agadir basin
Middle Cretaceous (Figure 19)	Guiraud et al., (2005)   Morocco Ye et al., (2017)   Reguibat Shield	Ali et al., (2014)   Tarfaya basin Pratt et al., (2015)   Rif basin Essafroui et al., (2015)   Massif Ancien Meister et al., (2016)   Kem Kem beds Mourlot et al., (2018)   DSDP wells Azdimousa et al., (2019)   Rif

(Continues)

**TABLE 3** (Continued)

SandS map	Palaeo-reconstruction*	Provenance study
(mid-late) Late Cretaceous (Figure 20)	Ranke et al., (1982)   Tarfaya basin Fabre et al., (1996)   Taoudeni basin Ait Brahim et al., (2002)   Atlas Systems Sibuet et al., (2012)   Atlantic van de Bogaard, (2013)   Canary Islands Ye et al., (2017)   Reguibat Shield	Ali et al., (2014)   Tarfaya basin Mourlot et al., (2018)   DSDP wells
Palaeogene (Figure 21)	Ranke et al., (1982)   Tarfaya basin Herbig and Trappe, (1994)   Meseta Ait Brahim et al., (2002)   Atlas Systems Guiraud et al., (2005)   Morocco van de Bogaard, (2013)   Canary Islands Leprêtre et al. (2018)   Rif system	Azdimoussa et al., (2019)   Rif
Neogene (Figure 22)	Ranke et al., (1982)   Tarfaya basin Leprêtre et al. (2018)   Rif system	Ali et al., (2014)   Tarfaya basin Azdimoussa et al., (2019)   Rif

\*Including palaeogeography, depositional environment and stress/structural maps.

generally provided surface geology control points, with the exception of the Permian, for which there are few outcrops. Additional outcrop and fossil data were incorporated from studies (Table 3).

Several “modifications” to the stratigraphy were added to our composite geological map (Figure 2a) based on new fieldwork or new published data, especially around the Anti-Atlas (see details part 3.2.2) and in the Central High-Atlas. In the latter, the so-called “Couches Rouge” terrestrial redbeds that have historically (and on the 1:1,000,000 map) been attributed a Middle and Late Jurassic age (Hollard et al., 1985) are re-dated to the Middle and Late Jurassic and middle Cretaceous (Barremian to Aptian) (Charrière & Haddoumi, 2016).

The well database (Figure 12) is composed of DSDP and IODP well reports, confidential oil exploration well reports and completion logs accessed from the “Office National des Hydrocarbures et des Mines” (ONHYM). Detailed well data from published work (notably Michard et al., 2008), and limited well data such as total depth (TD), formation at TD or stratigraphy from published studies or company reports were also used.

Large-scale reviews of the Moroccan geological history have been carried out in several studies (e.g. Le Roy et al., 1997; Nemčok et al., 2005; Ranke et al., 1982; Sibuet et al., 2012; Ye et al., 2017) and the results have been collated and integrated into our SandS maps. Several types of palaeo-reconstructions are used as the basis for depositional environments (sub-continental scale, e.g. Ye et al., 2017; to sub-basin scale, e.g. Lubert, 2017) and also for the interpretation of tectonic regime (e.g. Ait Brahim et al., 2002). Depositional

environment reconstructions for the Phanerozoic at the scale of North Africa from Guiraud et al. (2005) were used to broadly constrain all SandS maps. Palaeogeography maps of C.R. Scotese (Paleomap project, 2013) are shown in the inserts below each SandS maps, but were not used in the reconstructions.

Sediment provenance analysis conducted in Morocco and surroundings are scarce. Five recent works investigated the provenance with detrital zircon U-Pb (Azdimoussa et al., 2019; Domènech et al., 2018; Marzoli et al., 2017; Pratt et al., 2015; Perez et al., 2019); one study used traced elements and radiogenic Nd-Sr isotopes (Ali et al., 2014), one using neodymium isotopes and major/trace elements from DSDP wells (Mourlot et al., 2018), and one produced detrital LTT ages (Sehrt, 2014). Several studies have also documented palaeocurrent directions in fluvial systems (e.g. Baudon et al., 2009; Brown, 1980; Fabuel-Perez et al., 2009; Mader et al., 2017). Provenance and palaeocurrent data are used to constrain “source-to-sink” arrows on the presented maps.

Finally, we use the exhumation maps presented in step 2 to constrain the source domains (areas undergoing denudation), while modifying their contours based on the control points described above. The SandS maps illustrate the source, transitional and sink domains from the Permian to Neogene, within a simplified structural framework.

### 3.4.2 | Building the Source-and-Sink maps

The SandS maps are defined according to the International Chronostratigraphic Chart (IUGS, 2020): Permian (300 to

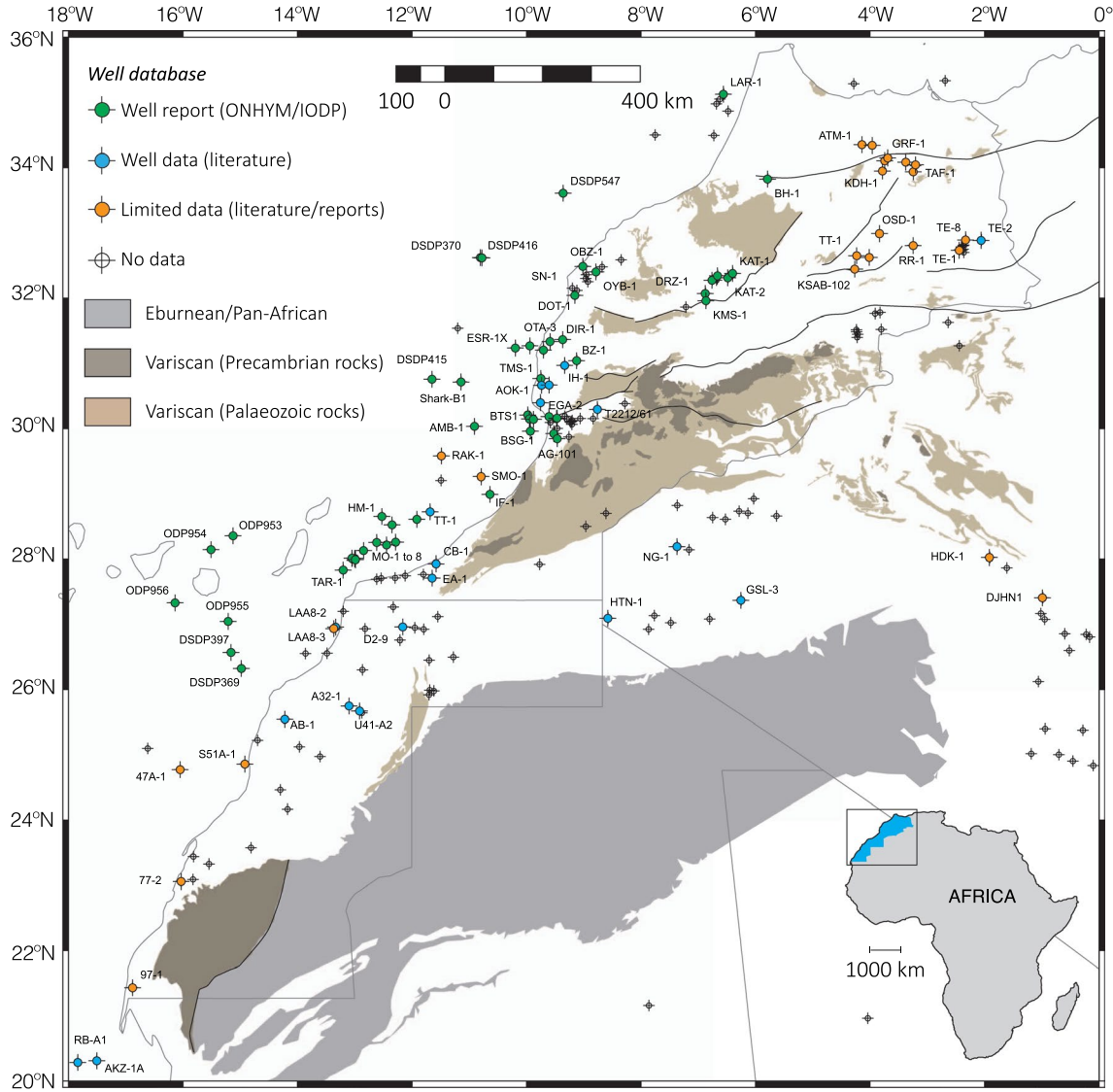


**FIGURE 12** Location of boreholes in Morocco and surrounding NW African countries (non exhaustive). Color-coded wells were used in the construction of the SandS maps

252 Ma; corresponding to period *a* from step 2; Figure 13), Triassic (252 to 201 Ma; period *b*; Figure 14), Early Jurassic (201 to 174 Ma; period *c*; Figure 15), Middle Jurassic (174 to 163 Ma; period *c*; Figure 16), Late Jurassic (163 to 145 Ma; period *d*; Figure 17), (early) Early Cretaceous (145 to 125 Ma; period *d*; Figure 18), middle Cretaceous (125 to 90 Ma; period *e*; Figure 19), (mid-late) Late Cretaceous (90 to 66 Ma; period *e*; Figure 20), Palaeogene (66 to 23 Ma; Figure 21) and Neogene (23 to 0 Ma; Figure 22). Exhumation maps from step 2 for periods *c*, *d* and *e* have therefore been used for two SandS maps each.

Four types of depositional environments are described in this study: terrestrial, transitional, shallow marine and marine. For most of the map control points, the depositional environments were already interpreted (Table 3). In

other instances, we interpreted the depositional environment based on lithology and/or fossil data. The ‘‘transitional’’ environment primarily suggests a coastal situation, but may account for areas characterized by fluctuation(s) between shallow marine and terrestrial environments. Source areas with low exhumation rates (between 0 and 0.01 km/Myr) may momentarily act as sedimentary bypass zones, as exemplified onshore in the Neogene map (Figure 21). Conversely, ‘‘terrestrial’’ domains may have contained source areas.

The construction of each map was completed by superimposing all the above-mentioned input layers. Source areas and faults were placed first, then data pertaining to the sink domains. Each feature (outcrop, well, fossil...) was then manually associated with a small coloured halo corresponding to the dominant depositional environment. The extent

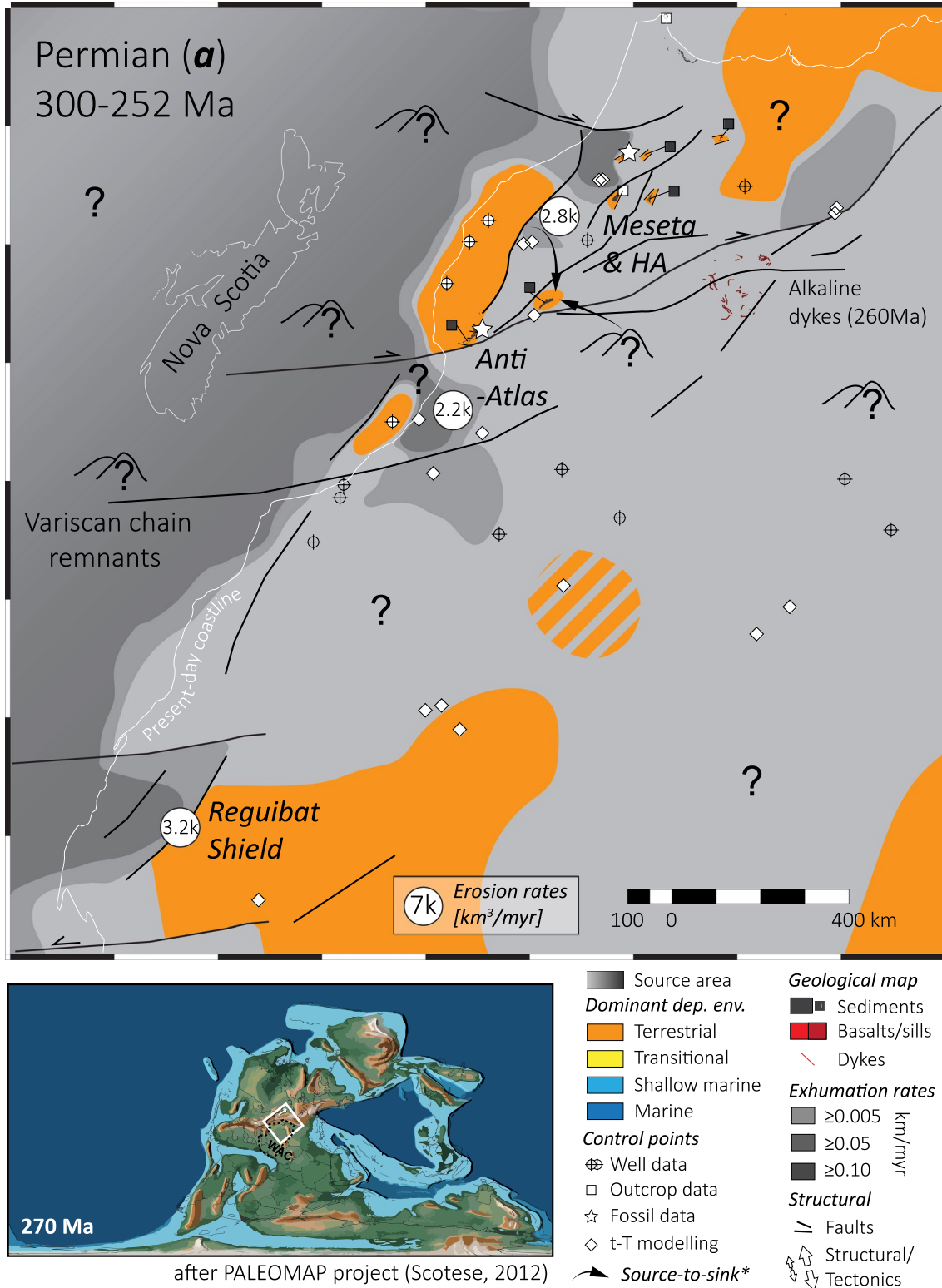


**FIGURE 13** Permian map (period *a* as defined in the part of this work). *General caption for all Source-and-Sink maps:* See list of references used to build this map, and the following ones, in Table 3. Dominant dep. env.: Dominant depositional environment. Source-to-sink\*: Simplified source-to-sink systems evidenced with provenance study or palaeocurrents. Structural/tectonics: directional result of compression/extension and shortening/stretching in local and regional studies respectively. Well data: full (white) points mean that sediments of that age were preserved; empty (transparent) points illustrate that sediments were not deposited or not preserved. WAC: Western African Craton. Hatched grey lines highlight modification made to the interpolation results from step 2. Black squares are highlighting sediments from the surficial geology layer if isolated and barely visible at their original scale

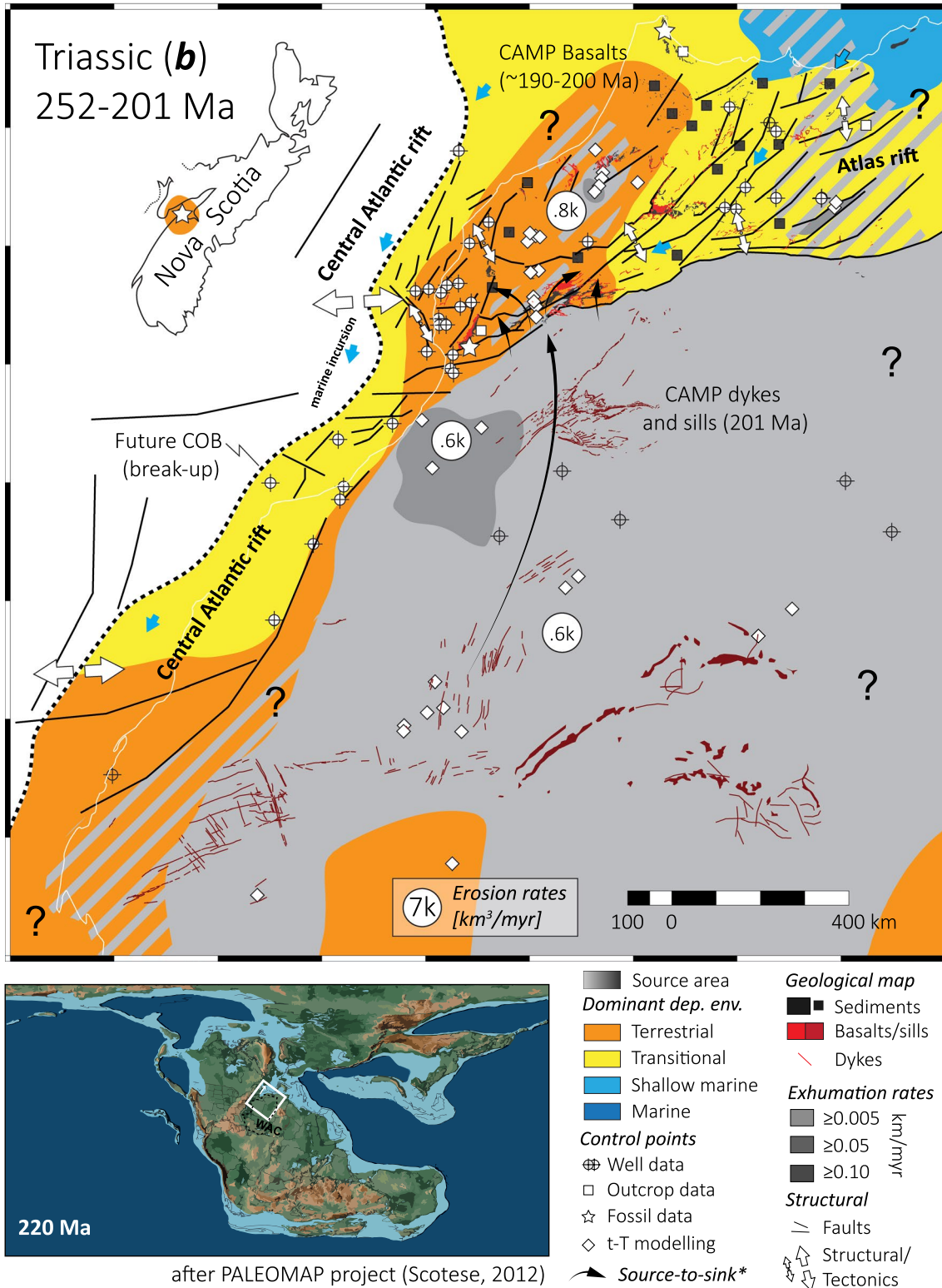


**FIGURE 14** Triassic map (period *b*). Illustrated dykes and basalts are from the Central Atlantic Magmatic Province (CAMP). See caption of Figure 13 for additional information

of the source areas was modified at this stage, modification highlighted by the grey hatched lines and finally the map completed by connecting depositional environments together. A descriptions of each SandS map and observed patterns are presented in Section 4.

### 3.4.3 | Limitations of the source-and-sink maps

Data quality, data density and temporal resolution are highly variable across the area covered by the SandS maps. This leads

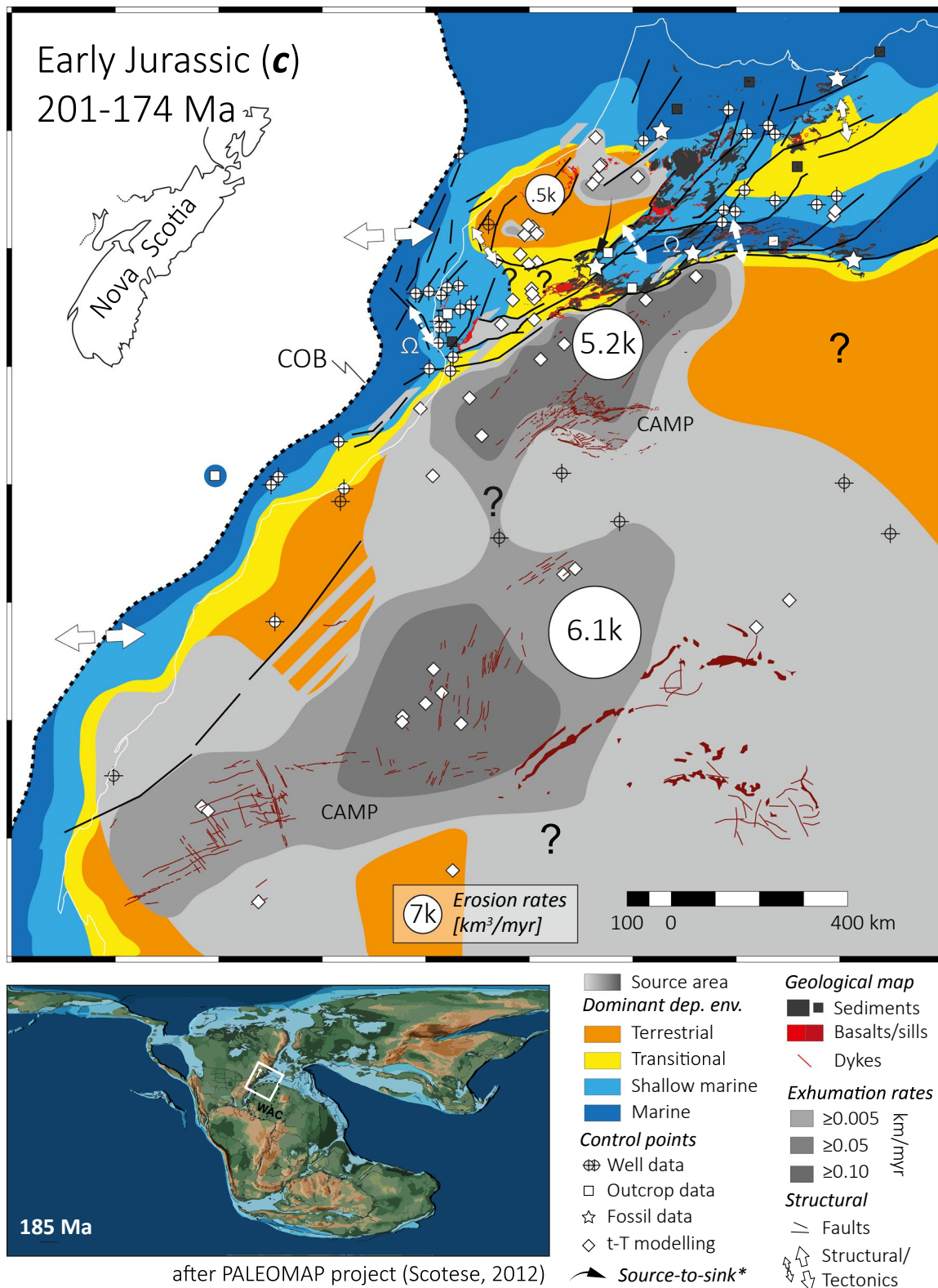


**FIGURE 15** Early Jurassic map (period c). CAMP: Central Atlantic Magmatic Province. See caption of Figure 13 for additional information. Ω: Triassic salt mobilization (after Moragas et al., 2018)

to variable robustness of the presented maps, which complicates the comparisons from one to another. Stratigraphic age is the primary uncertainty, as several Phanerozoic layers in Morocco and the surrounding areas have undifferentiated

ages (e.g. Hollard et al., 1985). These intervals may contain some dated marine sequences or magmatic intrusions, but these are generally local and extrapolation still has to be made to similar but nonconstrained facies.



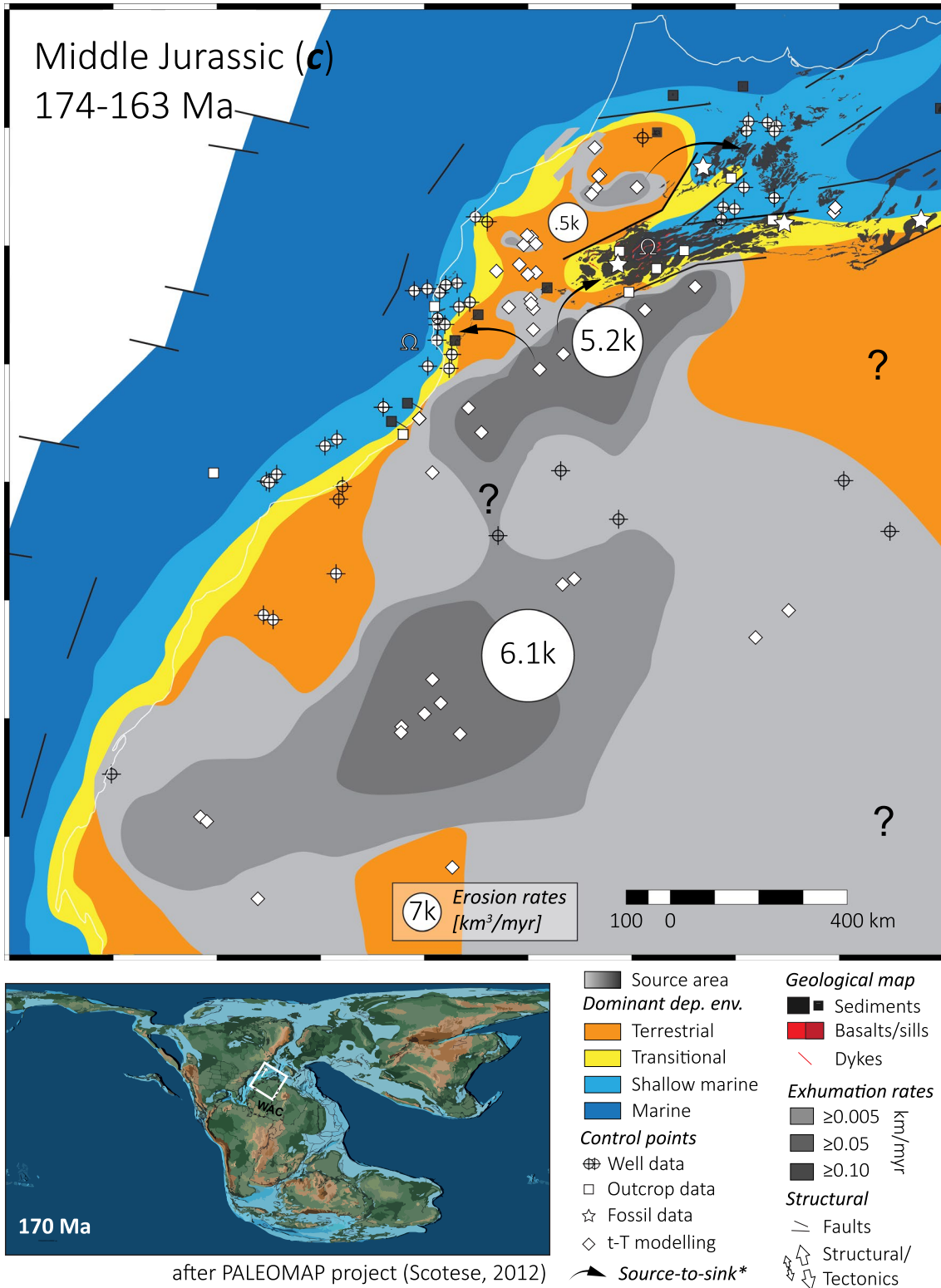


**FIGURE 16** Middle Jurassic map (period c). See caption of Figure 13 for additional information. Ω: Triassic salt mobilization (after Moragas et al., 2018)

The Permian map is characterized by having the most uncertain dominant depositional environments, as it is constrained with very limited data, while the Neogene is a data-rich time interval and the corresponding map is of higher resolution.

A variable aspect is the time-window duration that each map covers. The temporal resolution of the Permian and Triassic maps is low, ca. 50 Myr, compared to the short Middle Jurassic interval (ca. 11 Myr). It is also important

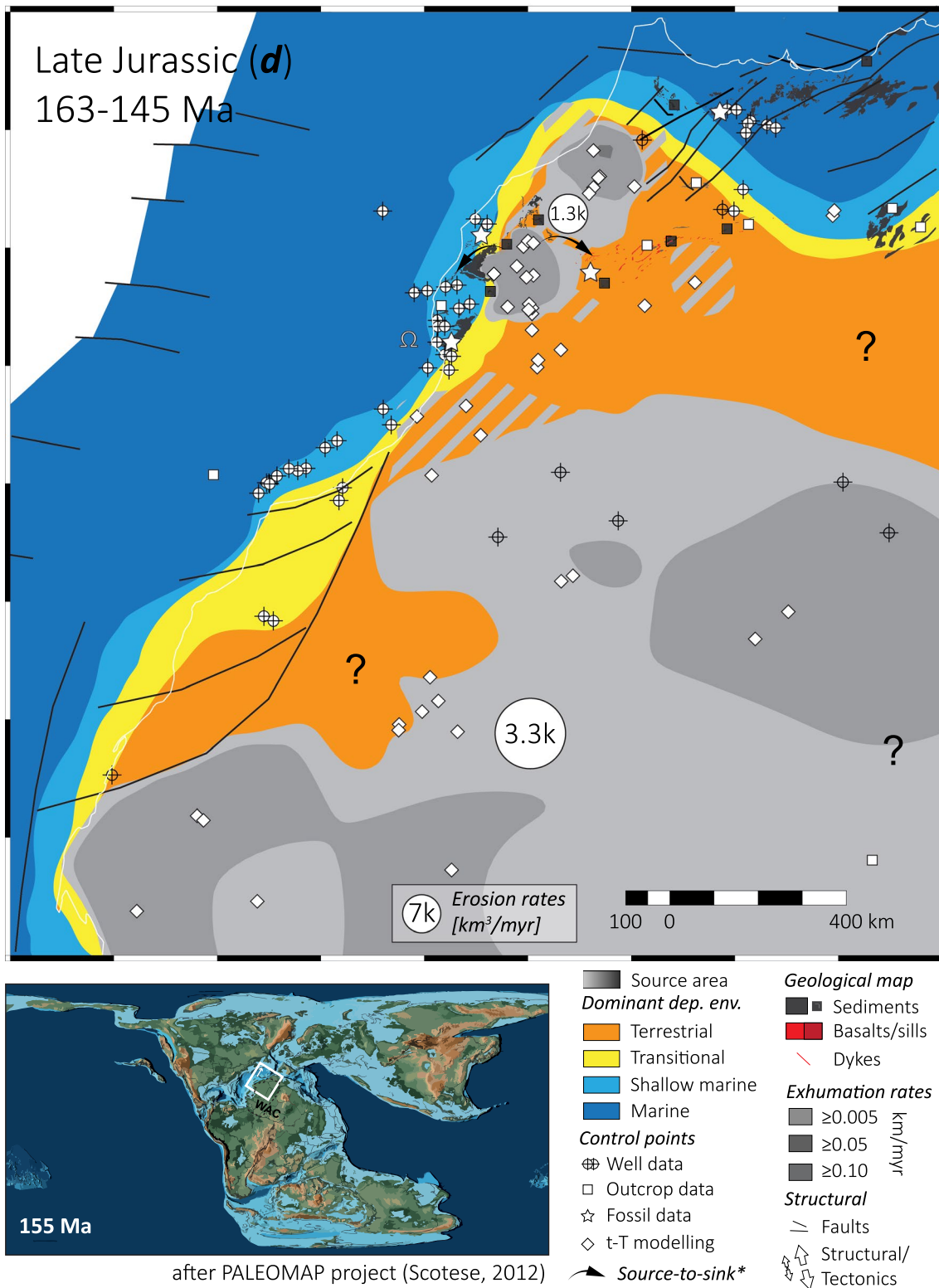


**FIGURE 17** Late Jurassic map (period *d*). See caption of Figure 13 for additional information. Ω: Triassic salt mobilization (after Moragas et al., 2018)

to note that the Triassic map is mostly composed of Late Triassic data, as Early and Middle Triassic sediments are rarely documented in the stratigraphy of Morocco. The

most accurate dating in the Triassic is obtained at the end of the sequence, where CAMP dykes and sills are radiometrically dated.

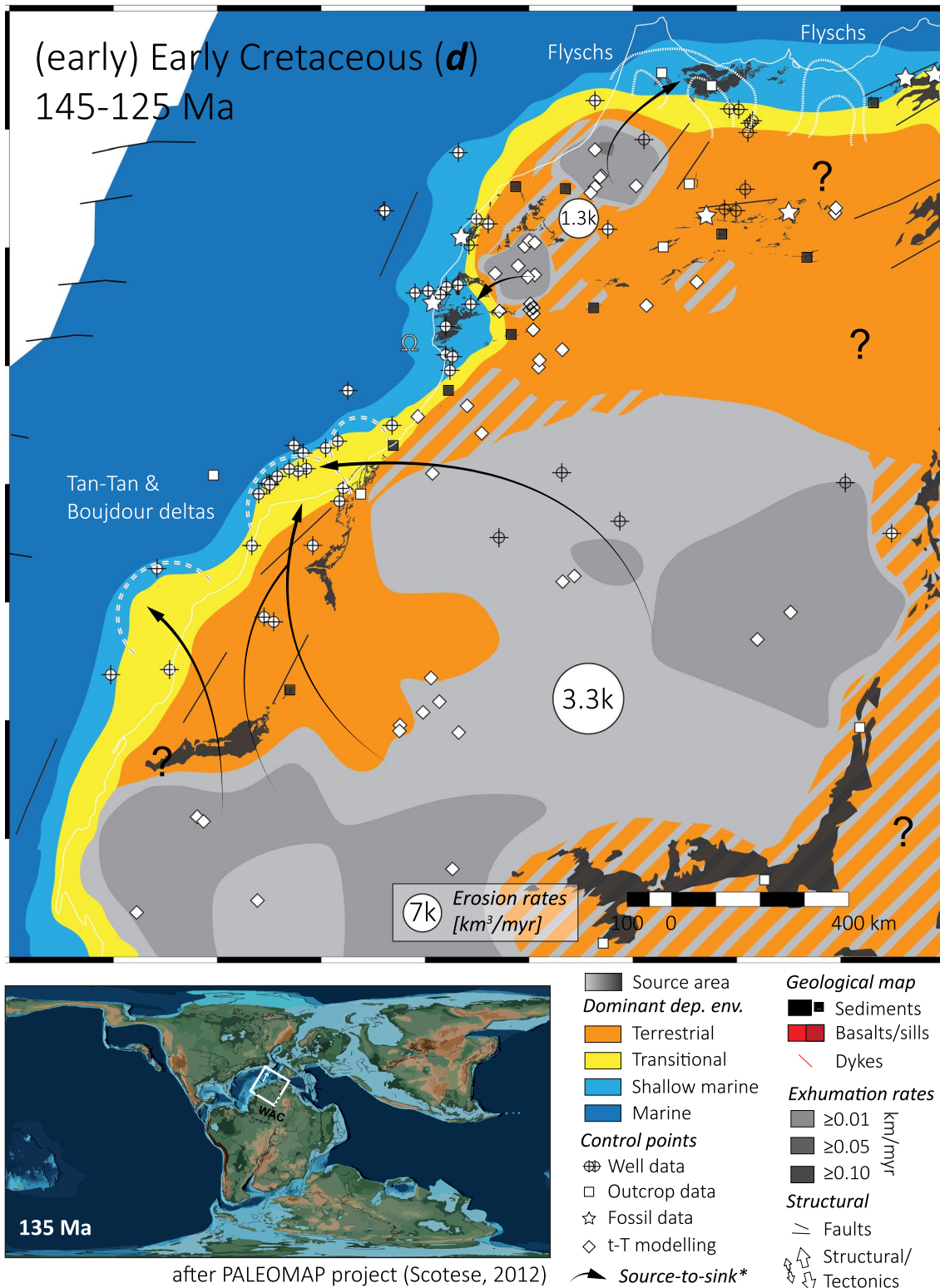


**FIGURE 18** (early) Early Cretaceous map (period *d*). See caption of Figure 13 for additional information.  $\Omega$ : Triassic salt mobilization (after Moragas et al., 2018)

Ye et al. (2017) presented a technique whereby the onlapping relationships between the Mesozoic sediments and their Precambrian/Palaeozoic basement are used as a

proxy to reconstruct the original extent of the basin (after Sloss & Scherer, 1975), which in turn provides the areal extent of the exhuming/emerged zones. We do not follow

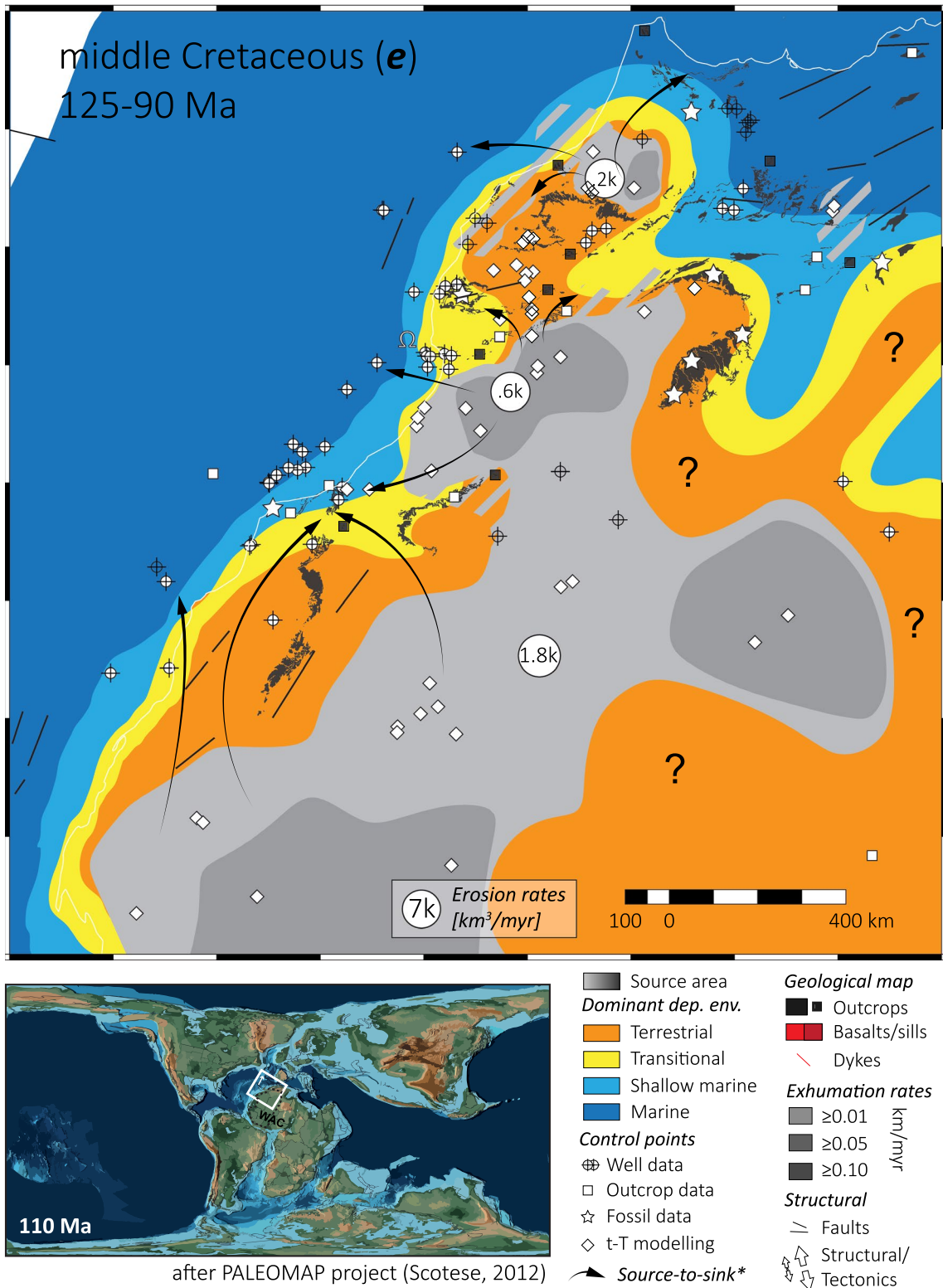


**FIGURE 19** middle Cretaceous map (period e). See caption of Figure 13 for additional information. Ω: Triassic salt mobilization (after Moragas et al., 2018)

this approach, as we lack the data on the slope values. These angles are often small and hard to measure in the field. Little published data exist on this subject and it is

sometimes unknown if the sediments are truncated, overlapping or simply completely missing. In this work, we assume that the interpolation results (using data from both

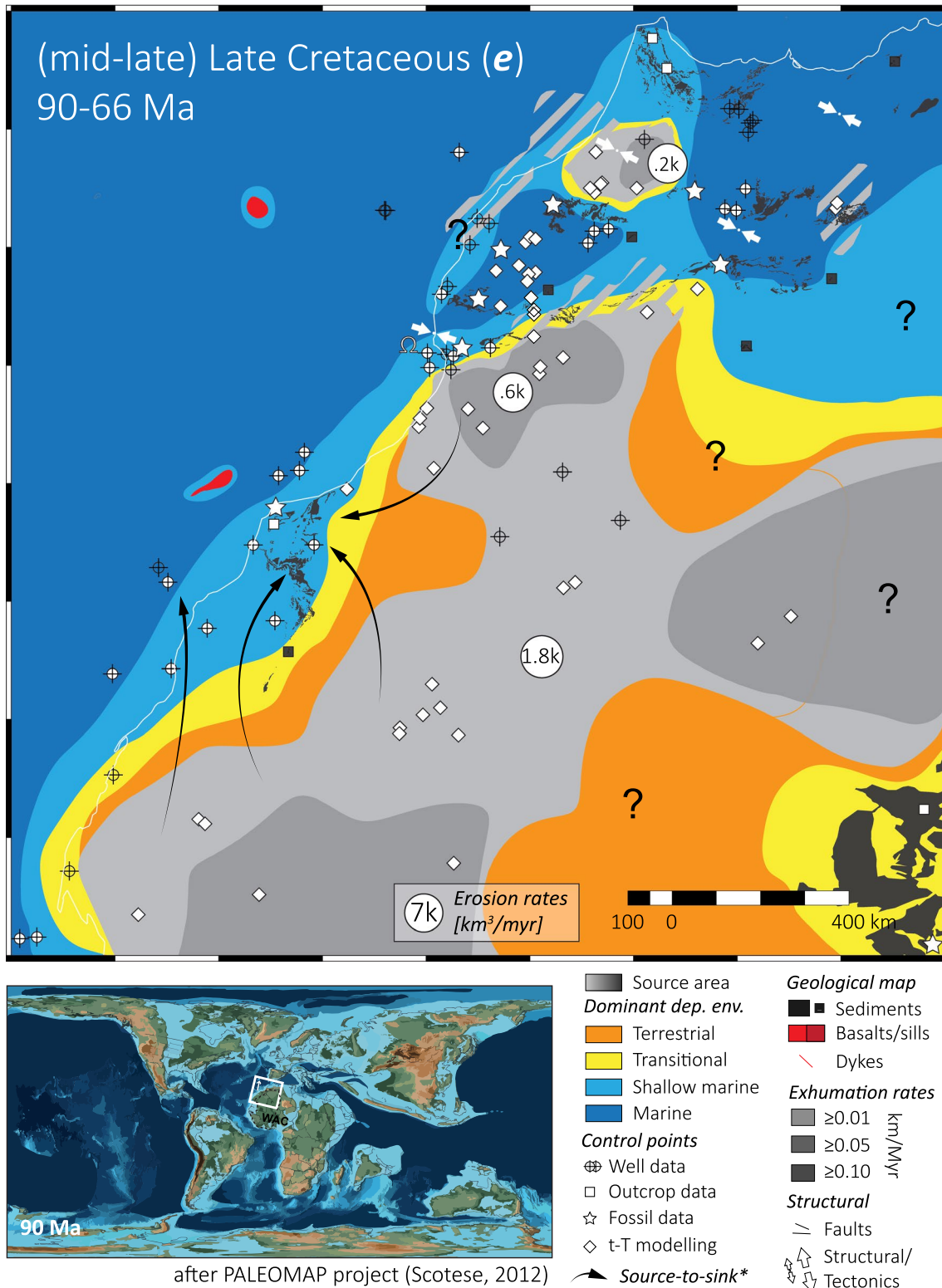


**FIGURE 20** (mid-late) Late Cretaceous map (period *e*). See caption of Figure 13 for additional information. Ω: Triassic salt mobilization (after Moragas et al., 2018)

source and sink domains) are a fair approximation of the extent of the source and depositional areas.

Moreover, our SandS maps use the present-day unrestored geography and geology as base maps. In many

areas this is acceptable (Figure 10 **insert**), however, there may be more substantial implications (and induced uncertainty) in areas such as the Atlas and Rif belts, for which Cenozoic upheaval was mostly caused by N-S shortening

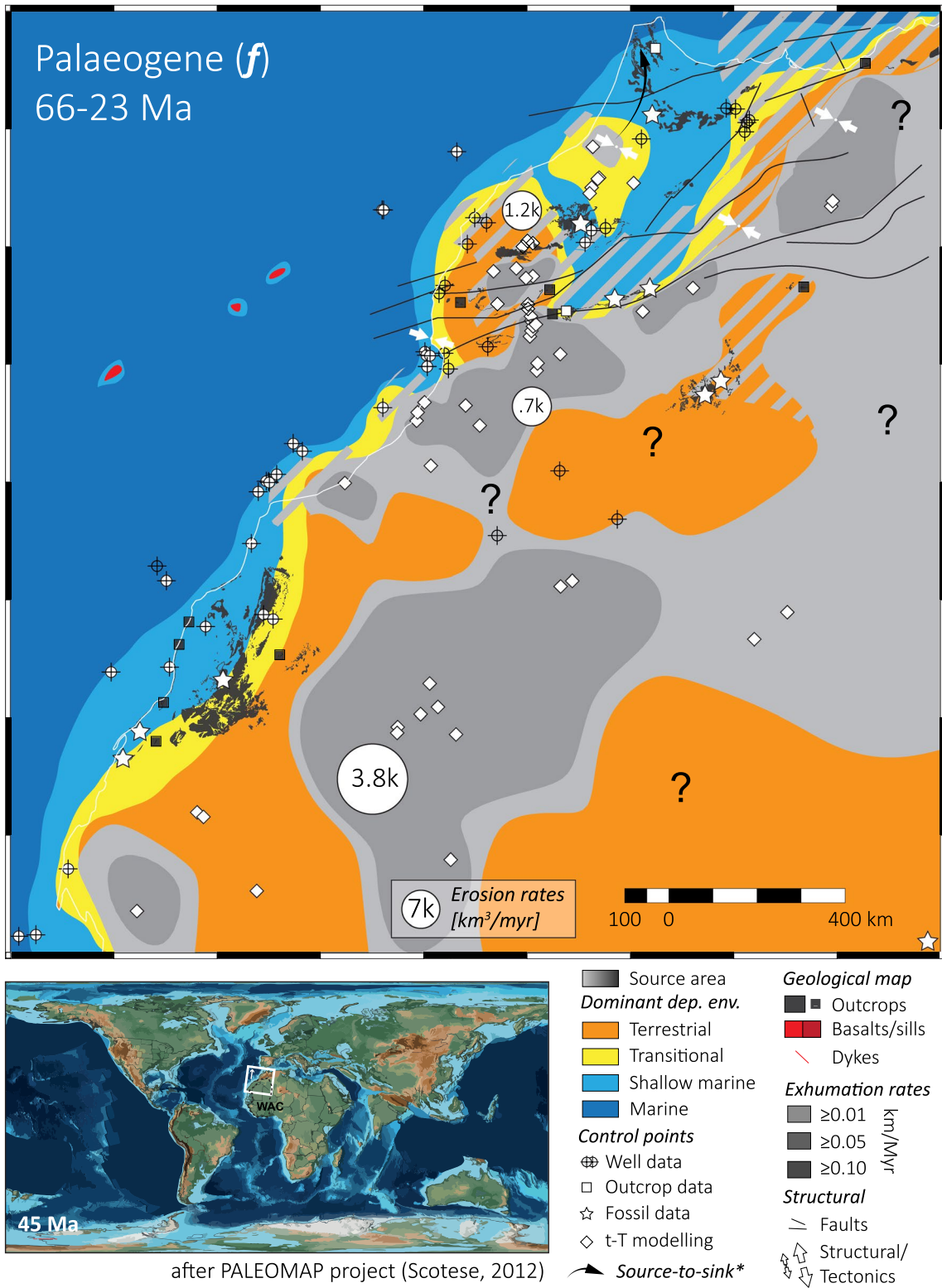


FIGURE 21 Palaeogene map (period f). See caption of Figure 13 for additional information

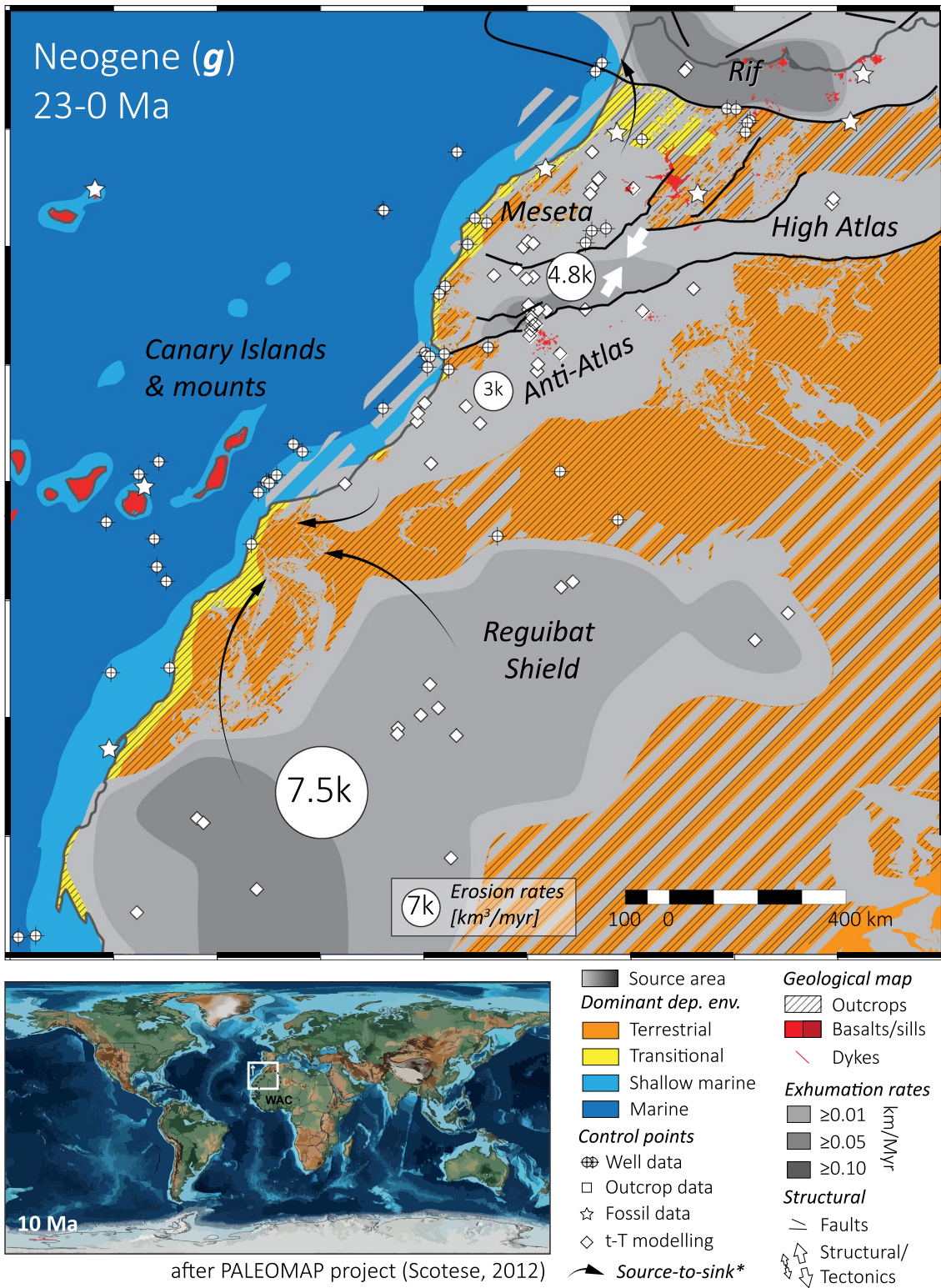


FIGURE 22 Neogene map (period g). See caption of Figure 13 for additional information

(e.g. Michard et al., 2008) associated with major strike-slip motion (Ellero et al., 2020).

## 4 | SOURCE-AND-SINK (SANDS) MAPS

### 4.1 | Pre-rift: Permian and Triassic

During the Permian (Figure 13), erosion of the remnants of the Variscan chain (e.g. Hmich et al., 2006; Lorenz, 1988), mostly effected the Meseta and Western Anti-Atlas. Known Permian deposition occurred in the Eastern Meseta, Doukkala and Argana Valley basins. Subsiding domains include the Central and Eastern Reguibat Shield (Leprêtre et al., 2015). We estimate the volume of produced sediments to ca.  $1.2 \times 10^6 \text{ km}^3$ , of which little is preserved today. Our working hypothesis is that Permian sediments were re-worked during the Triassic. Another possibility is that detrital material may have travelled outside of the study area to the south, using the Reguibat Shield as a transient sink.

From the Permian to the Early Triassic (periods *a* to *b*; Figures 13 and 14), the eroded area, which initially included the entire Variscan Orogenic belt, became restricted to the Meseta and the Anti-Atlas. The eastern Reguibat Shield is also affected by erosion in the Triassic. The occurrence of transitional depositional environments is another important change, resulting from Tethysian marine incursions as far as the Tarfaya basin (e.g. Leleu et al., 2016; Ranke et al., 1982; Scotese, 2012). The erosion that occurred in the Anti-Atlas during the Triassic is supported by sedimentary provenance analyses and palaeocurrents conducted in the Massif Ancien (Baudon et al., 2009; Brown, 1980; Domènech et al., 2018) that evidence a drainage systems organized perpendicular to the Anti-Atlas trends.

### 4.2 | Syn-rift: Triassic and Early Jurassic

During the Triassic (period *b*; Figure 14), the northern Meseta (estimated volume of eroded material: ca.  $>40,000 \text{ km}^3$ ), the Anti-Atlas (ca.  $30,000 \text{ km}^3$ ) and the Reguibat Shield (ca.  $30,000 \text{ km}^3$ ) were being eroded. A large portion of the Meseta shows considerable burial (e.g. Ghorbal et al., 2008), comparable to the Triassic burial documented in the Central Atlantic and High Atlas rift zones (e.g. Gouiza et al., 2010; Moragas et al., 2018 respectively). The Central Atlantic and Atlas rift zones (i.e. present-day rifted margin and High Atlas mountains respectively) were subsiding, except perhaps for a part of the Massif Ancien, which acted as a major drainage divide as suggested by Domènech et al., (2018; Figure 14). This massif is believed to have formed a positive structural relief sourcing Triassic

sediments to the Argana and Oukaimeden valley (palaeocurrents; e.g. Baudon et al., 2012; Mader et al., 2017). Red clastics overlying Precambrian basement in the northern central Anti-Atlas are mapped as Triassic or older, where basaltic flows overlying them yielded ages of  $205.9 \pm 7.9$  and  $207.8 \pm 6.5 \text{ Ma}$  (Fiechtner et al., 1992). This implies that, while the core of the Anti-Atlas continued to exhume (c.  $0.04 \text{ km/Myr}$ ), its northern margin was stable or subsiding (including the Souss and Ouarzazate basins).

From the Late Triassic to Early Jurassic (periods *b* to *c*; Figures 14 and 15), marine transgressions affected the Atlas and Central Atlantic rift (cf. blue arrows on Figure 14). The only significant change in source areas is an exhumation event occurring in the western Reguibat Shield (up to  $0.06 \text{ km/Myr}$ ) starting from the Early Jurassic (Leprêtre et al., 2015; Figure 15). A recent provenance study by Marzoli et al. (2017), using detrital zircon U-Pb ages, shows that sediments intercalated with the CAMP basalts in the western High Atlas have been sourced from the Meseta domain. For at least part of the Early Jurassic, there was no sea connection between the Western and Central High Atlas. This can be seen in the Early Jurassic record, where facies associations show continental and paralic deposits in the western part of the Central High Atlas, and a general deepening towards the east (Krencker et al., 2020). Sediment supply and accumulation over the Massif Ancien was likely large enough to prevent a marine connection (Krencker et al., 2020).

### 4.3 | Early Post-rift: Early Jurassic–early Early Cretaceous

The Early and Middle Jurassic (period *c*; Figures 15 and 16) are marked by enhanced erosion in the Anti-Atlas and Reguibat Shield, and to some extent in the Meseta (see volumes of eroded material in Table 3). Period *c* has the most active erosion rate for the Anti-Atlas and it is likely that the Anti-Atlas formed a topographic swell, as obtained exhumation rates are higher in the central part of the belt (up to  $0.16 \text{ km/Myr}$ ; e.g. Gouiza et al., 2017; Figure 15). Middle Jurassic redbeds are recorded in the onshore basins north and west of the Anti-Atlas (Tarfaya, Agadir-Essaouira, Central High Atlas, Sidi-Ifni Margin and Souss basins; see Table 3 and references therein), while in the basins south and east of the Anti-Atlas, no Jurassic sediments are recognized (e.g. Hollard et al., 1985; Michard et al., 2008). This supports an exhuming Anti-Atlas and Reguibat Shield, linked by an exhuming or stable Tindouf area.

Although the Jurassic is dominated by carbonates, there are significant periods of discrete siliciclastic influx. The Early Jurassic is dominated by carbonate sedimentation but has up to 40% of fine-grained siliciclastics (10%–20% on average), most abundant in the Central High Atlas and in the



Essaouira-Agadir Basin during most of the Early and Middle Jurassic (Duval-Arnould, 2019). Coarse-grained clastic sediments are also deposited in the Central and Western High Atlas during the Toarcian. Middle Jurassic rocks are composed of mudstones to coarse clastics (alluvial plain) and mixed carbonate siliciclastics in the Western and Central High Atlas respectively (Joussiaume, 2016; Malaval, 2016). These observations point towards the presence of an active source of clastic sediments in the vicinity of these basins during the Early to Middle Jurassic, corroborating the results of t-T studies conducted in the Anti-Atlas (e.g. Gouiza et al., 2017; Oukassou et al., 2013; Ruiz et al., 2011).

The Early and Middle Jurassic (period *c*; Figures 15 and 16) are fairly similar in terms of depositional environments. Exhumation patterns are identical on both SandS maps as they originate from the same exhumation map, presented in Figure 10c. Provenance studies carried out on Middle Jurassic sediments show evidence of sedimentary transport from the Meseta to the Middle Atlas (based on detrital zircon geochronology; Pratt et al., 2015), and from the Anti-Atlas to the Essaouira-Agadir Basin (based on palaeocurrents; Stets, 1992). Mobilization of Triassic salt occurred in the High Atlas and Essaouira-Agadir salt basins from the Early until the Middle Jurassic (e.g. Moragas et al., 2018), presumably where the sedimentary overburden was thickest (Figures 15 and 16). Salt mobilization in the High Atlas basin stopped prior to the Late Jurassic, but continued in the coastal basin until the Late Cretaceous (Moragas et al., 2018).

Exhumation/burial rates are negative in the Anti-Atlas (i.e. indicating subsidence). In the western part of the belt an observed positive rate (Figure 8) could be due to a t-T modelling inconsistency or it could record remnant relief from the previous period. A provenance study of Lower Cretaceous sediments from the north Tarfaya Basin (Ali et al., 2014) showed that they were sourced from the Reguibat Shield only. It suggests that the positive vertical movement rate calculated for the western Anti-Atlas for period *d* should be discarded, and that the t-T modelling results for that specific sample are inconsistent with the rest of the t-T modelling (Gouiza et al., 2017). We therefore considered no active source area in the western Anti-Atlas during the Late Jurassic in the corresponding SandS map (Figure 17).

From the Middle to Late Jurassic, our results show a shift in location of sediment production, from the Anti-Atlas to the Meseta. The Late Jurassic (period *d*; Figure 17) shows a major shift in the sediment source areas: the Anti-Atlas is no longer an active source, while the Meseta region was undergoing erosion (up to 0.07 km/Myr; e.g. Ghorbal et al., 2008). A high-resolution clay mineralogy study, carried out in folded Jurassic sediments of the Essaouira-Agadir Basin (Oujahain et al., 2011), shows a clear shift in either the sediment source lithology or area, between the Middle and Late Jurassic, passing from a chlorite- to an illite-dominated assemblage. It is possible that Middle

Jurassic erosion of the Anti-Atlas cut down to the Precambrian, hence, reaching metamorphosed Palaeozoic series, a source of chlorite minerals. The Meseta is also a documented source area during the Late Jurassic, as suggested by palaeocurrents measured in the western High Atlas (Stets, 1992).

The transition between the Jurassic and the Cretaceous (period *d*; Figures 17 and 18) was fairly quiescent. The coastline shifted towards the north in the Middle Atlas/Rif areas, and towards the west in the Tarfaya basin. The latter change was accompanied by the onset of large Early Cretaceous deltaic systems (Tan-Tan and Boujdour deltas; Figure 18). The entire Reguibat Shield had been an active source of sediments since the Early Jurassic and remained such during the Early Cretaceous. The prograding delta systems suggest an acceleration of exhumation or a change in source lithology in the Reguibat Shield in the earliest Cretaceous. An acceleration is not observed in the t-T modelling for that region (Figure 10d), therefore, it is possible that erosion in the Reguibat Shield reached the granitic basement at the end of the Jurassic, with near-complete removal of the metapelitic Palaeozoic cover prior to the Cretaceous.

Exhumation of the Meseta/Atlas massifs (rates of up to 0.1 km/Myr; ca. 50,000 km<sup>3</sup>/Myr) from Late Jurassic to Early Cretaceous (period *d*) was first described in Ghorbal et al., (2008). The preserved onshore basins in the Meseta do not record Upper Jurassic sediments, except in the coastal Doukkala basin (Figure 18). It suggests an exposed surface larger than that of the presently outcropping basement.

In the Late Jurassic and Early Cretaceous, it is not known whether the Tindouf basin was sourcing sediments to the Tarfaya Basin deltas, acting as a transient sink, or simply stable, as the only two wells that were sampled are located at the transition with the Anti-Atlas in the NW of the basin. The t-T models from the shallowest samples of these wells show mild exhumation rates according to our calculations (ca. 0.04 km/Myr).

A sedimentary provenance study conducted in the north Tarfaya Basin showed that the Lower Cretaceous and Upper Cretaceous sediments were sourced from the Reguibat Shield, and from both the Reguibat Shield and the Anti-Atlas respectively (Ali et al., 2014; Figures 18 and 19). During period *d*, the Reguibat Shield witnessed substantial erosion (ca. 3,300 km<sup>3</sup>/Myr), and it is interpreted to be the source of the Lower Cretaceous sediments deposited in the Boujdour and Tan-Tan deltas (with potentially a contribution from part of the south Tindouf basin), with a volume of eroded material of about 125,000 km<sup>3</sup>.

#### 4.4 | Late Post-rift and Atlas orogeny: middle Cretaceous to Neogene

The Cretaceous (periods *d* and *e*; Figures 18, 19 and 20) is characterized by another shift in source areas. The Anti-Atlas

basement, which was subsiding during the Early Cretaceous, was exhumed again from the middle Cretaceous onwards (Aptian-Turonian; up to 0.04 km/Myr; Gouiza et al., 2017; Figure 18). Meanwhile, the southern massifs of the Meseta underwent burial during the middle Cretaceous after a prolonged exhumation episode (e.g. Ghorbal et al., 2008). Widespread coarse detrital sediments are described from the Early Cretaceous (e.g. Davison, 2005; Frizon de Lamotte et al., 2009; Lubner, 2017). The transition from shallow marine to continental depositional environments occurred between the early and the middle Cretaceous in the Essaouira-Agadir basin. The fluvial deposits record a general palaeocurrent direction towards the west during the Latest Barremian to Early Aptian (Lubner, 2017). In the Late Aptian and Albian times, the area was drowned once again with the establishment of shallow marine conditions (Lubner, 2017).

In the Tarfaya Basin, Aptian-Albian (middle Cretaceous) fluvial units exposed along coastal outcrops display a mean palaeocurrent direction towards the northwest (Arantegui, 2018). Sediment provenance analyses suggest that only the Reguibat Shield (including the Mauritanides) was exporting clastic sediments to the north Tarfaya basin during the Early Cretaceous, while the western(?) Anti-Atlas partly supplied clastics to the coastal basin from Late Cretaceous onwards (Ali et al., 2014). Pratt et al. (2015) collected Albian sediments deposited in the Rif basin, and traced the provenance to two sources: the Meseta and another unknown area. Finally, Mourlot et al., (2018) undertook a large-scale provenance study targeting Albian to Maastrichtian sediments from DSDP wells (from north to south offshore Morocco sites 370, 416, 415 and 369 were sampled) along the NW African coast. They used the major and trace element concentrations from these marine sediments, as well as Nd isotopes, to constrain continental crust signatures. Their results show that the sediments from the DSDP wells north of Agadir have signatures from the Meseta, the Anti-Atlas, and the Reguibat Shield during the middle Cretaceous. DSDP Well 369, in the offshore Tarfaya basin, has a continuous record of sediments with a Reguibat Shield signature throughout the Albian and Late Cretaceous (Mourlot et al., 2018). Azdimoussa et al. (2019) analysed detrital zircon for U-Pb ages and documented similar potential source areas for Aptian-Albian, Palaeogene (Eocene) and Neogene (early Miocene) sediments deposited in the north-western Rif. These potential source areas, namely, the Meseta, the Triassic sediments from the High Atlas or the northern West African Craton (Azdimoussa et al., 2019), would require several local, or regional to sub-continental drainage systems (to export eroded material towards the Rif basin) respectively. In our maps, we have displayed the most local required system, i.e. between the exhuming Meseta massifs and the northern tip of the Rif (Figures 19, 21, and 22). Although the source of detrital material deposited in the Rif may indeed be the

Reguibat Shield, sediment fairways between the two massifs were probably disconnected by the Anti-Atlas acting as a geographical barrier, deflecting such routing towards the present-day northeast.

Cenomanian-Turonian outcrops onlap Palaeozoic basement (western Anti-Atlas; Abioui et al., 2019) and are characterized by having similar facies with a widespread occurrence around the Anti-Atlas (Figure 19) (Eastern Anti-Atlas; Guimerà et al., 2011). Sauropods and crocodylian ichnofacies from the Guir Hamada (Benyoucef et al., 2015) showed that an emerged land was nearby, which was likely the Anti-Atlas (Abioui et al., 2019; Charton, 2018; Gouiza et al., 2017).

In the late Early to Late Cretaceous (period *e*; Figure 20), subsiding domains are dominant in the study area. This period is characterized by a rise in global sea level (Cenomanian-Turonian transgression; e.g. Piqué et al., 2006), which transgressed the interior of Morocco and Algeria (e.g. Upper Cretaceous deposits in the Guir Hamada; e.g. Benyoucef et al., 2015). It appears to have partially submerged the Reguibat shield, the Tindouf basin (except its central part) and the borders of the Anti-Atlas. A Cenomanian-Turonian carbonate platform with low detrital influx prevailed in the Central High Atlas, while on the Atlantic and Tethysian margins, Turonian organic-rich black muds were deposited, in fault bounded basins where relatively deeper marine environment prevailed (Wang, 2018). Erosion was first localized in the centre of the Anti-Atlas (ca. 600 km<sup>3</sup>/Myr), then extended to the eastern and western regions. During the middle Cretaceous, the central Anti-Atlas became an active source area and exhumation of the Meseta slowed down (from up to 0.06 down to 0.02 km/Myr). By the end of the Cretaceous, the entire Anti-Atlas s.s. was sourcing sediments to surrounding basins, and most of the Meseta and High Atlas domains were subsiding and progressively drowned.

The Palaeogene and Neogene (periods *f* and *g*; Figures 21 and 22) are characterized by the Atlas orogeny, which records high exhumation rates in the High Atlas and Rif (up to 0.20 and 0.49 km/Myr, respectively) and to a lesser extent in the Anti-Atlas and Reguibat Shield (up to 0.05 and 0.10 km/Myr, respectively). We estimate the volume of eroded material from the study area during the Palaeogene and Neogene to ca. 0.3 x 10<sup>6</sup> and 0.8 x 10<sup>6</sup> km<sup>3</sup> respectively. During the Palaeogene (Figure 21), a large portion of the study area was emerged. Epicontinental basins developed around the exhuming massifs of the Meseta and the High Atlas, and shallow marine setting persisted in the Tarfaya Basin.

The Neogene (Figure 22) shows only minor differences with the present-day situation, with nearly all of Morocco emergent. Important sediment source areas are the Meseta, the High Atlas, the Anti-Atlas and the Reguibat Shield. Some shallow marine sinks developed in the North Tarfaya, southern Settat and Gharb basins, and along the Mediterranean coast in the Rif domain.

## 5 | DISCUSSION

### 5.1 | Implications for Moroccan source-to-sink systems

The investigation of large-scale denudation patterns has highlighted three regions that act as important sediment sources: the Reguibat Shield, the Anti-Atlas and the High Atlas/Meseta. The Reguibat Shield is marked by burial from the Permian to the Triassic, followed by exhumation from the Jurassic onwards (exhumation rates: 0.01–0.06 km/Myr; cumulative denudation of ca. 970,000 km<sup>3</sup>). We interpret that the Reguibat shield was the main source of sediments for the Cretaceous deltas, offshore Tarfaya basin.

In the Anti-Atlas, basement rocks were deeply buried in the Permian and then exhumed between the Triassic and the Middle Jurassic (0.01–0.16 km/Myr; cumulative denudation of ca. 330,000 km<sup>3</sup>). Renewed burial during the Late Jurassic/Early Cretaceous was followed by a final exhumation from the Late Cretaceous onwards (0.01–0.05 km/Myr; ca. 130,000 km<sup>3</sup>).

Presently outcropping Variscan age rocks in the High Atlas and Meseta were near the surface during the Permian/Late Triassic, buried until the Middle Jurassic, exhumed in the Late Jurassic/Early Cretaceous (0.01–0.09 km/Myr; cumulative denudation of ca. 50,000 km<sup>3</sup>), buried again during the Late Cretaceous and finally exhumed during the Cenozoic (0.01–0.20 km/Myr; ca. 160,000 km<sup>3</sup>). The Triassic-Middle Jurassic burial event was synchronous to Atlasic rifting, and temperature-to-depth conversion indicates rapid burial from close to the surface down to 4 km. In turn suggesting that subsidence associated with the Central Atlantic and/or the High Atlas rift zone(s) extended over nearly the entire Meseta.

Our results show that sediment source areas in Morocco since the Permian have varied in location and size and were not always active simultaneously (Figure 23). The present-day extent of the Precambrian and Variscan basement correlates fairly well to the areas that have experienced exhumation since the Permian. A few exceptions exist (e.g. centre Tindouf Basin, Hauts Plateau, etc...; Figure 23), which can be explained by the fact that their sediment cover prevented the basement from being sampled and analysed by LTT or they could represent uncertainty due to the way the exhumation maps were designed (Figure 10).

We conclude that the Anti-Atlas, the High Atlas and the Meseta massifs have all been important sediment sources to the surrounding sedimentary basins through the investigated periods. The results also highlight the Reguibat Shield as a vast and long-lived source areas (Figure 23), and may therefore be the most important supplier of clastics material to the onshore and offshore Meso-Cenozoic basins in Morocco and its surrounding; either directly as exemplified for the Tarfaya Basin (Ali et al., 2014) or through several sediment reworking cycles. The contrast in exhumation histories between the

Anti-Atlas and the Atlas/Meseta regions, characterized by several shifts of detrital sediment sources, can be explained in terms of movements of different fault bounded terrains separated by a long-lived major lithospheric shear zones (Ellero et al., 2020).

The SandS maps illustrate the increasing occurrence of terrigenous sediment in the southern regions, with the presence of the Reguibat Shield as a major detrital material source (feeding the Tarfaya-Dakhla and Taoudeni Basins). This interpretation supports the palaeoreconstructions of Ye et al., (2017) that also identified the Reguibat Shield as an important sedimentary source. Important fluvial systems also existed between the massif and the Taoudeni Basin (southernmost basin on Figure 1) and the Mauritania-Senegal Basin. These source-to-sink systems likely existed since the Triassic, and were active in the Berriasian (Early Cretaceous), Cenozoic and to a lesser extent during the Aptian-Albian and Late Cretaceous (Ye et al., 2017).

The coastal Essaouira-Agadir and Tarfaya basins have accumulated a near complete succession of deposits since the Permo-Triassic, as well as the present-day offshore passive margin domain (Tari & Jabour, 2013; Figure 9). Although major erosional unconformities are documented in the Doukkala, Essaouira-Agadir and Tarfaya Basins as well as offshore in the continental margin (Abou Ali et al., 2005; El Jorfi et al., 2015; Gouiza, 2011; Le Roy et al., 1997), the relatively continuous subsidence in these regions suggests that the widespread erosional exhumations were more focused around the documented source areas.

### 5.2 | Mass balance: onshore sources to offshore sinks

The total estimated eroded volume rates (Table 2) can be compared to published sedimentation rates from Helm (2009; Figure 24), as exemplified in Tinker et al., (2008) in South Africa. The sedimentation rates in the offshore domain and the coastal basins were obtained using interpreted stratigraphic thickness integrated from nine interpreted seismic profiles perpendicular to the coast (Helm, 2009), and extended by extrapolation and/or well control to the basin (using DSDP wells). Detrital sedimentation rates from the Triassic to the Neogene were then estimated and adjusted to the proportion of clastic sediments recorded in the control wells (Helm, 2009).

Results from the erosion rate modelling are interpreted to approximate the detrital sedimentation flux (i.e. disregarding routing of sediment in onshore basins, climate, lithology of the source area or suspended load, and the detrital component exiting the system to the distal offshore). In this case study, the comparison shows that the siliciclastic volumes deposited in the offshore/coastal basins and the eroded volume of

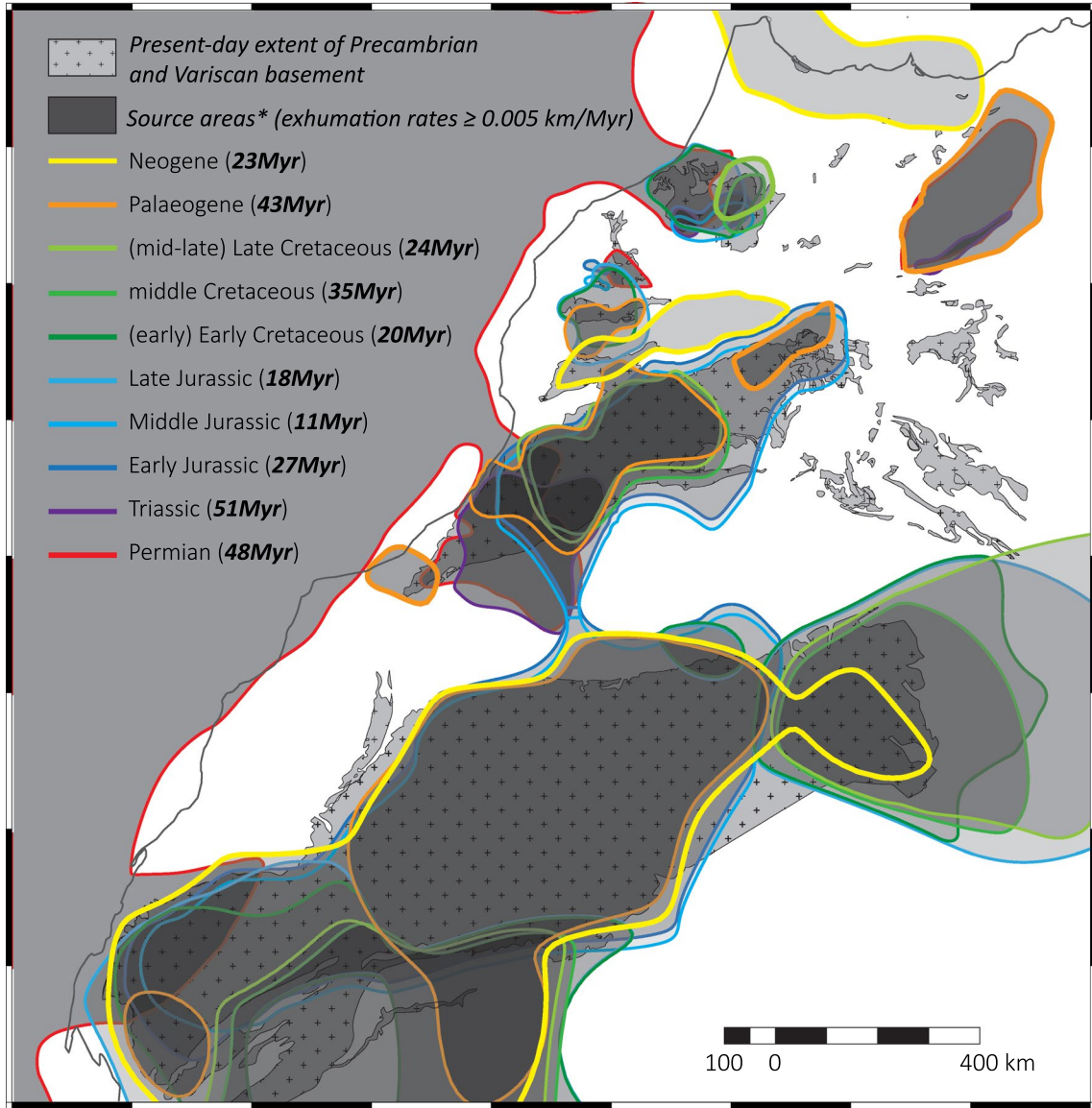


**FIGURE 23** Stacked polygons for exhumation rates  $\geq 0.005$  km/Myr, for each period of the SandS maps (Figures 13-22), superimposed to the extent of Precambrian and Variscan basement outcrops (after Hollard et al., (1985)). \*The transparency for each layer depends on the time duration of related period (e.g. transparency for Palaeocene source areas is 43%)

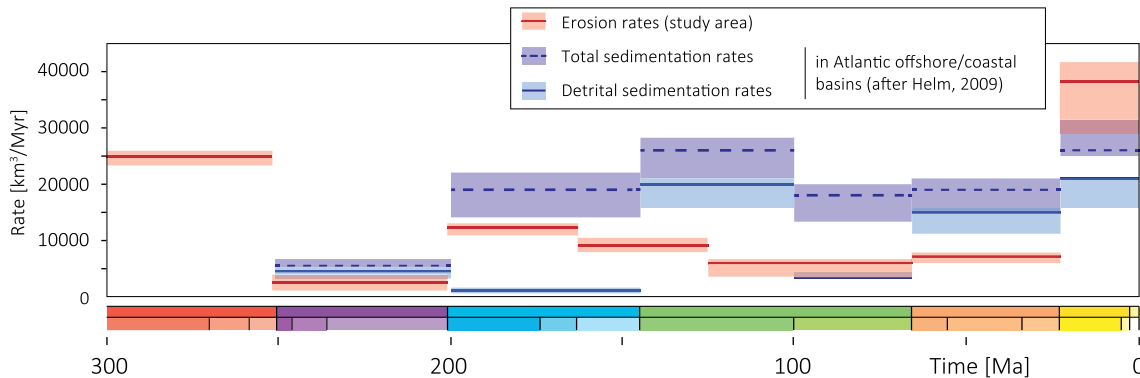


**FIGURE 24** Comparison of the total erosion rates to sedimentation rates in Moroccan offshore and coastal basins (after Helm, 2009). Note that it may be expected that the results should not match perfectly, as a proportion of the eroded material could be removed as dissolved carbonate, reworked after deposition, exported towards Algeria, Mauritania and Mali, or as fines detrital material that could have been transported over long distance beyond the study area of Helm (2009) and ours

material from the interpolation grid are, for the most part, of the same order of magnitude (Figure 24). Deposition and erosion rates are very similar, with relative increases/and decreases matching during the Triassic and Late Cretaceous. The exception is during the Jurassic period, when, according to our results, around 12,000 km<sup>3</sup>/Myr of material were eroded, while the offshore seems to record much lower volumes, about 1,000 to 2,000 km<sup>3</sup>/Myr of detrital sediments (after Helm, 2009). Such discrepancies, with influx higher than recorded sedimentation rates, could be explained by numerous reasons:

- Erosion in the Reguibat Shield, Anti-Atlas, Tindouf and Meseta may have removed fine-grained and/or carbonate-rich meta-sediments from the upper part of the Palaeozoic section. Hence, little coarse detrital material would be recorded in the Atlantic basins, where platform limestones are dominant.
- fluvial system pathways could have re-routed sediments to the east towards the Meso-Cenozoic Algerian and/or Tunisian basins, for instance
- the geothermal gradient could have been higher during rifting, which would result in much lower exhumation rates;

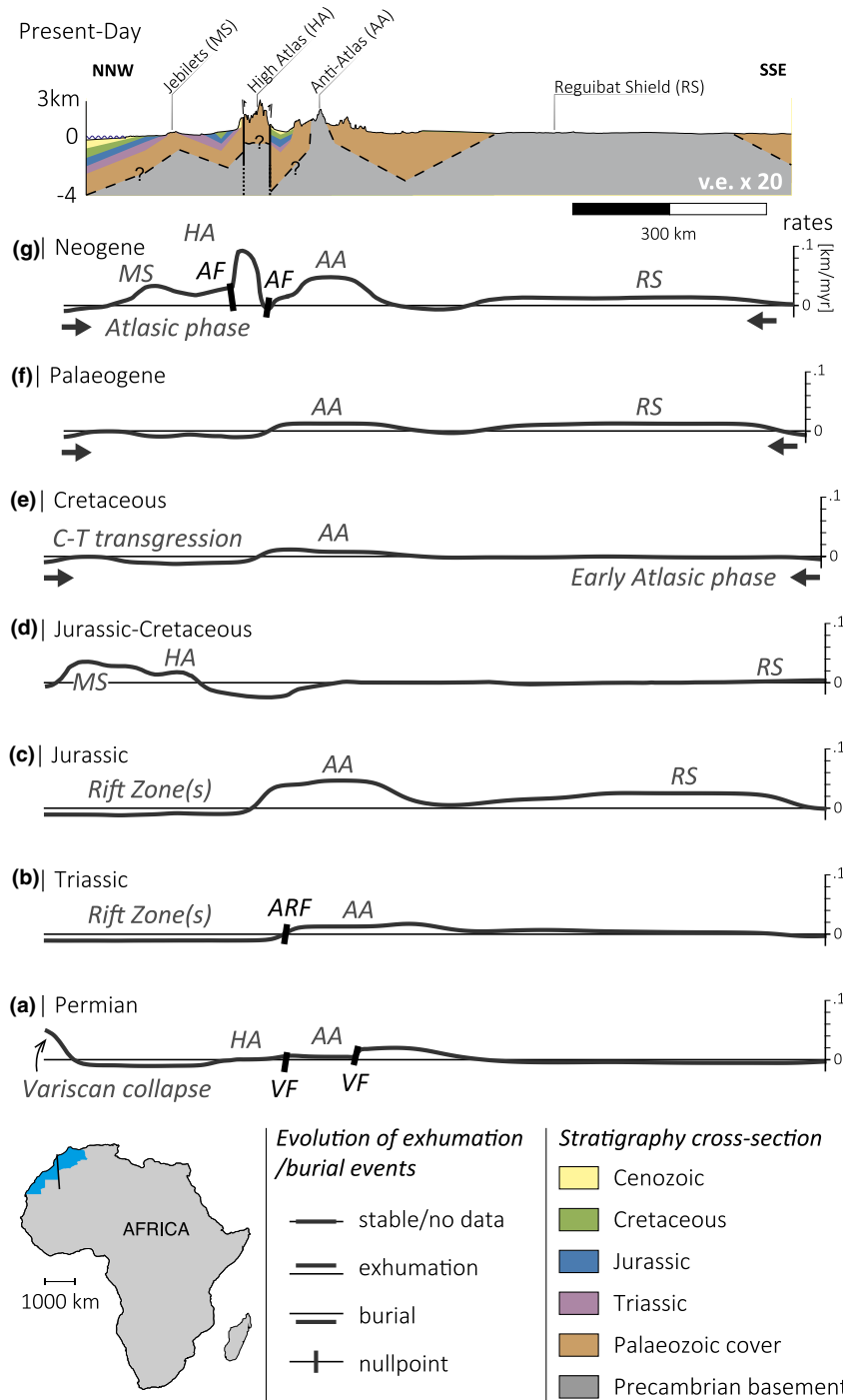


**FIGURE 25** Highly schematic NNW-SSE evolution of exhumation/burial events as evidenced by the presented workflow from Permian to Neogene (a-g). AF, Atlas fault; ARF, Atlas rift fault; C-T, Cenomanian-Turonian; VF, Variscan fault

- d. the offshore study of Helm (2009) did not account for compaction, meaning that sedimentation rates plotted against the erosion rates are minimum estimates.
- e. the limitation of only using nine sections (seismic lines) as reference along ~2000 km of coast means that depocenters may have been missed or overestimated;
- f. the algorithm extrapolated outside of data point coverage (e.g. centre of Tindouf Basin);
- g. longshore and/or contourite systems may have transported the temporarily stored material on the Moroccan shelf beyond the study area, or bypassed to the deeper basins.
- h. the volume of sediments that has been eroded from the shelf/slope, as recognized in offshore unconformities (e.g. Tari & Jabour, 2013), cannot be quantified (e.g. Tinker et al., 2008).

For times when the sedimentation rates are significantly higher than the erosion rates (Early Cretaceous and Palaeogene), it is possible that:

- a. a substantial sedimentary source may be unidentified if it lacks an LTT/t-T study (see previous part and Figure 23);
- b. selected t-T models are underestimating the cooling in the related time periods in one or several known sedimentary sources;
- c. the volume of detrital sediments calculated using offshore wells (Helm, 2009) may not be representative when up-scaled to the entire Atlantic margin.

### 5.3 | Exhumation/burial wavelengths

The half wavelengths of the exhumation/burial events can be estimated from the evolution of subsidence and exhumation observed along a cross-section trending perpendicular to the strike of the Jebilet Massif, High Atlas, Anti-Atlas and Reguibat Shield (Figure 25). The half wavelengths, expressed as the distance between successive null points, are between ca. 50 and 600 km for the exhuming domains, and ca. 40 and 200 km for the subsiding domains.

The Tindouf Basin remains fairly unconstrained in terms of vertical movements and therefore these wavelengths should be treated with caution, especially before the Late Cretaceous. The longest half wavelength is observed during the syn-rift stage for the Reguibat Shield to Anti-Atlas area. The half wavelengths shorten towards the north, where subsidence prevails in all illustrated periods. The exhumation/burial events may have driven regression or transgression, with positive feedback with eustatic sea-level changes.

Proposed mechanisms for the vertical movements are large-scale processes (see Teixell et al., 2009) that act at

wavelengths from one to several hundreds of kilometres (e.g. Şengör, 2003; Babault et al., 2008; Frizon de Lamotte et al., 2009). They include rift flank uplift (evidence does not support this in the study area), mantle-driven doming, lithospheric flexure, crustal-scale folding and erosional unloading. For the subsidence episodes, sedimentary loading was likely enhanced by crustal thinning (rift zone), thermal cooling (old rift), lithospheric flexure and crustal-scale folding (see Teixell et al., 2009).

## 6 | CONCLUSIONS

We present a methodology to use t-T modelling results as a proxy to define and quantify exhumation events. We display a series of exhumation maps from the Permian to the present-day in eastern Morocco and its surroundings, from which erosion patterns and erosion rates have been extracted. This allows analysis of the possible mechanism(s) responsible for the observed vertical movements.

The presented findings have implications for the evolution of the Central Atlantic rifted margins and for our understanding of the Meso-Cenozoic Moroccan source-to-sink systems. The investigation of denudation patterns at a large scale has highlighted three sediment source regions for the NW Africa basins: the Reguibat, the Anti-Atlas and the High Atlas/Meseta.

During the Permian, terrestrial basins located across the Meseta were sourced with material eroded from the Variscan chain. In the Middle to Late Triassic, widespread rifting allowed more extensive deposition across Morocco. Active sedimentary source areas were the northern Meseta, the western Anti-Atlas and the central Reguibat Shield. Initially, most of Morocco was dominated by continental deposits, with a gradual transgression inland from the Tethys to the east and the proto-Atlantic to the west extending terrestrial/transitional marine environments, across the High Atlas, the Meseta and the Tarfaya basins as well as part of the Reguibat Shield.

Throughout the Jurassic, shallow marine and frankly marine environments dominate, with periods of discrete siliciclastic input. Active sedimentary source areas were the Anti-Atlas, the Reguibat Shield and the Meseta massifs. A substantial shift in detrital source areas was evidenced from the Anti-Atlas to the Meseta/High Atlas at the transition between the Middle and the Late Jurassic (ca. 163 Ma).

In the Early Cretaceous, terrestrial environments cover a substantial portion of the study area, especially between 145 and 125 Ma. Another considerable source shift from the Meseta/High Atlas to the Anti-Atlas was evidenced at the transition between the early Early and the middle Cretaceous (ca. 125 Ma). Finally, during the Cenozoic, almost all the presently outcropping basement areas provided sediments to the coastal and foreland basins.

The presented workflow enables past large-scale source-to-sink domains to be constrained, which is lacking by design in local LTT studies (e.g. Charton et al., 2018).

## ACKNOWLEDGEMENTS

This study was part of the first author's doctoral thesis project, with financial support from the Netherlands research centre for Integrated Solid Earth Sciences (ISES) and the North Africa Research Group (NARG). We acknowledge the National Office of Hydrocarbons and Mines (ONHYM) for providing data to the NARG. All NARG members are thanked for scientific discussions and support. Angel Arantegui and Tim Luber are thanked for discussions about Early Cretaceous source-to-sink systems in the Tarfaya and Essaouira-Agadir basins respectively. Emmanuel Roquette, Delphine Rouby, Antonio Teixell and Mohamed Gouiza are acknowledged for proofreading an earlier version of the manuscript (Thesis chapters). Emilie Chaillan is thanked for digitizing the Cretaceous outcrops from the NW African geological maps. Basin Research Editor, Kerry Gallagher, is greatly thanked for his comments and advices. Finally, we deeply thank David Hodgson, Mar Moragas, Mohamed Gouiza and two anonymous reviewers for their constructive comments that greatly improved the original manuscript.

## CONFLICT OF INTEREST

The authors have no conflict of interest to declare.

## PEER REVIEW

The peer review history for this article is available at <https://publons.com/publon/10.1111/bre.12517>.

## DATA AVAILABILITY STATEMENT

The well data that support the findings of this study are available on request from the corresponding author. The data are not publicly available due to confidential restrictions. All other data are available as supplementary file 2.

## ORCID

Rémi Charton  <https://orcid.org/0000-0002-0064-256X>

## REFERENCES

- Abioui, M., Ferry, S., Grosheny, D., Içame, N., Robert, E., & Benssaou, M. (2019). The Cretaceous marine onlap on Palaeozoic deposits (Smara-Lâayoune Basin, South Morocco). Comparison with neighbouring regions. *Comptes Rendus Geoscience*, *351*(7), 498–507. <https://doi.org/10.1016/j.crte.2019.09.003>
- Abou Ali, N., Hafid, M., Chellai, E. H., Nahim, M., & Zizi, M. (2005). Structure de socle, sismostratigraphie et héritage structural au cours du rifting au niveau de la marge d'Ifni/Tan-Tan (Maroc sud-occidental). *Comptes Rendus Geosciences*, *337*, 1267–1276. [16/j.crte.2005.07.003](https://doi.org/10.1016/j.crte.2005.07.003)
- Adaci, M., Tabuce, R., Mebrouk, F., Bensalah, M., Fabre, P.-H., Hautier, L., Jaeger, J.-J., Lazzari, V., Mahboubi, M., Marivaux, L., Otero, O., Peigné, S., & Tong, H. (2007). Nouveaux sites à vertébrés paléogènes dans la région des Gour Lazib (Sahara Nord-occidental, Algérie). *Comptes Rendus Palevol*, *6*, 535–544. <https://doi.org/10.1016/j.crpv.2007.09.001>
- Ait Boughrou, A., Boulanouar, M., Yacoubi, M., & Coineau, N. (2007). The first Microcharon (Crustacea Isopoda, Microparasellidae) from the Moroccan North Saharan Platform. *Origin and Palaeobiogeography: Contribution to Zoology*, *76*, 19–32. <https://doi.org/10.1163/18759866-07601003>
- Ait Brahim, L., Chotin, P., Hinaj, S., Abdelouafi, A., El Adraoui, A., Nakcha, C., Dhont, D., Charroud, M., Sossey Alaoui, F., Amrhar, M., Bouaza, A., Tabyaoui, H., & Chaouni, A. (2002). Paleostress evolution in the Moroccan African margin from Triassic to Present. *Tectonophysics*, *357*, 187–205. [https://doi.org/10.1016/S0040-1951\(02\)00368-2](https://doi.org/10.1016/S0040-1951(02)00368-2)
- Ali, S., Stattegger, K., Garbe-Schönberg, D., Frank, M., Kraft, S., & Kuhnt, W. (2014). The provenance of Cretaceous to Quaternary sediments in the Tarfaya basin, SW Morocco: Evidence from trace element geochemistry and radiogenic Nd–Sr isotopes. *Journal of African Earth Sciences*, *90*, 64–76. <https://doi.org/10.1016/j.jafrearsci.2013.11.010>
- Aloui, T., Dasgupta, P., & Chaabani, F. (2012). Facies pattern of the Sidi Aïch Formation: Reconstruction of Barremian paleogeography of Central North Africa. *Journal of African Earth Sciences*, *71*, 18–42.
- Ambroggi, R., & Lapparent, A. (1954). Découverte d'empreintes de pas de Reptiles dans le Maestrichtien d'Agadir (Maroc): Compte Rendu sommaire des séances de la Société géologique de France, 51–52.
- Amidon, W. H., Roden-Tice, M., Anderson, A. J., McKeon, R. E., & Shuster, D. L. (2016). Late Cretaceous unroofing of the White Mountains, New Hampshire, USA: An episode of passive margin rejuvenation? *Geology*, *44*, 415–418. <https://doi.org/10.1130/G37429.1>
- Andreu, B., & Tronchetti, G. (1994). Ostracodes et foraminifères du Crétacé supérieur du synclinal d'El Koubbat, Moyen Atlas, Maroc. Biostratigraphie, Paléoenvironnements, Paléobiogéographie, systématique des ostracodes: Congrès français de stratigraphie, 1, Toulouse.
- Aquit, M., Kuhnt, W., Holbourn, A., Chellai, E. H., Stattegger, K., Kluth, O., & Jabour, H. (2013). Late Cretaceous paleoenvironmental evolution of the Tarfaya Atlantic coastal Basin, SW Morocco. *Cretaceous Research*, *45*, 288–305. <https://doi.org/10.1016/j.cretres.2013.05.004>
- Arab, M., Bracène, R., Roure, F., Zazoun, R. S., Mahdjoub, Y., & Badji, R. (2015). Source rocks and related petroleum systems of the Chelif Basin, (western Tellian domain, north Algeria). *Marine and Petroleum Geology*, *64*, 363–385. <https://doi.org/10.1016/j.marpetgeo.2015.03.017>
- Arantegui, A. (2018). Characterisation of Mesozoic Depositional Systems along the Atlantic Passive Margin of Morocco. North Aaiun-Tarfaya Basin: University of Manchester, Ph.D. Thesis, 169 p.
- Arantegui, A., Jerrett, R., Schröder, S., Bulot, L. G., Gatto, R., Monari, S., & Redfern, J. (2019). Constraining Mesozoic early post-rift depositional systems evolution along the eastern Central Atlantic margin. *Sedimentary Geology*, *386*, 31–51. <https://doi.org/10.1016/j.sedgeo.2019.03.005>
- Azdimouza, A., Bourgeois, J., Poupeau, G., Vázquez, M., Asebriy, L., & Labrin, E. (2013). Fission track thermochronology of the Beni Bousera peridotite massif (Internal Rif, Morocco) and the exhumation of ultramafic rocks in the Gibraltar Arc. *Arabian Journal of Geosciences*, *7*, 1993–2005. <https://doi.org/10.1007/s12517-013-0924-3>

- Azdimousa, A., Jabaloy-Sánchez, A., Talavera, C., Asebriy, L., González-Lodeiro, F., & Evans, N. J. (2019). Detrital zircon U-Pb ages in the Rif Belt (northern Morocco): Paleogeographic implications. *Gondwana Research*, *70*, 133–150. <https://doi.org/10.1016/j.gr.2018.12.008>
- Babault, J., Teixell, A., Arboleya, M. L., & Charroud, M. (2008). A Late Cenozoic age for long-wavelength surface uplift of the Atlas Mountains of Morocco. *Terra Nova*, *20*(2), 102–107. <https://doi.org/10.1111/j.1365-3121.2008.00794.x>
- Balestrieri, M. L., Moratti, G., Bigazzi, G., & Algouti, A. (2009). Neogene exhumation of the Marrakech High Atlas (Morocco) recorded by apatite fission-track analysis. *Terra Nova*, *21*, 75–82. <https://doi.org/10.1111/j.1365-3121.2008.00857.x>
- Barbero, L., Jabaloy, A., Gómez-Ortiz, D., Pérez-Peña, J. V., Rodríguez-Peces, M. J., Tejero, R., Estupiñán, J., Azdimousa, A., Vázquez, M., & Asebriy, L. (2011). Evidence for surface uplift of the Atlas Mountains and the surrounding peripheral plateaux: Combining apatite fission-track results and geomorphic indicators in the Western Moroccan Meseta (coastal Variscan Paleozoic basement). *Tectonophysics*, *502*, 90–104. <https://doi.org/10.1016/j.tecto.2010.01.005>
- Barbero, L., Teixell, A., Arboleya, M.-L., Río, P. D., Reiners, P. W., & Bougadir, B. (2007). Jurassic-to-present thermal history of the central High Atlas (Morocco) assessed by low-temperature thermochronology. *Terra Nova*, *19*, 58–64. <https://doi.org/10.1111/j.1365-3121.2006.00715.x>
- Baudon, C., Fabuel-Perez, I., & Redfern, J. (2009). Structural style and evolution of a Late Triassic rift basin in the Central High Atlas, Morocco: Controls on sediment deposition. *Geological Journal*, *44*, 677–691. <https://doi.org/10.1002/gj.1195>
- Baudon, C., Redfern, J., & Van Den Driessche, J. (2012). Permo-Triassic structural evolution of the Argana Valley, impact of the Atlantic rifting in the High Atlas, Morocco. *Journal of African Earth Sciences*, *65*, 91–104. <https://doi.org/10.1016/j.jafrearsci.2012.02.002>
- Beauvais, L. (1986). Monographie des madréporaires du Jurassique inférieur du Maroc. *Palaontographica*, *194*, 1–68.
- Benest, M. (1985). Evolution de la plate-forme de l'Ouest algérien et du Nord-Ouest marocain au cours du Jurassique supérieur et au début du Crétacé. Stratigraphic, milieux de depot et dynamique sédimentaire: Documents du Laboratoire de Géologie de Lyon, *95*, 581.
- Benvenuti, M., Moratti, G., & Algouti, A. (2017). Stratigraphic and structural revision of the Upper Mesozoic succession of the Dadès valley, eastern Ouarzazate Basin (Morocco). *Journal of African Earth Sciences*, *135*, 1–45. <https://doi.org/10.1016/j.jafrearsci.2017.01.018>
- Benyoucef, M., Malti, F.-Z., Adaci, M., Fellah, A. H., Abbache, A., Cherif, A., Sidhoum, R., & Bensalah, M. (2015). Évolution lithostratigraphique, paléoenvironnementale et paléogéographique du flysch de Ben-Zireg (Viséen inférieur, Algérie). *Geodiversitas*, *37*, 5–29. <https://doi.org/10.5252/g2015n1a1>
- Benzaggagh, M. (2016). Tholeiitic basalts and ophiolitic complexes of the Mesorif Zone (External Rif, Morocco) at the Jurassic-Cretaceous boundary and the importance of the Ouerrha Accident in the palaeogeographic and geodynamic evolution of the Rif Mountains. *Boletín Geológico Y Minero*, *127*, 389–406.
- Benzaggagh, M., Latil, J.-L., Oumhamed, M., & Ferré, B. (2017). Stratigraphic succession (Albian to lower? Cenomanian) and upper Albian ammonites and biozones from the Talerhza Basin (South Riffian Ridges, northern Morocco). *Cretaceous Research*, *73*, 71–90. <https://doi.org/10.1016/j.cretres.2017.01.005>
- Bertotti, G., & Gouiza, M. (2012). Post-rift vertical movements and horizontal deformations in the eastern margin of the Central Atlantic: Middle Jurassic to Early Cretaceous evolution of Morocco. *International Journal of Earth Sciences*, *101*, 2151–2165. <https://doi.org/10.1007/s00531-012-0773-4>
- Best, M. W., & Boekschoten, G. J. (1981). On the coral fauna in the Miocene reef at Baixo, Porto Santo (Eastern Atlantic). *Netherlands Journal of Zoology*, *32*, 412–418.
- Bhattacharya, J. P., Copeland, P., Lawton, T. F., & Holbrook, J. (2016). Estimation of source area, river paleo-discharge, paleoslope, and sediment budgets of linked deep-time depositional systems and implications for hydrocarbon potential. *Earth-Science Reviews*, *153*, 77–110. <https://doi.org/10.1016/j.earscirev.2015.10.013>
- Blain, H.-A., Sesé, C., Rubio-Jara, S., Panera, J., Uribelarrea, D., & Pérez-González, A. (2013). Reconstitution paléoenvironnementale et paléoclimatique du Pléistocène supérieur ancien (MIS 5a) dans le Centre de l'Espagne: Les petits vertébrés (Amphibia, Reptilia and Mammalia) des gisements de HAT et PRERESA (Sud-est de Madrid). *Revue De L'association Française Pour L'étude Du Quaternaire*, *24*, 191–205. <https://doi.org/10.4000/quaternaire.6604>
- Boleli, E. (1952). Plateau des phosphates "hydrogéologie du Maroc": Notes et Mémoires du Service Géologique du Maroc. Vol. 77, 197–204.
- Bourillot, R., Neige, P., Pierre, A., & Durlot, C. (2008). Early-Middle Jurassic Lytoceratid Ammonites with constrictions from Morocco: Palaeobiogeographical and evolutionary implications. *Palaentology*, *51*, 597–609. <https://doi.org/10.1111/j.1475-4983.2008.00766.x>
- Bridwell, R. J. (1976). Lithospheric thinning and the late Cenozoic thermal and tectonic regime of the northern Rio Grande rift: New Mexico Geological Society Field Conference, 27, Vermq'o Park.
- Broutin, J., Aassoumi, H., El Wartiti, M., Freydet, P., Kerp, H., Quesada, C., & Toutin-Morin, N. (1998). The Permian basins of Tiddas, Bou Achouch and Khenifra (Central Morocco). Biostratigraphic and palaeophytogeographic implications. *Mémoires Du Muséum National D'histoire Naturelle*, *179*, 257–278.
- Broutin, J., Ferrandini, J., & Saber, H. (1989). Implications stratigraphiques et paléogéographiques de la découverte d'une flore permienne eur-américaine dans le Haut-Atlas occidental (Maroc). *Comptes rendus de l'Académie des sciences*, Vol. 308 (pp. 1509–1514).
- Brown, R. H. (1980). Triassic rocks of Argana Valley, southern Morocco, and their regional structural implications. *AAPG Bulletin*, *64*, 988–1003.
- Casini, L., Cuccuru, S., Puccini, A., Oggiano, G., & Rossi, P. (2015). Evolution of the corsica-sardinia batholith and late-orogenic shearing of the variscides. *Tectonophysics*, *646*, 65–78. <https://doi.org/10.1016/j.tecto.2015.01.017>
- Cavin, L., Tong, H., Boudad, L., Meister, C., Piuz, A., Tabouelle, J., Aarab, M., Amiot, R., Buffetaut, E., Dyke, G., Hua, S., & Le Loeuff, J. (2010). Vertebrate assemblages from the early Late Cretaceous of southeastern Morocco: An overview. *Journal of African Earth Sciences*, *57*, 391–412. <https://doi.org/10.1016/j.jafrearsci.2009.12.007>
- Chalouan, A., Michard, A., Kadiri El, K., Negro, F., de Lamotte, D. F., Soto, J. I., & Saddiqi, O. (2008). The Rif Belt. In: *Continental Evolution: The Geology of Morocco*. Springer. 203–302.
- Charrière, A., & Haddoumi, H. (2016). Les «Couches rouges» continentales jurassico-crétacées des Atlas marocains (Moyen Atlas, Haut Atlas central et oriental): Bilan stratigraphique, paléogéographies successives et cadre géodynamique. *Boletín Geológico Y Minero*, *127*, 407–430.



- Charton, R. (2018). Phanerozoic Vertical Movements in Morocco. PhD Thesis, TUDelft, 165. <https://doi.org/10.4233/uuid:fda35870-18d9-4ca3-9443-199a1dcb0250>
- Charton, R., Bertotti, G., Arantegui, A., & Bulot, L. (2018). The Sidi Ifni transect across the rifted margin of Morocco (Central Atlantic): Vertical movements constrained by low-temperature thermochronology. *Journal of African Earth Sciences*, *141*, 22–32. <https://doi.org/10.1016/j.jafrearsci.2018.01.006>
- Chevalier, J. P., & Choubert, G. (1962). Les madréporaires miocènes du Maroc. Éditions du Service géologique du Maroc, 173, p. 1–74.
- Chopin, F., Corsini, M., Schulmann, K., El Houicha, M., Ghienne, J.-F., & Edel, J.-B. (2014). Tectonic evolution of the Rehamna metamorphic dome (Morocco) in the context of the Alleghanian-Variscan orogeny. *Tectonics*, *33*, 1154–1177. <https://doi.org/10.1002/2014TC003539>
- Choubert, G., Faure-Muret, A., & Hottinger, L. (1966). Aperçu géologique du bassin côtier de Tarfaya: Editions du Service géologique du Maroc (p. 285).
- Clift, P. D., Dewey, J. F., Draut, A. E., Chew, D. M., Mange, M., & Ryan, P. D. (2004). Rapid tectonic exhumation, detachment faulting and orogenic collapse in the Caledonides of western Ireland. *Tectonophysics*, *384*, 91–113. <https://doi.org/10.1016/j.tecto.2004.03.009>
- Cloetingh, S., & Burov, E. (2011). Lithospheric folding and sedimentary basin evolution: A review and analysis of formation mechanisms. *Basin Research*, *23*, 257–290. <https://doi.org/10.1111/j.1365-2117.2010.00490.x>
- Collier, J. S., McDermott, C., Warner, G., Gyori, N., Schnabel, M., McDermott, K., & Horn, B. W. (2017). New constraints on the age and style of continental breakup in the South Atlantic from magnetic anomaly data. *Earth and Planetary Science Letters*, *477*, 27–40. <https://doi.org/10.1016/j.epsl.2017.08.007>
- Dartevelle, E., & Schwetz, J. (1937). Mollusques récoltés dans le Bas-Congo. *Annales De La Société Royale Zoologique De Belgique*, *68*, 49–65.
- Davies, J. H. F. L., Marzoli, A., Bertrand, H., Youbi, N., Ernesto, M., & Schaltegger, U. (2017). End-Triassic mass extinction started by intrusive CAMP activity: Nature. *Communications*, *8*, 15596. <https://doi.org/10.1038/ncomms15596>
- Davison, I. (2005). Central Atlantic margin basins of North West Africa: Geology and hydrocarbon potential (Morocco to Guinea). *Journal of African Earth Sciences*, *43*, 254–274. <https://doi.org/10.1016/j.jafrearsci.2005.07.018>
- Dhondt, A. V., Malchus, N., Boumaza, L., & Jaillard, E. (1999). Cretaceous Oysters from North Africa: Origin and Distribution. *Bulletin De La Société Géologique De France*, *170*, 67–76.
- Domenech, M. (2015). Rift opening and inversion in the Marrakech High Atlas: integrated structural and thermochronologic study. Universitat Autònoma de Barcelona, Ph.D. Thesis, 157.
- Domènech, M., Stockli, D., & Teixell, A. (2018). Detrital zircon U-Pb provenance and paleogeography of Triassic rift basins in the Marrakech High Atlas. *Terra Nova*, *30*, 310–318. <https://doi.org/10.1111/ter.12340>
- Domènech, M., Teixell, A., & Stöckli, D. F. (2016). Magnitude of rift-related burial and orogenic contraction in the Marrakech High Atlas revealed by zircon (U-Th)/He thermochronology and thermal modeling. *Tectonics*, *35*, 2609–2635. <https://doi.org/10.1002/2016TC004283>
- Doubinger, J. (1956). Contribution à l'étude des flores autuno-stéphaniennes. *Société Géologique De France*, *35*, 1–180.
- Duval-Arnould, A. (2019). Controls on stratigraphic development of shelf margin carbonates. Jurassic Atlantic margin – Essaouira-Agadir Basin, Western Morocco: PhD Thesis, University of Manchester, 287.
- Echarfaoui, H., Hafid, M., Salem, A. AiT., & Abderrahmane, AiT. F. (2002). Analyse sismo-stratigraphique du bassin d'Abda (Maroc occidental), exemple de structures inverses pendant le rifting atlantique. *Comptes Rendus Geoscience*, *334*, 371–377. [https://doi.org/10.1016/S1631-0713\(02\)01768-6](https://doi.org/10.1016/S1631-0713(02)01768-6)
- Ehlers, T. A. (2005). Crustal thermal processes and the interpretation of thermochronometer data. *Reviews in Mineralogy and Geochemistry*, *58*, 315–350. <https://doi.org/10.2138/rmg.2005.58.12>
- El Harfi, A., Lang, J., Salomon, J., & Chellai, E. (2001). Cenozoic sedimentary dynamics of the Ouarzazate foreland basin (Central High Atlas Mountains, Morocco). *International Journal of Earth Sciences*, *90*, 393–411. <https://doi.org/10.1007/s005310000115>
- El Jorfi, L., Süß, M. P., Aigner, T., & Mhammedi, N. (2015). Triassic – quaternary sequence stratigraphy of the tarfaya basin (moroccan Atlantic): structural evolution, eustasy and sedimentation. *Journal of Petroleum Geology*, *38*, 77–98. <https://doi.org/10.1111/jpg.12599>
- El Haimer, F. Z. (2014). Mouvements verticaux post-Varisques des domaines Mesetien et Atlasique: Thermochronology basse température sur apatite et zircon. Université Hassan II, Ph.D. Thesis, 124 p.
- Ellero, A., Malusà, M. G., Ottria, G., Ouanaïmi, H., & Froitzheim, N. (2020). Transpressional structuring of the High Atlas belt, Morocco. *Journal of Structural Geology*, *135*, 104021. <https://doi.org/10.1016/j.jsg.2020.104021>
- Ellouz, N., Patriat, M., Gaulier, J.-M., Bouatmani, R., & Sabounji, S. (2003). From rifting to Alpine inversion: Mesozoic and Cenozoic subsidence history of some Moroccan basins. *Sedimentary Geology*, *156*, 185–212. [https://doi.org/10.1016/S0037-0738\(02\)00288-9](https://doi.org/10.1016/S0037-0738(02)00288-9)
- England, P., & Molnar, P. (1990). Surface uplift, uplift of rocks, and exhumation of rocks. *Geology*, *18*(12), 1173–1177. [https://doi.org/10.1130/0091-7613\(1990\)018<1173:SUORA>2.3.CO;2](https://doi.org/10.1130/0091-7613(1990)018<1173:SUORA>2.3.CO;2)
- Ennouchi, E. (1954). La faune néolithique de Toulkine (Haut Atlas): Comptes rendus des séances mensuelles de la société des sciences naturelles et physiques du Maroc, Vol. 20 (pp. 140–141).
- Essafroui, B., Ferry, S., Groshény, D., Içame, N., El Aouli, H., Masrour, M., Bulot, L. G., Géraud, Y., & Aoutem, M. (2015). Sequence stratigraphic architecture of marine to fluvial deposits across a passive margin (Cenomanian, Atlantic margin, Morocco, Agadir transect). *Carnets de géologie*. <https://doi.org/10.4267/2042/56909>
- Ettachfini, M., Rey, J., Taj-Eddine, K., & Tavera, J. M. (1998). The Valanginian of the Safi Basin (Atlantic Morocco) and its ammonite fauna. *Palaeobiogeographical Implications: Comptes Rendus De L'académie Des Sciences*, *5*, 319–325.
- Fabre, J., Arnaud-Vanneau, A., Belhadj, Z., & Monod, T. (1996). Evolution des terrains méso-cénozoïques d'une marge à l'autre du craton ouest africain, entre le Tanezrouft (Algérie) et l'Adrar de Mauritanie. *Mémoires Du Service Géologique De L'algerie*, *8*, 187–229.
- Fabuel-Perez, I., Redfern, J., & Hodgetts, D. (2009). Sedimentology of an intra-montane rift-controlled fluvial dominated succession: The Upper Triassic Oukaïmeden Sandstone Formation. *Central High Atlas, Morocco: Sedimentary Geology*, *218*, 103–140. <https://doi.org/10.1016/j.sedgeo.2009.04.006>
- Feroni, A. C., Ellero, A., Malusa, M. G., Musumeci, G., Ottria, G., Polino, R., & Leoni, L. (2010). Transpressional tectonics and nappe stacking along the Southern Variscan Front of Morocco.

- International Journal of Earth Sciences*, 99, 1111–1122. <https://doi.org/10.1007/s00531-009-0449-x>
- Fetah, M., Bensaid, M., & Dahmani, M. (1990). Carte Géologique du Maroc. Zawyat Ahancal (1 : 100,000): Ministère de l'Énergie et des Mines.
- Fiechtner, L., Friedrichsen, H., & Hammerschmidt, K. (1992). Geochemistry and geochronology of early mesozoic tholeiites from central Morocco. *Geologische Rundschau*, 81, 45–62. <https://doi.org/10.1007/BF01764538>
- Flowers, R. M., & Ehlers, T. A. (2018). Rock erodibility and the interpretation of low-temperature thermochronologic data. *Earth and Planetary Science Letters*, 482, 312–323. <https://doi.org/10.1016/j.epsl.2017.11.018>
- Frizon de Lamotte, D., Crespo-Blanc, A., Saint-Bézar, B., Comas, M., Fernandez, M., Zeyen, H., Ayarza, P., Robert-Charrue, C., Chalouan, A., & Zizi, M. (2004). TRANSMED Transect I: Iberian Meseta-Guadalquivir Basin–Betic Cordillera-Alboran Sea–Rif–Moroccan Meseta-High Atlas–Sahara Platform. In: *The TRANSMED Atlas: The Mediterranean Region from Crust to Mantle*, Springer, p. 141.
- Frizon de Lamotte, D., Fourdan, B., Leleu, S., Leparmentier, F., & de Clarens, P. (2015). Style of rifting and the stages of Pangea breakup. *Tectonics*, 34, 1009–1029. <https://doi.org/10.1002/2014TC003760>
- Frizon de Lamotte, D., Leturmy, P., Missenard, Y., Khomsi, S., Ruiz, G., Saddiqi, O., Guillocheau, F., & Michard, A. (2009). Mesozoic and Cenozoic vertical movements in the Atlas system (Algeria, Morocco, Tunisia): An overview. *Tectonophysics*, 475(1), 9–28. <https://doi.org/10.1016/j.tecto.2008.10.024>
- Frizon de Lamotte, D., Raulin, C., Mouchot, N., Wrobel-Daveau, J.-C., Blanpied, C., & Ringenbach, J.-C. (2011). The southernmost margin of the Tethys realm during the Mesozoic and Cenozoic: Initial geometry and timing of the inversion processes. *Tectonics*, 30, TC3002. <https://doi.org/10.1029/2010TC002691>
- Frizon de Lamotte, D., Tavakoli-Shirazi, S., Leturmy, P., Averbuch, O., Mouchot, N., Raulin, C., Leparmentier, F., Blanpied, C., & Ringenbach, J. C. (2013). Evidence for Late Devonian vertical movements and extensional deformation in northern Africa and Arabia: Integration in the geodynamics of the Devonian world. *Tectonics*, 32, 107–122. <https://doi.org/10.1002/tect.20007>
- Gaffney, E. S., Tong, H., & Meylan, P. A. (2006). Evolution of the side-necked turtles: The families Bothremydidae, Euraxemydidae, and Araripemydidae. *Bulletin of the American Museum of Natural History*, 300, 698. [https://doi.org/10.1206/0003-0090\(2006\)300\[1:EOTSTT\]2.0.CO;2](https://doi.org/10.1206/0003-0090(2006)300[1:EOTSTT]2.0.CO;2)
- Gallagher, K. (2012). Transdimensional inverse thermal history modeling for quantitative thermochronology. *Journal of Geophysical Research: Solid Earth*, 117, 2156–2202. <https://doi.org/10.1029/2011JB008825>
- Gallagher, K., Brown, R., & Johnson, C. (1998). Fission track analysis and its applications to geological problems. *Annual Review of Earth and Planetary Sciences*, 26, 519–572. <https://doi.org/10.1146/annurev.earth.26.1.519>
- Gallagher, K., Hawkesworth, C. J., & Mantovani, M. S. M. (1994). The denudation history of the onshore continental margin of SE Brazil inferred from apatite fission track data. *Journal of Geophysical Research: Solid Earth*, 99(B9), 18117–18145.
- Ghorbal, B. (2009). Mesozoic to Quaternary thermo-tectonic evolution of Morocco (NW Africa): Vrije Universiteit Amsterdam, Ph.D. Thesis, 226 p.
- Ghorbal, B., Bertotti, G., Foeken, J., & Andriessen, P. (2008). Unexpected Jurassic to Neogene vertical movements in 'stable' parts of NW Africa revealed by low temperature geochronology. *Terra Nova*, 20, 355–363. <https://doi.org/10.1111/j.1365-3121.2008.00828.x>
- Gimeno-Vives, O., Mohn, G., Bosse, V., Haissen, F., Zaghloul, M. N., Atouabat, A., & Frizon de Lamotte, D. (2019). The Mesozoic margin of the Maghreb Tethys in the Rif belt (Morocco): Evidence for polyphase rifting and related magmatic activity. *Tectonics*, 38, 2894–2918. <https://doi.org/10.1029/2019TC005508>
- Gingerich, P. D., & Zouhri, S. (2015). New fauna of archaeocete whales (Mammalia, Cetacea) from the Bartonian middle Eocene of southern Morocco. *Journal of African Earth Sciences*, 111, 273–286. <https://doi.org/10.1016/j.jafrearsci.2015.08.006>
- Girard, J. P., Eichenseer, H., Kabbej, A., & Idris, K. M. (2015). Regional Synthesis of Thermal-Burial Regimes in the Paleozoic-Proterozoic Series of the Taoudeni Basin, Adrar, Mauritania: Fluid Inclusion and Thermochronology Data. In *International Petroleum Technology Conference*. International Petroleum Technology Conference. <https://doi.org/10.2523/IPTC-18423-MS>
- Gomez, F., Beauchamp, W., & Barazangi, M. (2000). Role of the Atlas Mountains (northwest Africa) within the African-Eurasian plate-boundary zone. *Geology*, 28, 775–778. [https://doi.org/10.1130/0091-7613\(2000\)28<775:ROTAMN>2.0.CO;2](https://doi.org/10.1130/0091-7613(2000)28<775:ROTAMN>2.0.CO;2)
- Gouiza, M. (2011). Mesozoic source-to-sink systems in NW Africa: Geology of vertical movements during the birth and growth of the Moroccan rifted margin. Vrije Universiteit Amsterdam, Ph.D. Thesis, 170 p.
- Gouiza, M., Bertotti, G., & Andriessen, P. A. (2018). Mesozoic and Cenozoic thermal history of the Western Reguibat Shield (West African Craton). *Terra Nova*, 30, 135–145. <https://doi.org/10.1111/ter.12318>
- Gouiza, M., Bertotti, G., Charton, R., Haimoudane, K., Dunkl, I., & Anczkiewicz, A. A. (2019). New Evidence of 'Anomalous' Vertical Movements along the Hinterland of the Atlantic NW African Margin. *Journal of Geophysical Research: Solid Earth*, 124(12), 13333–13353. <https://doi.org/10.1029/2019JB017914>
- Gouiza, M., Bertotti, G., Hafid, M., & Cloetingh, S. A. P. L. (2010). Kinematic and thermal evolution of the Moroccan rifted continental margin: Doukkala-High Atlas transect. *Tectonics*, 29(5). <https://doi.org/10.1029/2009TC002464>
- Gouiza, M., Charton, R., Bertotti, G., Andriessen, P., & Storms, J. E. A. (2017). Post-Variscan evolution of the Anti-Atlas belt of Morocco constrained from low-temperature geochronology. *International Journal of Earth Sciences*, 106, 593–616. <https://doi.org/10.1007/s00531-016-1325-0>
- Green, P. F., Japsen, P., Chalmers, J. A., Bonow, J. M., & Duddy, I. R. (2018). Post-breakup burial and exhumation of passive continental margins: Seven propositions to inform geodynamic models. *Gondwana Research*, 53, 58–81. <https://doi.org/10.1016/j.gr.2017.03.007>
- Grimaud, J., Rouby, D., Chardon, D., & Beauvais, A. (2018). Cenozoic sediment budget of West Africa and the Niger delta. *Basin Research*, 30, 169–186. <https://doi.org/10.1111/bre.12248>
- Groune, K., Halim, M., Benmakhlouf, M., Arsalane, S., Lemee, L., & Ambles, A. (2013). Organic geochemical and mineralogical characterization of the Moroccan Rif bituminous rocks. *Journal of Materials and Environmental Science*, 4, 472–481.
- Guillocheau, F., Rouby, D., Robin, C., Helm, C., Rolland, N., Le Carlier de Veslud, C., & Braun, J. (2012). Quantification and causes of the terrigenous sediment budget at the scale of a continental margin: A new method applied to the Namibia-South Africa margin. *Basin Research*, 24, 3–30. <https://doi.org/10.1111/j.1365-2117.2011.00511.x>

- Guimerà, J., Arboleya, M. L., & Teixell, A. (2011). Structural control on present-day topography of a basement massif: The Central and Eastern Anti-Atlas (Morocco). *Geologica Acta: An International Earth Science Journal*, 9, 55–65. <https://doi.org/10.1344/105.000001643>
- Guiraud, R. (1998). Mesozoic rifting and basin inversion along the northern African Tethyan margin: An overview: Geological Society. *London, Special Publications*, 132, 217–229. <https://doi.org/10.1144/GSL.SP.1998.132.01.13>
- Guiraud, R., Bosworth, W., Thierry, J., & Delplanque, A. (2005). Phanerozoic geological evolution of Northern and Central Africa: An overview. *Journal of African Earth Sciences*, 43, 83–143. <https://doi.org/10.1016/j.jafrearsci.2005.07.017>
- Haddoumi, H., Allain, R., Meslouh, S., Metais, G., Monbaron, M., Pons, D., Rage, J. C., Vullo, R., Zouhri, S., & Gheerbrant, E. (2016). Guelb el Ahmar (Bathonian, Anoual Syncline, eastern Morocco): first continental flora and fauna including mammals from the Middle Jurassic of Africa. *Gondwana Research*, 29(1), 290–319.
- Haddoumi, H., Charriere, A., & Mojon, P.-O. (2010). Stratigraphie et sédimentologie des «Couches rouges» continentales du Jurassique-Crétacé du Haut Atlas central (Maroc): implications paléogéographiques et géodynamiques. *Geobios*, 43, 433–451. <https://doi.org/10.1016/j.geobios.2010.01.001>
- Hafid, M., Zizi, M., Bally, A. W., & Ait Salem, A. (2006). Structural styles of the western onshore and offshore termination of the High Atlas, Morocco. *Comptes Rendus Geoscience*, 338, 50–64. <https://doi.org/10.1016/j.crte.2005.10.007>
- Hayford, E. K., Lisker, F., & Apaalse, L. (2008). Cretaceous rifting of the Ghana transform margin-Evidence from on shore apatite fission track data and optimum thermal history models. *Ghana Journal of Science*, 48.
- Helland-Hansen, W., Sømme, T. O., Martinsen, O. J., Lunt, I., & Thurmond, J. (2016). Deciphering earth's natural hourglasses: perspectives on source-to-sink analysis. *Journal of Sedimentary Research*, 86, 1008–1033. <https://doi.org/10.2110/jsr.2016.56>
- Helm, C. (2009). Quantification des flux sédimentaires anciens à l'échelle d'un continent: Le cas de l'Afrique au Méso-Cénozoïque. Université Rennes, Ph.D. Thesis, 364 p.
- Herbig, H. G., & Trappe, J. (1994). Stratigraphy of the Subatlas Group (Maastrichtian-Middle Eocene, Morocco). *Newsletters on Stratigraphy*, 125–165. <https://doi.org/10.1127/nos/30/1994/125>
- Hill, R. V., McCartney, J. A., Roberts, E., Bouaré, M., Sissoko, F., & O'leary, M. A. (2008). Dyrosaurid (Crocodyliformes: Mesoeucrocodylia) Fossils from the Upper Cretaceous and Paleogene of Mali: Implications for Phylogeny and Survivorship across the K/T Boundary. *American Museum Novitates*, 3631, 1–21. <https://doi.org/10.1206/598.1>
- Hmich, D., Schneider, J. W., Saber, H., Voigt, S., & El Wartiti, M. (2006). New continental Carboniferous and Permian faunas of Morocco: Implications for biostratigraphy, palaeobiogeography and palaeoclimate. *Geological Society, London, Special Publications*, 265, 297–324. <https://doi.org/10.1144/GSL.SP.2006.265.01.14>
- Hollard, H., Choubert, G., Bronner, G., Marchand, J., & Sougy, J. (1985). Carte Géologique du Maroc, (1:1,000,000; 2 sheets). Notes et Mémoires du Service Géologique du Maroc.
- Hssaida, T., Chahidi, S., Benzaggagh, M., Riding, J. B., & Oumalch, F. (2014). Associations de kystes de dinoflagellés des séries du Jurassique supérieur (Oxfordien–Tithonien) du Rif externe (Pré-rif interne et Mésorif, Maroc) et comparaisons régionales. *Annales De Paléontologie*, 100(4), 327–342. <https://doi.org/10.1016/j.annpal.2014.03.001>
- Ibrahim, N., Varricchio, D. J., Sereno, P. C., Wilson, J. A., Dutheil, D. B., Martill, D. M., Baidder, L., & Zouhri, S. (2014). Dinosaur Footprints and Other Ichnofauna from the Cretaceous Kem Kem Beds of Morocco. *PLoS One*, 9, e90751–e90815. <https://doi.org/10.1371/journal.pone.0090751>
- Japsen, P., Bonow, J. M., Green, P. F., Chalmers, J. A., & Lidmar-Bergström, K. (2006). Elevated, passive continental margins: Long-term highs or Neogene uplifts? *New Evidence from West Greenland: Earth and Planetary Science Letters*, 248, 330–339. <https://doi.org/10.1016/j.epsl.2006.05.036>
- Japsen, P., Bonow, J. M., Green, P. F., Chalmers, J. A., & Lidmar-Bergström, K. (2009). Formation, uplift and dissection of planation surfaces at passive continental margins - a new approach. *Earth Surface Processes and Landforms*, 34, 683–699. <https://doi.org/10.1002/esp.1766>
- Japsen, P., Bonow, J. M., Green, P. F., Cobbold, P. R., Chiassi, D., Lilletveit, R., Magnavita, L. P., & Pedreira, A. (2012). Episodic burial and exhumation in NE Brazil after opening of the South Atlantic. *Geological Society of America Bulletin*, 124, 800–816. <https://doi.org/10.1130/B30515.1>
- Japsen, P., Chalmers, J. A., Green, P. F., & Bonow, J. M. (2012). Elevated, passive continental margins: Not rift shoulders, but expressions of episodic, post-rift burial and exhumation. *Global and Planetary Change*, 90–91, 73–86. <https://doi.org/10.1016/j.gloplacha.2011.05.004>
- Japsen, P., Green, P. F., Bonow, J. M., Chalmers, J. A., & Rasmussen, E. S. (2016). Burial and exhumation history of southernmost Norway estimated from apatite fission-track analysis data constrained by geological observations and stratigraphic landscape analysis. *NGF Abstract and Proceedings*, 1, 26–28.
- Japsen, P., Green, P. F., Bonow, J. M., Hinchey, A. M., & Wilton, D. H. C. (2016). Burial and exhumation history of the Labrador-Newfoundland margin: first observations. *Geological Survey of Denmark and Greenland (GEUS) Bulletin*, 35, 91–94. <https://doi.org/10.34194/geusb.v35.4947>
- Jelinek, A. R., Chemale, F. Jr, van der Beek, P. A., Guadagnin, F., Cupertino, J. A., & Viana, A. (2014). Denudation history and landscape evolution of the northern East-Brazilian continental margin from apatite fission-track thermochronology. *Journal of South American Earth Sciences*, 54, 158–181. <https://doi.org/10.1016/j.jsames.2014.06.001>
- Jenny, J., & Jossen, J. A. (1982). Découverte d'empreintes de pas de Dinosaures dans le Jurassique inférieur (Pliensbachien) du Haut-Atlas central (Maroc). *Comptes Rendues Hebdomadaires Séances Académie De Sciences*, 294, 223–226.
- Joussiaume, R. (2016). Les relations entre diapirisme et sédimentation: Exemple du Jurassique moyen de la région d'Imilchil, Haut-Atlas central, Maroc. PhD Thesis, Université de Bordeaux.
- Jouve, S., Laroche, M. O., Bouya, B., & Amaghaz, M. (2005). A new dyrosaurid crocodyliform from the Palaeocene of Morocco and a phylogenetic analysis of Dyrosauridae. *Acta Palaeontologica Polonica*, 50, 1–14.
- Juez-Larre, J., & Andriessen, P. (2006). Tectonothermal evolution of the northeastern margin of Iberia since the break-up of Pangea to present, revealed by low-temperature fission-track and (U–Th)/He thermochronology: A case history of the Catalan Coastal Ranges. *Earth and Planetary Science Letters*, 243, 159–180. <https://doi.org/10.1016/j.epsl.2005.12.026>

- Kammerer, C. F., Nesbitt, S. J., & Shubin, N. H. (2011). The first silesaurid dinosauriform from the Late Triassic of Morocco. *Acta Palaeontologica Polonica*, *57*, 277–284. <https://doi.org/10.4202/app.2011.0015>
- Karroum, M., Mandour El, A., Khattach, D., Cassas, A., Himi, M., Rochdane, S., Laftouhi, N.-E., & Khalil, N. (2014). Fonctionnement hydrogéologique du bassin de la Bahira (Maroc central): Apport de l'analyse des données géologiques et gravimétriques. *Canadian Journal of Earth Sciences*, *51*, 517–526. <https://doi.org/10.1139/cjes-2013-0130>
- Ketcham, R. A. (2005). Forward and inverse modeling of low-temperature thermochronometry data. *Reviews in Mineralogy and Geochemistry*, *58*, 275–314. <https://doi.org/10.2138/rmg.2005.58.11>
- Ketcham, R. A., Donelick, R. A., & Donelick, M. B. (2000). AFTSolve: A program for multi-kinetic modeling of apatite fission-track data. *Geological Materials Research*, *2*, 1–32.
- Koeniguer, J.-C. (1967). Etude paléoxylologique du rio de oro. *Notas Y Comunicaciones Instituto Geologico Y Minero De España*, *96*, 39–66.
- Krencker, F. N., Fantasia, A., Danisch, J., Martindale, R., Kabiri, L., El Ouali, M., & Bodin, S. (2020). Two-phased collapse of the shallow-water carbonate factory during the late Pliensbachian-Toarcian driven by changing climate and enhanced continental weathering in the Northwestern Gondwana Margin. *Earth-Science Reviews*, 103254. [https://www.sciencedirect.com/science/article/pii/S0012825220303007?casa\\_token=eps3KNGXtUoAAAAA:UO889mmTKGyZDz5c8DR6ghgF\\_uFwWzKQO5od6eSWW6CB0AcUhfTULAsWXkqBq1qxOgduh90aLFY](https://www.sciencedirect.com/science/article/pii/S0012825220303007?casa_token=eps3KNGXtUoAAAAA:UO889mmTKGyZDz5c8DR6ghgF_uFwWzKQO5od6eSWW6CB0AcUhfTULAsWXkqBq1qxOgduh90aLFY)
- Labails, C., Olivet, J.-L., Aslanian, D., & Roest, W. R. (2010). An alternative early opening scenario for the Central Atlantic Ocean. *Earth and Planetary Science Letters*, *297*, 355–368. <https://doi.org/10.1016/j.epsl.2010.06.024>
- Lafforgue, L. (2016). Place de la minéralisation de manganèse de Bouarfâ dans l'évolution méso-cénozoïque de l'oriental marocain. Doctoral dissertation, Paris Saclay, 360.
- Lagnaoui, A., Klein, H., Saber, H., Fekkak, A., Belahmira, A., & Schneider, J. W. (2016). New discoveries of archosaur and other tetrapod footprints from the Timezgadiouine Formation (Irohalene Member, Upper Triassic) of the Argana Basin, western High Atlas, Morocco – Ichnotaxonomic implications. *Palaeogeography, Palaeoclimatology, Palaeoecology*, *453*, 1–9. <https://doi.org/10.1016/j.palaeo.2016.03.022>
- Lanari, R., Fellin, M. G., Faccenna, C., Balestrieri, M. L., Pazzaglia, F. J., Youbi, N., & Maden, C. (2020). Exhumation and surface evolution of the Western High-Atlas and surrounding regions as constrained by low-temperature thermochronology. *Tectonics*, *39*(3), 2019TC005562. <https://doi.org/10.1029/2019TC005562>
- Laville, E., & Piqué, A. (1992). Jurassic penetrative deformation and Cenozoic uplift in the central High Atlas (Morocco): a tectonic model. *Structural and orogenic inversions. Geologische Rundschau*, *81*(1), 157–170.
- Le Roy, P., Piqué, A., Le Gall, B., Ait Brahim, L., Morabet, A. M., & Demnati, A. (1997). Les bassins cotiers triasico-liasiques du Maroc occidental et la diachronie du rifting intra-continental de l'Atlantique central. *Bulletin De La Société Géologique De France*, *168*, 637–648.
- Lee, C. W. (1983). Bivalve mounds and reefs of the Central High Atlas, Morocco: palaeogeography. *Palaeoclimatology, Palaeoecology*, *43*, 153–168. [https://doi.org/10.1016/0031-0182\(83\)90052-4](https://doi.org/10.1016/0031-0182(83)90052-4)
- Leleu, S., Hartley, A. J., van Oosterhout, C., Kennan, L., Ruckwied, K., & Gerdes, K. (2016). Structural, stratigraphic and sedimentological characterisation of a wide rift system: The Triassic rift system of the Central Atlantic Domain. *Earth Science Reviews*, *158*, 89–124. <https://doi.org/10.1016/j.earscirev.2016.03.008>
- Leprêtre, R. (2015). Evolution Phanérozoïque du Craton Ouest Africain et de ses bordures Nord et Ouest. Université Paris 11, Ph.D. Thesis, 423.
- Leprêtre, R., Barbarand, J., Missenard, Y., Gautheron, C., Pinna-Jamme, R., & Saddiqi, O. (2017). Mesozoic evolution of NW Africa: Implications for the Central Atlantic Ocean dynamics. *Journal of the Geological Society*, *174*, 817–835. <https://doi.org/10.1144/jgs2016-100>
- Leprêtre, R., Barbarand, J., Missenard, Y., & Leparmentier, F. (2014). Vertical movements along the northern border of the West African Craton: The Reguibat Shield and adjacent basins. *Geological Magazine*, *151*, 1–14.
- Leprêtre, R., Frizon de Lamotte, D., Combiér, V., Gimeno-Vives, O., Mohn, G., & Eschard, R. (2018). The Tell-Riforogenic system (Morocco, Algeria, Tunisia) and the structural heritage of the southern Tethys margin: BSGF. *BSGF-Earth Sciences Bulletin*, *189*, 10. <https://doi.org/10.1051/bsgf/2018009>
- Leprêtre, R., Missenard, Y., Barbarand, J., Gautheron, C., Saddiqi, O., & Pinna-Jamme, R. (2015). Postrift history of the eastern central Atlantic passive margin: Insights from the Saharan region of South Morocco. *Journal of Geophysical Research: Solid Earth*, *120*, 4645–4666. <https://doi.org/10.1002/2014JB011549>
- Leroy, M., Gueydan, F., & Dauteuil, O. (2008). Uplift and strength evolution of passive margins inferred from 2-D conductive modelling. *Geophysical Journal International*, *172*, 464–476. <https://doi.org/10.1111/j.1365-246X.2007.03566.x>
- Logan, P., & Duddy, I. (1998). An investigation of the thermal history of the Ahnet and Reggane Basins, Central Algeria, and the consequences for hydrocarbon generation and accumulation. *Geological Society, London, Special Publications*, *132*, 131–155. <https://doi.org/10.1144/GSL.SP.1998.132.01.07>
- Lorenz, J. C. (1988). Synthesis of Late Paleozoic and Triassic red-bed sedimentation in Morocco. In: *The Atlas System of Morocco* Springer, p. 139–168.
- Luber, T. (2017). Integrated Analysis of Lower Cretaceous Stratigraphy and depositional systems: The Essaouira-Agadir basin of Morocco. University of Manchester, Ph.D. Thesis, 257 p.
- Luth, S. W., & Willingshofer, E. (2008). Mapping of the post-collisional cooling history of the Eastern Alps. *Swiss Journal of Geosciences*, *101*, 207–223. <https://doi.org/10.1007/s00015-008-1294-9>
- Mader, N. K., Redfern, J., & El Ouataoui, M. (2017). Sedimentology of the Essaouira Basin (Meskala Field) in context of regional sediment distribution patterns during upper Triassic pluvial events. *Journal of African Earth Sciences*, *130*, 293–318. <https://doi.org/10.1016/j.jafrearsci.2017.02.012>
- Mahammed, F., Läng, E., Mami, L., Mekahli, L., Benhamou, M., Bouterfa, B., Kacemi, A., Chérif, S.-A., Chaouati, H., & Taquet, P. (2005). The 'giant of Ksour', a Middle Jurassic sauropod dinosaur from Algeria. *Comptes Rendus Palevol*, *4*, 707–714. <https://doi.org/10.1016/j.crpv.2005.07.001>
- Malaval, M. (2016). Enregistrement sédimentaire de l'activité diapirique associée à la ride du Jbel Azourki, Haut Atlas central, Maroc: impact sur la géométrie des dépôts et la distribution des faciès des systèmes carbonatés et mixtes du Jurassique inférieur. PhD Thesis, Université Bordeaux 3.
- Malusà, M. G., Danisik, M., & Kuhlemann, J. (2016). Tracking the Adriatic-slab travel beneath the Tethyan margin of Corsica-Sardinia

- by low-temperature thermochronology. *Gondwana Research*, 31, 135–149. <https://doi.org/10.1016/j.gr.2014.12.011>
- Malusà, M. G., & Fitzgerald, P. G. (2019a). Fission-Track Thermochronology and its Application to Geology: Springer Textbooks in Earth Sciences, Geography and Environment. Springer, Cham, 393 p. <https://doi.org/10.1007/978-3-319-89421-8>
- Malusà, M. G., & Fitzgerald, P. G. (2019b). From Cooling to Exhumation: Setting the Reference Frame for the Interpretation of Thermochronologic Data. In M. Malusà, & P. Fitzgerald (Eds.), *Fission-Track Thermochronology and its Application to Geology: Springer Textbooks in Earth Sciences, Geography and Environment* (pp. 147–164). Springer.
- Malusà, M. G., Polino, R., Feroni, A. C., Ellero, A., Ottria, G., Baidder, L., & Musumeci, G. (2007). Post-Variscan tectonics in eastern Anti-Atlas (Morocco). *Terra Nova*, 19, 481–489. <https://doi.org/10.1111/j.1365-3121.2007.00775.x>
- Mansour, E. M. (1991). Thermochronologie par la méthode des traces de fission dans l'apatite. Application aux massifs de l'Argentera-Mercantour (Alpes occidentales) et des Jebilet (Meseta marocaine). Université Joseph-Fourier - Grenoble I, PhD Thesis, 197 p.
- Manspeizer, W., Puffer, J. H., & Cousminer, H. L. (1978). Separation of Morocco and eastern North America: A Triassic-Liassic stratigraphic record. *Geological Society of America Bulletin*, 89, 901–920. [https://doi.org/10.1130/0016-7606\(1978\)89<901:SOMAEN>2.0.CO;2](https://doi.org/10.1130/0016-7606(1978)89<901:SOMAEN>2.0.CO;2)
- Mareschal, J. C., & Jaupart, C. (2004). Variations of surface heat flow and lithospheric thermal structure beneath the North American craton. *Earth and Planetary Science Letters*, 223, 65–77. <https://doi.org/10.1016/j.epsl.2004.04.002>
- Marivaux, L., Adnet, S., Benammi, M., Tabuce, R., & Benammi, M. (2017). Anomaluroid rodents from the earliest Oligocene of Dakhla, Morocco, reveal the long-lived and morphologically conservative pattern of the Anomaluridae and Nonanomaluridae during the Tertiary in Africa. *Journal of Systematic Palaeontology*, 15, 539–569. <https://doi.org/10.1080/14772019.2016.1206977>
- Marzoli, A., Davies, J. H. F. L., Youbi, N., Merle, R., Corso, J. D., Dunkley, D. J., Fioretti, A. M., Bellieni, G., Medina, F., Wotzlaw, J.-F., McHone, G., Font, E., & Bensalah, M. K. (2017). Proterozoic to Mesozoic evolution of North-West Africa and Peri-Gondwana microplates: Detrital zircon ages from Morocco and Canada. *Lithos*, 278, 1–44. <https://doi.org/10.1016/j.lithos.2017.01.016>
- Matton, G., & Jébrak, M. (2009). The Cretaceous Peri-Atlantic Alkaline Pulse (PAAP): Deep mantle plume origin or shallow lithospheric break-up? *Tectonophysics*, 469, 1–12. <https://doi.org/10.1016/j.tecto.2009.01.001>
- Mazzoli, S., Jankowski, L., Szaniawski, R., & Zattin, M. (2010). Low-T thermochronometric evidence for post-thrusting (<11 Ma) exhumation in the Western Outer Carpathians, Poland. *Comptes Rendus Geoscience*, 342, 162–169. <https://doi.org/10.1016/j.crte.2009.11.001>
- Meister, C., Piuze, A., Cavin, L., Boudad, L., Bacchia, F., Ettachfani, E. M., & Benyoucef, M. (2017). Late Cretaceous (Cenomanian-Turonian) ammonites from southern Morocco and south western Algeria. *Arabian Journal of Geosciences*, 10(1), 1. <https://doi.org/10.1007/s12517-016-2714-1>
- Mekahli, L., Elmi, S., & Benhamou, M. (2004). Biostratigraphy, sedimentology and tectono-eustatic events of the Lower and Middle Jurassic of the Ksour Mountains (Western Saharian Atlas, Southern Algeria). *International Geological Congress*, 32, Florence.
- Merino-Tomé, Ó., Della Porta, G., Pierre, A., Kenter, J. A. M., Durllet, C., & Verwer, K. (2017). Intact seismic-scale platforms and ramps in the Lower to Middle Jurassic of Morocco: Implications for stratal anatomy and lithofacies partitioning. *AAPG Bulletin*, 101, 205–513. <https://doi.org/10.1306/011817DIG17029>
- Michard, A., Ibouh, H., & Charrière, A. (2011). Syncline-topped anticlinal ridges from the High Atlas: A Moroccan conundrum, and inspiring structures from the Syrian Arc, Israel. *Terra Nova*, 23, 314–323. <https://doi.org/10.1111/j.1365-3121.2011.01016.x>
- Michard, A., Saddiqi, O., Chalouan, A., & de Lamotte, D. F. (2008). Continental Evolution: The Geology of Morocco. Springer, 424 p.
- Michard, A., Soulaïmani, A., Hoepffner, C., Ouanaïmi, H., Baidder, L., Rjimat, E. C., & Saddiqi, O. (2010). The South-Western Branch of the Variscan Belt: Evidence from Morocco. *Tectonophysics*, 492, 1–24. <https://doi.org/10.1016/j.tecto.2010.05.021>
- Middlemiss, F. A. (1980). Lower Cretaceous Terebratulidae from south-western Morocco and their biogeography. *Palaeontology*, 23, 515–556.
- Miles, P., Bouysse, P., & De Souza, K. (2012). Structural Map of the Atlantic Ocean, CCGM-CGMW.
- Missenard, Y. (2006). Le relief des Atlas Marocains: Contribution des processus asthénosphériques et du raccourcissement crustal, aspects chronologiques. Université de Cergy Pontoise, Ph.D. Thesis, 236 p.
- Missenard, Y., & Cadoux, A. (2011). Can Moroccan Atlas lithospheric thinning and volcanism be induced by Edge-Driven Convection? *Terra Nova*, 24, 27–33. <https://doi.org/10.1111/j.1365-3121.2011.01033.x>
- Monbaron, M. (1978). New Occurrences Of Big Dinosaurian Bones In The Jurassic-Cretaceous Basin Of Taguelft (Atlas Of Beni-mellal, Morocco). *Comptes Rendus Hebdomadaires Des Seances De L'Academie Des Sciences*, 287, 1277–1279.
- Monbaron, M., & Taquet, P. (1981). Découverte du squelette complet d'un grand Cétiosaure (Dinosaure Sauropode) dans le bassin jurassique moyen de Tilougguit (Haut-Atlas central, Maroc). *Compte Rendu De L'Academie Des Sciences De Paris*, 292, 243–246.
- Montero, P., Haissen, F., Mouttaqi, A., Molina, J. F., Errami, A., Sadki, O., Cambeses, A., & Bea, F. (2016). Contrasting SHRIMP U-Pb zircon ages of two carbonatite complexes from the peri-cratonic terranes of the reguibat shield: Implications for the lateral extension of the West African craton. *Gondwana Research*, 38, 238–250. <https://doi.org/10.1016/j.gr.2015.12.005>
- Moragas, M., Vergés, J., Saura, E., Martín-Martín, J., Messenger, G., Merino-Tomé, Ó., Suárez-Ruiz, I., Razin, P., Grélaud, C., Malaval, M., Joussiaume, R., & Hunt, D. W. (2018). Jurassic rifting to post-rift subsidence analysis in the Central High Atlas and its relation to salt diapirism. *Basin Research*, 30, 336–362. <https://doi.org/10.1111/bre.12223>
- Mourlot, Y., Roddaz, M., Dera, G., Calvès, G., Kim, J.-H., Chaboureaud, A.-C., Mounic, S., & Raïsson, F. (2018). Geochemical evidence for large-scale drainage reorganization in Northwest Africa during the Cretaceous. *Geochemistry, Geophysics, Geosystems*, 19, 1690–1712. <https://doi.org/10.1029/2018GC007448>
- Mulder, E. W., Bardet, N., Godefroit, P., & Jagt, J. W. (2000). *Elasmosaur remains from the Maastrichtian type area, and a review of latest Cretaceous elasmosaurs (Reptilia, Plesiosauroidea): Bulletin de l'Institut royal des Sciences naturelles de Belgique*, Vol. 70 (pp. 161–178).
- Najih, A., Montero, P., Verati, C., Charaf Chabou, M., Fekkak, A., Baidder, L., Ezzouhairi, H., Bea, F., & Michard, A. (2019). Initial

- Pangean rifting north of the West African Craton: Insights from late Permian U-Pb and  $40\text{Ar}/39\text{Ar}$  dating of alkaline magmatism from the Eastern Anti-Atlas (Morocco). *Journal of Geodynamics*, *132*, 101670. <https://doi.org/10.1016/j.jog.2019.101670>
- Nemčok, M., Stuart, C., Segall, M. P., & Allen, R. B. (2005). Structural development of southern Morocco: Interaction of tectonics and deposition. Annual Bob F. Perkins Research Conference, 25, Houston. 151–202.
- Nouri, J., Díaz-Martínez, I., & Pérez-Lorente, F. (2011). Tetractyl Footprints of an Unknown Affinity Theropod Dinosaur from the Upper Jurassic of Morocco (C. Lalueza-Fox, Ed.). *PLoS One*, *6*, e26882–e26887. <https://doi.org/10.1371/journal.pone.0026882>
- Oujahin, B., Daoudi, L., Laduron, D., Rocha, F., & Naud, J. (2011). Jurassic Clay Mineral Sedimentation Control Factors in the Essaouira Basin (Western High Atlas, Morocco). *Geologica Belgica*, *14*, 129–141.
- Oujidi, M., & Elmi, S. (2000). Evolution de l'architecture des monts d'Oujda (Maroc oriental) pendant le Trias et au début du Jurassique. *Bulletin De La Société Géologique De France*, *171*, 169–179. <https://doi.org/10.2113/171.2.169>
- Oukassou, M., Charrière, A., Lagnaoui, A., Gibb, S., Michard, A., & Saddiqi, O. (2016). First occurrence of the Ichnogenus *Selenichnites* from the Middle Jurassic Strata of the Skoura Syncline (Middle Atlas, Morocco). *Palaeoecological and Palaeoenvironmental Context: Comptes Rendus Palevol*, *15*, 461–471. <https://doi.org/10.1016/j.crpv.2015.09.013>
- Oukassou, M., Saddiqi, O., Barbarand, J., Sebti, S., Baïdier, L., & Michard, A. (2013). Post-Variscan exhumation of the Central Anti-Atlas (Morocco) constrained by zircon and apatite fission-track thermochronology. *Terra Nova*, *25*, 151–159. <https://doi.org/10.1111/ter.12019>
- Ourribane, M., Chellai, E. H., & Zaghib-Turki, D. (2000). Rôle des microbialites et des «micro-encroûtants» dans la lithification récifale: Exemples du Jurassique supérieur de l'Atlas maghrébin (Maroc et Tunisie). *Comptes Rendus De L'académie Des Sciences*, *330*, 407–414. [https://doi.org/10.1016/S1251-8050\(00\)00157-9](https://doi.org/10.1016/S1251-8050(00)00157-9)
- Pagel, M., Barbarand, J., Beaufort, D., Gautheron, C., & Pironon, J. (2014). Bassins sédimentaires Les marqueurs de leur histoire thermique. Ed Sciences, Société Géologique de France (p. 226).
- Perez, N. D., Teixell, A., Gómez-Gras, D., & Stockli, D. F. (2019). Reconstructing extensional basin architecture and provenance in the Marrakech High Atlas of Morocco: Implications for rift basins and inversion tectonics. *Tectonics*, *38*(5), 1584–1608. <https://doi.org/10.1029/2018TC005413>
- Piqué, A., Soulaïmani, A., Laville, E., Amrhar, M., Bouabdelli, M., Hoepffner, C., & Chalouan, A. (2006). Géologie du Maroc: Editions Geode. 287 p
- Pratt, J. R., Barbeau, D. L. Jr, Garver, J. I., Emran, A., & Izykowski, T. M. (2015). Detrital Zircon Geochronology of Mesozoic Sediments in the Rif and Middle Atlas Belts of Morocco: Provenance Constraints and Refinement of the West African Signature. *The Journal of Geology*, *123*, 177–200. <https://doi.org/10.1086/681218>
- Rage, J.-C. (1976). Les Squamates du Miocène de Beni Mella, Maroc. *Géologie Méditerranéenne*, *3*, 57–69.
- Rage, J.-C., & Wouters, G. (1979). Découverte du plus ancien Palaeopheidé (Reptilia, Serpentes) dans le Maestrichtien du Maroc. *Geobios*, *12*, 293–296.
- Ranke, U., & von Rad, U., Wissmann, G. (1982). Stratigraphy, Facies and Tectonic Development of the On- and Offshore Aaiun-Tarfaya Basin — A Review. In: *Geology of the Northwest African Continental Margin*, Springer. 86–105.
- Romagny, A., Münch, P., Cornée, J. J., Corsini, M., Azdimousa, A., Melinte-Dobrinescu, M. C., Drinia, H., Bonno, M., Arnaud, N., Monié, P., Quillévéré, F., & Ben Moussa, A. (2014). Late Miocene to present-day exhumation and uplift of the Internal Zone of the Rif chain: Insights from low-temperature thermochronometry and basin analysis. *Journal of Geodynamics*, *77*, 39–55. <https://doi.org/10.1016/j.jog.2014.01.006>
- Ruiz, G. M. H., Sebti, S., Negro, F., Saddiqi, O., Frizon de Lamotte, D., Stockli, D., Foeken, J., Stuart, F., Barbarand, J., & Schaer, J. P. (2011). From central Atlantic continental rift to Neogene uplift - western Anti-Atlas (Morocco). *Terra Nova*, *23*, 35–41. <https://doi.org/10.1111/j.1365-3121.2010.00980.x>
- Sabil, N. (1995). La datation par traces de fission: Aspects méthodologiques et applications thermochronologiques en contexte alpin et de marge continentale. Université de Grenoble, Ph.D. Thesis, 245 p.
- Saddiqi, O., El Haimer, F.-Z., Michard, A., Barbarand, J., Ruiz, G., Mansour, E. M., Leturmy, P., & Frizon de Lamotte, D. (2009). Apatite fission-track analyses on basement granites from south-western Meseta, Morocco: Paleogeographic implications and interpretation of AFT age discrepancies. *Tectonophysics*, *475*, 29–37. <https://doi.org/10.1016/j.tecto.2009.01.007>
- Saint-Martin, J.-P. (1990). Les formations récifales coralliennes du Miocène supérieur d'Algérie et du Maroc. *Mémoires Du Muséum National D'histoires Naturelles De Paris*, *56*, 1–373.
- Samaka, F., & Bouhaddioui, D. (2003). Evaluation du Potentiel Petrolier du Bassin de Souss et de l'Offshore d'Agadir. ONHYM, Rapport inédit, 34 p.
- Sanders, M. T., Bardin, J., Benzaggagh, M., & Cecca, F. (2015). Early Toarcian (Jurassic) belemnites from northeastern Gondwana (South Riffian ridges, Morocco). *Paläontologische Zeitschrift*, *89*, 51–62. <https://doi.org/10.1007/s12542-013-0214-0>
- Scotese, C. R. (2012). The Paleomap Project. [www.scotese.com](http://www.scotese.com)
- Sebti, S. (2011). Mouvements verticaux de l'Anti-Atlas occidental marocain (Kerdous and Ifni). Thermochronologie par traces de fission: Université Hassan II, Ph.D. Thesis, 172 p.
- Sebti, S., Saddiqi, O., El Haimer, F. Z., Michard, A., Ruiz, G., Bousquet, R., & de Lamotte, D. F. (2009). Vertical movements at the fringe of the West African Craton: First zircon fission track datings from the Anti-Atlas Precambrian basement, Morocco. *Comptes Rendus Geoscience*, *341*(1), 71–77.
- Sehrt, M. (2014). Variscan to Neogene long-term landscape evolution at the Moroccan passive continental margin (Tarfaya Basin and western Anti-Atlas). University of Heidelberg, Ph.D. Thesis, 174 p.
- Sehrt, M., Glasmacher, U. A., Stockli, D. F., Jabour, H., & Kluth, O. (2017a). The southern Moroccan passive continental margin: An example of differentiated long-term landscape evolution in Gondwana. *Gondwana Research*, *53*, 129–144. <https://doi.org/10.1016/j.gr.2017.03.013>
- Sehrt, M., Glasmacher, U. A., Stockli, D. F., Jabour, H., & Kluth, O. (2017b). Meso-/Cenozoic long-term landscape evolution at the southern Moroccan passive continental margin, Tarfaya Basin, recorded by low-temperature thermochronology. *Tectonophysics*, *717*, 499–518. <https://doi.org/10.1016/j.tecto.2017.08.028>
- Şengör, A. M. C., Özeren, S., Genç, T., & Zor, E. (2003). East Anatolian high plateau as a mantle-supported, north-south shortened domal structure. *Geophysical Research Letters*, *30*(24). <https://doi.org/10.1029/2003GL017858>

- Serge, E. L. M. I., Marok, A., Sebane, A., & Almeras, Y. (2009). Importance of the Mellala section (Traras Mountains, northwestern Algeria) for the correlation of the Pliensbachian-Toarcian boundary. *Volumina Jurassica*, 7(1), 37–46.
- Sibuet, J.-C., Rouzo, S., Srivastava, S., Dehler, S., Deptuck, M., & Karim, A. (2012). Plate tectonic reconstructions and paleogeographic maps of the central and North Atlantic oceans. *Canadian Journal of Earth Sciences*, 49, 1395–1415. <https://doi.org/10.1139/e2012-071>
- Sloss, L. L., & Scherer, W. (1975) Geometry of Sedimentary Basins: Applications to Devonian of North America and Europe. In: Whitten, E.H.T. Quantitative Studies in the Geological Sciences. *Geological Society of America Memoir*, 142, 71–88. <https://doi.org/10.1130/MEM142-p71>
- Stampfli, G. M., & Borel, G. D. (2002). A plate tectonic model for the Paleozoic and Mesozoic constrained by dynamic plate boundaries and restored synthetic oceanic isochrons. *Earth and Planetary Science Letters*, 196, 17–33. [https://doi.org/10.1016/S0012-821X\(01\)00588-X](https://doi.org/10.1016/S0012-821X(01)00588-X)
- Steiner, C., Hobson, A., Favre, P., Stampfli, G. M., & Hernandez, J. (1998). Mesozoic sequence of Fuerteventura (Canary Islands): Witness of Early Jurassic sea-floor spreading in the central Atlantic. *Geological Society of America Bulletin*, 110, 1304–1317. [https://doi.org/10.1130/0016-7606\(1998\)110<1304:MSOFCI>2.3.CO;2](https://doi.org/10.1130/0016-7606(1998)110<1304:MSOFCI>2.3.CO;2)
- Stets, J. (1992). Mid-Jurassic events in the western High Atlas (Morocco). *Geologische Rundschau*, 81, 69–84. <https://doi.org/10.1007/BF01764540>
- Tabuce, R., Adnet, S., Cappetta, H., Noubhani, A., & Quillevère, F. (2005). Aznag (Ouarzazate basin, Morocco), a new African middle Eocene (Lutetian) vertebrate-bearing locality with selachians and mammals. *Bulletin De La Société Géologique De France*, 176, 381–400. <https://doi.org/10.2113/176.4.381>
- Tari, G., & Jabour, H. (2013). Salt tectonics along the Atlantic margin of Morocco. *Geological Society, London, Special Publications*, 369, 337–353. <https://doi.org/10.1144/SP369.23>
- Teixell, A., Ayarza, P., Zeyen, H., Fernandez, M., & Arboleya, M.-L. (2005). Effects of mantle upwelling in a compressional setting: The Atlas Mountains of Morocco. *Terra Nova*, 17, 456–461. <https://doi.org/10.1111/j.1365-3121.2005.00633.x>
- Teixell, A., Bertotti, G., de Lamotte, D. F., & Charroud, M. (2009). The geology of vertical movements of the lithosphere: An overview. *Tectonophysics*, 475, 1–8. <https://doi.org/10.1016/j.tecto.2009.08.018>
- Tinker, J., de Wit, M., & Brown, R. (2008). Linking source and sink: Evaluating the balance between onshore erosion and offshore sediment accumulation since Gondwana break-up, South Africa. *Tectonophysics*, 455(1–4), 94–103. <https://doi.org/10.1016/j.tecto.2007.11.040>
- Trappe, J. (1991). Stratigraphy, facies distribution and paleogeography of the marine Paleogene from the Western High Atlas. *Morocco: Neues Jahrbuch Für Geologie Und Paläontologie*, 180, 279–321.
- van den Bogaard, P. (2013). The origin of the Canary Island Seamount Province - New ages of old seamounts. *Scientific Reports*, 3(1), 21077. <https://doi.org/10.1038/srep02107>
- van der Beek, P., Mbede, E., Andriessen, P., & Delvaux, D. (1998). Denudation history of the Malawi and Rukwa Rift flanks (East African Rift System) from apatite fission track thermochronology. *Journal of African Earth Sciences*, 26, 363–385. [https://doi.org/10.1016/S0899-5362\(98\)00021-9](https://doi.org/10.1016/S0899-5362(98)00021-9)
- Verati, C., Rapaille, R., Feraud, G., Marzoli, A., Bertrand, H., & Youbi, N. (2007). <sup>40</sup>Ar/<sup>39</sup>Ar ages and duration of the Central Atlantic Magmatic Province volcanism in Morocco and Portugal and its relation to the Triassic–Jurassic boundary. *Palaeogeography, Palaeoclimatology, Palaeoecology*, 244(1–4), 308–325. <https://doi.org/10.1016/j.palaeo.2006.06.033>
- Vermesch, P., & Tian, Y. (2014). Thermal history modelling: HeFTy vs. QTQt. *Earth Science Reviews*, 139, 279–290. <https://doi.org/10.1016/j.earscirev.2014.09.010>
- Wang, J. (2018). Controls on the organic-rich mudstones development across the Cenomanian-Turonian Oceanic Anoxic Event (OAE2) in Moroccan Basins. PhD Thesis, University of Manchester, 248 p.
- Wildman, M., Brown, R., Watkins, R., Carter, A., Gleadow, A., & Summerfield, M. (2015). Post break-up tectonic inversion across the southwestern cape of South Africa: New insights from apatite and zircon fission track thermochronometry. *Tectonophysics*, 654, 30–55. <https://doi.org/10.1016/j.tecto.2015.04.012>
- Wildman, M., Webster, D., Brown, R., Chardon, D., Rouby, D., Ye, J., & Dall'Asta, M. (2019). Long-term evolution of the West African transform margin: estimates of denudation from Benin using apatite thermochronology. *Journal of the Geological Society*, 176(1), 97–114.
- Wildman, M., Cogné, N., & Beucher, R. (2019). Fission-Track Thermochronology Applied to the Evolution of Passive Continental Margins. In M. Malusà, & P. Fitzgerald (Eds.), *Fission-Track Thermochronology and its Application to Geology. Springer Textbooks in Earth Sciences, Geography and Environment* (pp. 351–371). Springer.
- Wipf, M., Glasmacher, U. A., Stockli, D. F., Emmerich, A., Bechstädt, T., & Baur, H. (2009). Reconstruction of the differentiated long-term exhumation history of Fuerteventura, Canary Islands, Spain, through fission-track and (U-Th-Sm)/He data. *International Journal of Earth Sciences*, 99, 675–686. <https://doi.org/10.1007/s00531-008-0415-z>
- Withjack, M. O., & Schlische, R. W. (2005). A Review of Tectonic Events on the Passive Margin of Eastern North America. Bob S. Perkins Research Conference, 25, Houston, p. 203–235.
- Wrtiti, M. E., Broutin, J., Freytet, P., Larhib, M., & Toutin-Morin, N. (1990). Continental deposits in Permian basins of the Mesetian Morocco, geodynamic history. *Journal of African Earth Sciences*, 10, 361–368. [https://doi.org/10.1016/0899-5362\(90\)90067-O](https://doi.org/10.1016/0899-5362(90)90067-O)
- Yamato, P., Husson, L., Becker, T. W., & Pedoja, K. (2013). Passive margins getting squeezed in the mantle convection vice. *Tectonics*, 32, 1559–1570. <https://doi.org/10.1002/2013TC003375>
- Ye, J. (2016). Evolution topographique, tectonique et sédimentaire syn-à post-rift de la marge transformante ouest africaine. GET Toulouse, PhD Thesis, 273 p.
- Ye, J., Chardon, D., Rouby, D., Guillocheau, F., Dall'asta, M., Ferry, J.-N., & Broucke, O. (2017). Paleogeographic and structural evolution of northwestern Africa and its Atlantic margins since the early Mesozoic. *Geosphere*, 13, 1254–1284. <https://doi.org/10.1130/GES01426.1>
- Zarhloule, Y. (2004). Le Gradient Géothermique Profond Du Maroc: Détermination Et Cartographie. *Bulletin De L'institut Scientifique De Rabat*, 26, 11–25.
- Zeyen, H., Ayarza, P., Fernández, M., & Rimi, A. (2005). Lithospheric structure under the western African-European plate boundary: A transect across the Atlas Mountains and the Gulf of Cadiz. *Tectonics*, 24, TC2001. <https://doi.org/10.1029/2004TC001639>
- Zouhri, S., Gingerich, P. D., Elboudali, N., Sebti, S., Noubhani, A., Rahali, M., & Meslouh, S. (2014). New marine mammal faunas (Cetacea and Sirenia) and sea level change in the Samlat Formation, Upper Eocene, near Ad-Dakhla in southwestern Morocco. *Comptes*

*Rendus Palevol*, 13(7), 599–610. <https://doi.org/10.1016/j.crpv.2014.04.002>

Zouhri, S., Kchikach, A., Saddiqi, O., Haimer El, F. Z., Baïdier, L., & Michard, A. (2008). The Cretaceous-tertiary plateaus. In: Continental Evolution. The Geology of Morocco, Springer, p. 331–333.

### SUPPORTING INFORMATION

Additional supporting information may be found online in the Supporting Information section.

**How to cite this article:** Charton R, Bertotti G, Duval Arnould A, Storms JEA, Redfern J. Low-temperature thermochronology as a control on vertical movements for semi-quantitative source-to-sink analysis: A case study for the Permian to Neogene of Morocco and surroundings. *Basin Res.* 2021;33:1337–1383. <https://doi.org/10.1111/bre.12517>